UNIVERSIDAD AUTÓNOMA DE NUEVO LEÓN
FACULTAD DE INGENIERÍA CIVIL

THESIS

THIXOTROPY OF REACTIVE SUSPENSIONS: APPLICATION TO WHITE PORTLAND CEMENT SUSPENSIONS

PRESENT

OMAR FARID OJEDA-FARÍAS

AS A REQUIREMENT FOR THE DEGREE OF

DOCTOR EN INGENIERÍA CON ORIENTACIÓN EN MATERIALES DE CONSTRUCCIÓN

MAY, 2019

UNIVERSIDAD AUTÓNOMA DE NUEVO LEÓN

FACULTAD DE INGENIERÍA CIVIL

Thesis

THIXOTROPY OF REACTIVE SUSPENSIONS: APPLICATION TO WHITE PORTLAND CEMENT SUSPENSIONS

PRESENT

OMAR FARID OJEDA-FARÍAS

As a requirement for the degree of

Doctor en Ingeniería con Orientación en Materiales de Construcción

DIRECTOR

DR. JOSÉ MANUEL MENDOZA-RANGEL

CO-DIRECTOR

DR. PASCAL HÉBRAUD

San Nicolás de los Garza, Nuevo León, México **May 2019**

Cd. Universitaria a 12 de abril de 2019

Dr. César Antonio Juárez Alvarado
Subdirección de Estudios de Posgrado
Facultad de Ingeniería Civil - UANL
Presente:

Estimado Dr. Juárez

Por este medio le comunico que el M.I. Omar Farid Ojeda Farías, pasante del Doctorado en Ingeniería con Orientación en Materiales de Construcción, ha concluido satisfactoriamente su trabajo de tesis denominado: **"THIXOTROPY OF REACTIVE SUSPENSIONS: APPLICATION TO WHITE PORTLAND CEMENT SUSPENSIONS"**, por lo que no tengo inconveniente en solicitarle que amablemente gire las instrucciones para dar paso a los trámites correspondientes y atender la solicitud del Examen de Grado del M.I. Omar Farid Ojeda Farías para cumplir con los requisitos que exige el Reglamento de Exámenes Profesionales de nuestra Institución.

Sin otro en particular, le reitero mis distinguidas consideraciones y un afectuoso saludo.

Atentamente
"Alere Flammam Veritatis"

Dr. José Manuel Mendoza Rangel
Director de Tesis

Pascal Hébraud

Institut de Physique et de Chimie
des Matériaux de Strasbourg
23 rue du Loess
67034 Strasbourg Cedex
France

Tél. +33 (0) 3 88 10 71 85
E-Mail : pascal.hebraud@ipcms.unistra.fr

Strasbourg, April 29th 2019

Dr. Cesar Antonio Juárez Alvarado
Head of Postgraduate Studies
Civil Engineering School
Universidad Autónoma de Nuevo León

Object : Evaluation of the PhD thesis of Mr. Omar Farid Ojeda-Farías

Dear Dr. Alvarado,

In response to my designation as co-director of the thesis entitled "Thixotropy of reactive suspensions. Application to white portland cement suspensions", presented by Mr. Omar Farid Ojeda-Farías, as a prerequisite to obtain the degree of PhD of Engineering with orientation on Construction Materials, I acknowledge that I have read and evaluated the thesis and have indicated my comments, suggestions and corrections to the document.

Considering that the student has made the necessary modifications, I feel that the thesis document can be APPROVED so that Mr. Omar Farid Ojeda-Farías can proceed with the presentation to satisfy the requirements of the PhD of Engineering degree from the Universidad Autónoma de Nuevo Leon.

Please do not hesitate to contact me if you need any further information.

Yours sincerely,

Pascal Hébraud

Cd. Universitaria a 30 de abril de 2019

Dr. José Manuel Mendoza Rangel
Coordinador Académico de Posgrado
Facultad de Ingeniería Civil
Universidad Autónoma de Nuevo León
Presente:

Estimado Dr. Mendoza:

En atención a su oficio en el que me informa que fui designado como Revisor de la Tesis **"THIXOTROPY OF REACTIVE SUSPENSIONS: APPLICATION TO WHITE PORTLAND CEMENT SUSPENSIONS"**, que presenta el M.I. Omar Farid Ojeda Farías, como requisito parcial para obtener el grado de Doctor en Ingeniería con Orientación en Materiales de Construcción, me permito informar a usted que después de haber leído y evaluado la calidad de tesis, dictamino que la misma es APROBADA.

Sin otro en particular, le reitero mis distinguidas consideraciones y un afectuoso saludo.

Atentamente
"Alere Flammam Veritatis"

Dr. César Antonio Juárez Alvarado
REVISOR

UANL
UNIVERSIDAD AUTÓNOMA DE NUEVO LEÓN

FIC
FACULTAD DE INGENIERÍA CIVIL
INSTITUTO DE INGENIERÍA CIVIL

Cd. Universitaria a 30 de abril de 2019

Dr. César Antonio Juárez Alvarado
Subdirector de Estudios de Posgrado
Facultad de Ingeniería Civil
Universidad Autónoma de Nuevo León
Presente:

Estimado Dr. Juárez:

En atención a su oficio en el que me informa que fui designado como Revisor de la Tesis **"THIXOTROPY OF REACTIVE SUSPENSIONS: APPLICATION TO WHITE PORTLAND CEMENT SUSPENSIONS"**, que presenta el M.I. Omar Farid Ojeda Farías, como requisito parcial para obtener el grado de Doctor en Ingeniería con Orientación en Materiales de Construcción, me permito informar a usted que después de haber leído y evaluado la calidad de tesis, dictamino que la misma es APROBADA.

Sin otro en particular, le reitero mis distinguidas consideraciones y un afectuoso saludo.

Atentamente
"Alere Flammam Veritatis"

Dr. Alejandro Durán Herrera
REVISOR

Av. Universidad s/n, Ciudad Universitaria, C.P. 66455
San Nicolás de los Garza, Nuevo León, México.
Tel.: (81) 14424400 / Fax: (81) 14424443
http://www.fic.uanl.mx

ANIVERSARIO 1933•2018

DEDICATION

I would like to dedicate this work to special persons that are the most important in my life, my mother Silvia Farías and my father Benito Ojeda, without whom this thesis could not have been finished.

I would like also dedicate this work to my life mate Guadalupe Del angel, who supported me in all moments of this project.

My sincerely dedication.

ACKNOWLEDGMENT

I would like to thank the Universidad Autónoma de Nuevo León to give me the opportunity to do my Ph.D study.

I am also grateful to Facultad de Ingeniería Civil and especially to the Instituto de Ingeniería Civil for the support, facilities and equipment.

A special thank to all academics of PhD program in construction materials for their teachings and advice during the advance of this thesis. I also thank to concrete technology department, construction materials research laboratory, eco-materials department and postgraduates studies department.

I would like to express my gratitude to Institut de Physique et Chimie des Matériaux de Strasbourg (IPCMS) and especially the Department of Ultrafast Optics and Nanophotonics and BIOSOFT group, for the support, feedback, cooperation, stay and of course friendship during my Ph.D.

I am also grateful to Sika Technology – Central Research material physics for the support, facilities and confidence during the several stays.

I would like to thank the CONACYT for the scholarship of PhD No. 276361 and the support of the projects of research No. 155363 and 285976.

I would like to express mi sincere gratitude to my advisors Dr. José Manuel Mendoza-Rangel and Dr. Pascal Hébraud for their continuous support of my Ph.D study and research, for their patience, confidence, motivation, and immense knowledge. Their guidance helped me in all time of research. They are the best mentors I could have had.

My sincere thanks also to Dr. Didier Lootens, who provide me an opportunity to join his team of Sika, and who gave access to the laboratory and research facilities, furthermore, for show me how a leader should be.

Besides my advisors, I would like to thank the rest of my thesis committee: Dr. Alejandro Durán-Herrera, Dr. Ismael Flores Vivian, for their comments, suggestions and corrections that improved the quality of this thesis.

I would like to thank the Sika material physics team. Maxime Liard, Luka Oblak, Patrik Kuhn, Armin Bruehwiler, Raphael Bourquin, and all people that helped me during my visits to the laboratory.

I would like to thank my family: my parents and my brother and my sister for their support during my Ph.D.

Thanks to all my friends for their support during my PhD.

CONTENTS

LIST OF FIGURES

LIST OF TABLES

1 INTRODUCTION

1.1 Overview

Portland cement pastes are concentrated suspensions consisting of two interacting phases: solid and reactive with the binder and liquid with the water and its admixtures. The solid particles are composed of calcium silicate and aluminate phases, which once dispersed in water lead to strong ionic dissolution, saturation and precipitation of surface layers, followed by a period of low reactivity called dormant period. During this period hydrate products nucleate and grow to form portlandite, ettringite and CSH gel followed by a faster hydration process known as acceleration period. In the dormant period the consistency is workable until the ions precipitation starts the suspension setting.

The portland cement suspensions are complex fluids with thixotropic behavior due to the change of apparent viscosity at the several stress conditions. These suspensions exhibit physical thixotropy due to the attractive forces generated by Brownian motion and Van der Waals forces, forming aggregates by the growing of flocs and a gel structure. On the other hand, chemical thixotropy is a result of the chemical process of hydration, forming bridges of CSH products from the first minutes of mixing, as well as the ettringite needles as a consequence of C_3A fast reaction with gypsum and water.

Both, physical and chemical thixotropies driving the setting and hardening of portland cement suspensions as well as the rebuild-up of microstructure after the application of a pre-shear stress of higher value. Of the above, the variation of water to cement ratio, the use of chemical admixtures and the different shear rate conditions during mixing, transport and placing into the formworks is commonly studied for practical applications, due to deliberately or non-deliberately alters the thixotropy of cement suspensions, by the modification of attractive interactions or the kinetics during hydration.

For that reason, it is necessary to analyze those variables during rest and shear rate conditions in order to understand and control the flow properties of portland cement suspensions for application self-leveling extrusion, and pumping. In other words, we wish to obtain blends with high viscosity at rest but low flow resistance during their manipulation

1.2 Cement suspensions thixotropy

Thixotropy of portland cement suspensions in a fresh state is a property characteristic of Non-Newtonian time-dependent fluids. When a suspension previously at rest is subject to flow its viscosity decreases over time, but if the stress that produces the flow is interrupted the suspension recovers viscosity by rebuilding its microstructure. The thixotropic behavior of cement suspensions is a function of the blend design, the mixing protocol and the history of the applied shear rate.

The study of thixotropy in civil engineering is significant in self-leveling applications, extrusion, and pumping, where the value of yield stress plays an important role. If one suspension will be pumped the yield stress must be low, in other words, the viscosity should be decreased for getting the flow of suspension, but once placed in formwork an increase of viscosity in order to avoid segregation of particles is convenient. That is, the yield stress needs to be higher.

At present, the researches of thixotropy have been focused controlling the flow properties of cement suspensions by the use of chemical admixtures. In recent years technologies which 3D printing mortar, requires the adequate driving of suspensions and avoiding the segregation once placed. On the other hand, hardened properties such as 28 days strength and durability are the main considerations in the formulation of suspensions. Physical and chemical thixotropies have been studied but their representation and identification is a challenge yet, no having models that identifying the aggregation of particles for interacting force (physical part) and chemical reactions of silicoaluminates of cement particles (chemical part).

For that reason the implementation of new approach to study thixotropy is crucial, such is the case of analysis of dynamics by multi scattering light, which gives information of particle motion derived from thermal agitation, and it is possible to correlate with the rheology of suspension.

1.3 Scope of project

This project of research has the purpose to analyzing the thixotropy of white Portland cement suspensions and its alteration produced by solid volume fractions and presence of chemical admixtures. The variables were delimitated to four water-cement ratios, three concentrations of superplasticizer (HRWRA) and the combination of high concentration of superplasticizer with viscosity modifying admixture (VMA). These variables were selected due to their importance in extrusion and pumping both industry and scientific applications around of the world.

The methodology selected makes use of conventional rheometry by rotational test and the multi-scattering light technique in order to study the influence the variables mentioned above, therefore, the kinetics of each one of the suspensions will be studied both by rheology and diffusing wave spectroscopy.

With flow curves, thixotropy quantification and the dynamics obtained by intensity autocorrelation function, the evolution as well as the identification of physical and chemical thixotropy are discussed, identifying the transition between periods of kinetics.

2 BASIC THEORY

2.1 Portland Cement

The Portland cement is a hydraulic cement produced by pulverizing clinker, composed primarily of hydraulic calcium silicates, calcium aluminates, calcium aluminoferrite, and one or more forms of calcium sulfate (gypsum) is incorporated to make the finished product [1]. The Portland cement is an inorganic material finely ground that mixed with water, form a paste which sets and hardens by hydration reactions.

2.1.1 Production and composition of Portland cement

The raw materials for the manufacture of Portland cement are divided into calcareous components and clayey components. The main source of the calcareous component is limestone ($CaCO_3$) and the source of silica and aluminum oxide are clays or slates, which for its use in cement has contents of 55-60% SiO_2, 15-25% Al_2O_3 y 5-10% Fe_2O_3.

The manufacturing process of clinker involves the use of limestone and clay that are mixed and thermally processed to temperatures about 1300 - 1450 ºC. Two stages can be identifying during this process; Firstly, at the range of lower temperature of 1300 ºC, where the reaction is in a solid state because the presence of the liquid phase is very low. The next stage is at a high temperature; at which it is already about 25% of the melt [2]. A summary of reaction can be described as follows: At the temperature of about 100 ºC (drying zone) free water is expelled. In 750 ºC (preheating zone) the water of clay is lost. Between 750 ºC and 1000 ºC calcination occurs, bound to calcium carbonate is dissociated. In the burning zone when the temperature is between 1000 -1450 ºC, partial fusion of the mix occurs and the C_3S and C_2S form the clinker. Finally, in the cooling zone at temperatures of 1450 – 1300 ºC crystallization of melt occurs and the formation of calcium aluminate and calcium aluminoferrite is presented [3].

The raw materials mentioned above interact with one another inside the kiln to form complex products. These products are components of clinker specified by the oxide contents and by proportions of the four main compounds. In addition to the compounds, there are minor compounds that are a few percentages of the weight of cement; Table 2.1 gives the oxide composition of a typical Portland cement [4].

Table 2.1 Typical oxide composition of portland cement

Oxide	Typical oxide composition per cent
CaO	63
SiO_2	20
Al_2O_3	6
Fe_2O_3	3
MgO	1.5
SO_3	2
K_2O	
Na_2O	1

2.1.2 Classification of Portland cements

Around of the world, there are various names to define portland cement, names like 42.5 Portland cement, Type I cement, ordinary portland cement, CPO etc. are the most commonly in construction industry. For the division of cement into kinds, the cement composition plays an important role, because the hydraulic or pozzolanic additions conferring different properties like strength development, heat of hydration and resistance to several environmental attacks [5].

The fundamental performance properties that give the basis for its classification are the following:

- Strength of the mortars after 28 days of hardening (Class of cement)
- The rate of strength development
- Setting time
- Heat hydration
- Resistance to aggressive environmental

In this work we will use the classification from the main standards into civil engineering. According to American standards the portland cement is produced following the [6] specification, designating eight types of cement as is showed in Table 2.2. Additionally, by [7] standard, the blended hydraulic cement can be included in this classification, taken into account the slag and pozzolans employed in their production having six types of cement as is showed in Table 2.3.

Table 2.2 Types of portland cements according ASTM C 150

Type of cement	Denomination
Type I	Normal
Type IA	Air-entraining
Type II	Moderate sulfate resistance
Type IIA	Moderate sulfate resistance with air-entraining
Type III	High early strength
Type IIIA	High early strength with air-entraining
Type IV	Low heat of hydration
Type V	High sulfate resistance

Table 2.3 Types of blended hydraulic cements according ASTM C 595

Type of cement	Denomination
Type IS	Portland blast-furnace slag cement
Type IP	Portland-pozzolan cement
Type P	Portland-pozzolan cement. High strength at early age are not required
Type I(PM)	Pozzolan-modified portland cement
Type I(SM)	Slag-modified portland cement
Type S	Slag cement in combination with portland cement

In Mexico, the standard [8] classified the cement for type, strength and specials characteristics. Tables 2.4, 2.5 and 2.6 show the nomenclature used into the standard. The CPC is commercially common cement into the industry, and it can be found like CPC 30R, even though is possible to find the different combination.

Table 2.4 Classification of cements by type according NMX-C-414 ONNCCE

Type of cement	Denomination
CPO	Ordinary portland cement
CPP	Pozzolanic portland cement
CPEG	Portland cement with blast furnace slag
CPC	Compound portland cement
CPS	Portland cement with silica fume
CEG	Cement with blast furnace slag

Table 2.5 Classification of cements by strength according NMX-C-414 ONNCCE

Strength class	Compressive strength (MPa)			Setting time (min)	
	3 days	28 days	maximum	Initial	Final
20	-	20	40	45	600
30	-	30	50	45	600
30 R	20	30	50	45	600
40	-	40	-	45	600
40 R	30	40	-	45	600

Table 2.6 Classification of cements by special characteristics according NMX-C-414 ONNCCE

Nomenclature	Special characteristic
RS	Sulfate resistance
BRA	Low alkali aggregate reactivity
BCH	Low heat of hydration
B	White

Another common classification is concerning European standard UNE-EN 197-1:2011 [9] which look at five types of cement considering the cement with sulfate resistance. In this classification, the supplementary cementitious materials are taken into account as well as strength and heat of hydration. Table 2.7 shows the different types of cements commercially available.

Table 2.7 Types of cements according UNE-EN 197-1:2011

Types	Notation	
CEM I	Portland cement	CEM I
	Portland cement sulfate resistance	CEM I-SR 0
		CEM I-SR 3
		CEM I-SR 5
CEM II	Portland-slag cement	CEM II/A-S
		CEM II/B-S
	Portland-silica fume cement	CEM II/A-D
	Portland-pozzolana cement	CEM II/A-P
		CEM II/B-P
		CEM II/A-Q
		CEM II/B-Q
	Portland-fly ash cement	CEM II/A-V
		CEM II/B-V

		CEM II/A-W
		CEM II/B-W
	Portland-burnt shale cement	CEM II/A-T
		CEM II/B-T
	Portland-limestone cement	CEM II/A-L
		CEM II/B-L
		CEM II/A-LL
		CEM II/B-LL
	Portland-composite cement	CEM II/A-M
		CEM II/B-M
CEM III	Blast furnace cement	CEM III/A
		CEM III/B
		CEM III/C
	Blast furnace cement sulfate resistance	CEM III/B-SR
		CEM III/C-SR
CEM IV	Pozzolanic cement	CEM IV/A
		CEM IV/B
	Pozzolanic cement sulfate resistance	CEM IV/A-SR
		CEM IV/B-SR
CEM V	Composite cement	CEM V/A
		CEM V/B

Therefore, of classification for type and composition, each cement can be classified for strength at 28 days, Table 2.8 shows the cement with normal and high resistance according to standard UNE-EN 197-1:2011.

Table 2.8 Classification for strength of cements according to UNE-EN 197-1:2011

Resistance	**Compressive strength (MPa)**			
Class	**Initial Strength (2 and 7 days)**		**Normal Strength (28 days)**	
32,5 N	-	≥ 16,0	≥ 32,5	≤ 52,5
32,5 R	≥ 10,0	-		
42,5 N	≥ 10,0	-	≥ 42,5	≤ 62,5
42,5 R	≥ 20,0	-		
52,5 N	≥ 20,0	-	≥ 52,5	-
52,5 R	≥ 30,0	-		

2.1.2.1 White Portland cement

Into construction industry several types of cement are produced to meet various normal physical and chemical requirements, having the group of special portland cements like white portland cement [10]. White portland cement is made of selected raw materials containing negligible amounts of iron and magnesium oxide [1]. The color of cement is a function of its chemical composition and processing conditions. The common gray of commercial cements is due to the iron compounds and the burning of the clinker, therefore, white cement is obtained from low iron and magnesium oxides raw materials, special grinding process and selected fuel used in clinker manufacturing [11].

In recent years, concretes made with white portland cement has had special use in architectural design requirements, because its appearance and durability reduce production costs, due to 85% of whiteness it allows the preparation of successful mixtures with colorant pigments and obtain elements with several forms [12-14]

2.1.3 Individual cement compounds

The major phases of portland cement are tricalcium silicate ($3CaO \cdot SiO_2$), dicalcium silicate ($2CaO \cdot SiO_2$), tricalcium aluminate ($3CaO \cdot Al_2O_3$) and ferrite phase of average composition ($4CaO \cdot Al_2 \cdot O_3 \cdot Fe_2O_3$), which at cement chemistry notation: C = CaO, S = SiO_2, A = Al_2O_3, F = Fe_2O_3, $\bar{S}$ = SO_3, and H = H_2O. The tricalcium silicate is a solid solution containing Mg and Al and is called alite, having monoclinic or trigonal form. Alite is the most important component of normal portland cement constituting 50-60% and its main contribution is the development of strength. The dicalcium silicate called belite occurs in the β form containing Al and Mg as well and some K_2O. The belite contributes little to strength development at 28 days. The tricalcium aluminate constitutes 4-12% and the ferrite phase is a solid solution with variable composition from C_2F to C_6A_2F [15,16].

2.1.3.1 Tricalcium silicate and alite phase

Tricalcium silicate or alite (C_3S) is the major component of Portland cement clinker, values around of 50-70% can be found into a phase's composition in different polymorphs forms like triclinic, but at high temperatures, it can be transformed in monoclinic and trigonal as well. The main contribution of alite to the reactivity of portland cement is particularly up 28 days of age on a cement paste [17]. The structure is compound for ions Ca^{2+}, O^{2-}, and SiO_4^{4-} with incorporations of the oxides Al_2O_3 and MgO mainly. According to the literature the C_3S has 73.7% of CaO and 26.3% of SiO_2 [18].

2.1.3.2 Dicalcium silicate and belite phase

Dicalcium silicate or belite (C_2S) represents between 15-30% of clinker. Its reaction is similar to alite but significantly slower. There are several polymorphs of C_2S (α, α`, β and γ) but

generally is stabilized in β form. Its structure is compound for Ca^{+2} and SO_4^{4-} but the inclusion of other ions like K^+, Mg^{2+}, and Al^{3+} can be included. The composition of C_2S is around of 34.9% SiO_2 and 65.1% CaO, having inclusion between 4 – 6% of Al_2O_3 and Fe_2O_3 [18].

2.1.3.3 $Ca_3Al_2O_6$ and Aluminate phase in clinker

Tricalcium aluminate (C_3A) is found around 5-15% of the clinker. Its reaction normally is divided into two mechanisms, the first one is in the absence of a source of sulfate and second case is when sulfate (gypsum) is added in order to avoid the rapid reaction. It can present in differences polymorphs depending the quantity in weight of Na_2O (0 - 4% cubic, 3 – 8% orthorhombic and 5 – 7% monoclinic). The C_3A is compound for ions Ca^{2+} and rings of sixteen tetrahedrons of AlO_4. Its composition is 52.3% CaO and 37.7% Al_2O_3. This component is responsible for the phenomenon of the flash set, the formation of calcium aluminates hydrates and sulfoaluminates, in fact, higher amounts of C_3A may produce durability problems in elements formed by concrete [15].

2.1.3.4 Ferrite phase

Tetra calcium aluminoferrite (C_4AF) accounts for 5-15% of the clinker, its contribution of strength is to longer periods. The ferrite phase can be obtained with the components CaO, Al_2O_3 and Fe_2O_3 in the solid solution $Ca_2(Al_xFe_{1-x})_2O_5$, where $0 < x < 0.7$ and $C_4AF$is only a composition where x=0.5. The C_4AF have 46.1% CaO, 21.0 % Al_2O_3 and 32.9% Fe_2O_3 [18].

2.1.4 Hydration, setting and hardening

The hydration process involves a reaction between an anhydrite compound with water, resulting in a new component hydrated. During the hydration, the reactive particles of cement has an interaction with molecules of water, immediately after its dispersion in water a strong dissolution occurs followed by a period of low reactivity where calcium and sulfate hydrates nucleate and grow to form hydration products, after that the process becomes faster until reaching a rigid system observing a sol/gel transition [19,20].

The difference between setting and hardening can be observed in Figure 2.1, where the setting implies the sudden loss of plasticity of the paste, becomes it a rigid solid with weak mechanical properties. The term hardening (after of setting) implies the development of hardness and gain of mechanical strength. This process starts from the addition of water until the paste shows properties of hardy solid.

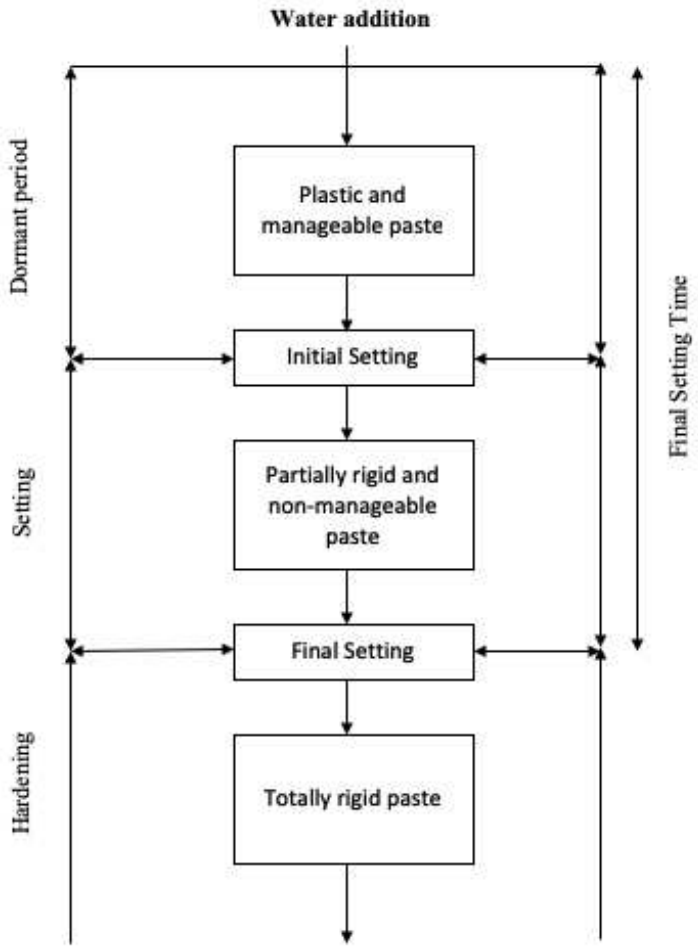

Figure 2.1 Setting and hardening in cement suspensions

As is presented by [21] cement hydration involves a collection of coupled chemical processes fall into one of the following categories:

1. Dissolution/dissociation involves detachment of molecular units from the surface of a solid in contact with water.
2. Diffusion describes the transport of solution components through the pore volume of cement paste or along of surface of solids in adsorption layers.
3. Growth involves surface attachment, the incorporation of molecular units into the structure of a crystalline or amorphous solid.
4. Nucleation due to the precipitation of solids heterogeneously on solid surface or homogeneously in solution when the bulk free energy driving force for forming the solid outweighs the energetic penalty of forming the new solid-liquid interface.
5. Complexation, reaction between simple ions to form ion complex or adsorbed molecular complexes on solid surfaces.

6. Adsorption, the accumulation of ions or other molecular units at interface, such as the surface of a solid particle in a liquid.

According to [22] the progress of hydration and its kinetics are influenced by the following factors:

- Phase composition of the cement and the presence of foreign ions
- Fineness of the cement, in particular by its particle size distribution and specific surface.
- Water-cement ratio used
- Curing temperature
- Presence of chemical admixture
- Presence of additives

The hydration processes in portland cement are complex and involve chemo-physical phenomena whose scales span nanometers to micrometers in length and from seconds to centuries in time [23].

2.1.4.1 Tricalcium silicate hydration

C_3S/alite constitutes between 50 and 70 % of Portland cement and mainly control the properties of cement paste, hence the importance of its study. The hydrate products obtained are $Ca(OH)_2$, o portlandite (CH), and calcium silicate hydrate semicrystalline called C-S-H gel, with Ca/Si molar ratio is between 0.7 and 2.3.

The generally accepted reaction for the hydration of C_3S is:

$$C_3S + 5.3\ H \rightarrow C_{1.7}SH_{4.0} + 1.3\ CH$$

A typical curve of C_3S hydration is presented in Figure 2.2 obtained by [21]. In order to discuss the kinetics mechanism, four periods indicated in the calorimetry curve are considered: (1) Initial reaction, (2) Period of slow reaction, (3) Acceleration period, and (4) Deceleration period.

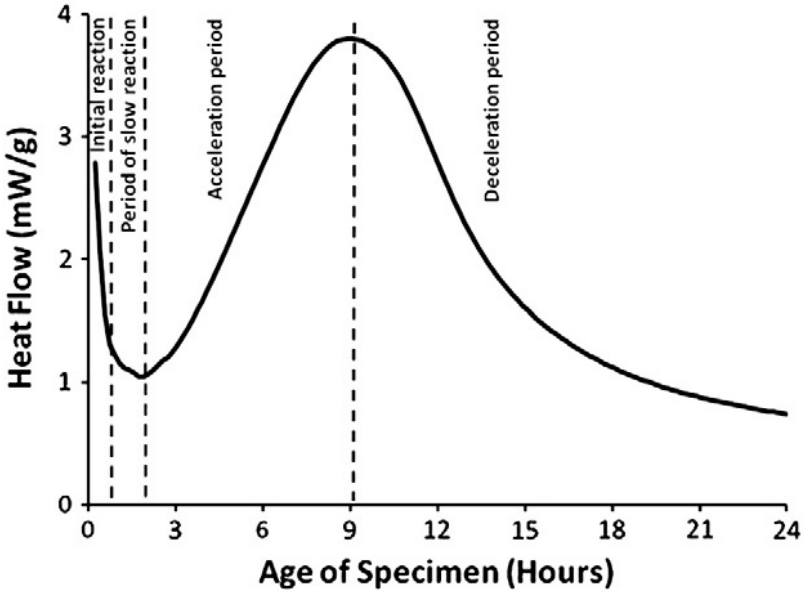

Figure 2.2 Rate of alite reaction as a function of time

The initial reaction (pre-induction period) is characterized by rapid reactions between particles of C_3S and water as well as a large exothermic signal related to the rapid dissolution of C_3S, on the order of seconds. This dissolution can reach equilibrium until the solutions are still undersaturated. The C_3S early deacceleration has been a topic of discussion, and several hypothesis have been discussed. One of these hypotheses is concerning a metastable barrier; This hypothesis implies that the metastable hydrate isolates the underlying alite from the solution. A set of studies provide strong evidence of a direct correlation between the length of slow reaction period and the rate of development of the surface hydrate.

During the period of low reaction (dormant period) the heat flow decreases drastically, the ion concentration of Ca^{2+} and OH^- increase. At the final of this period the precipitation of portlandite starts and the formation of CSH continued.

At the acceleration period, the nucleation of a stable form of C-S-H occurs. This formation occurs sometime after of the formation of a metastable hydrate layer on alite surfaces, and the growth of the stable C-S-H. This growth of C-S-H must be closely related to the development of its structure either as the aggregation of nanoscale particles or as large sheets of silicate layers. In this period C-S-H and portlandite starts to grow rapidly, being the trigger of this increase the precipitation of calcium hydroxide by two mechanisms; Either the presence of an inhibiting layer or the geochemical approach, both mentioned by Bullard and Flatt in [24,25].

Finally, the deceleration period is an important stage in cement pastes and concrete technology. This period is controlled by the diffusion process, consumption of small particles, and lack of space or water. The lack of water is important due to the total volume of hydrates is less than the combined volume of the reacting cement plus water causing chemical

shrinkage. On the other hand, it has been observed that the transition to diffusion rate control is responsible for the first period of deceleration immediately after the main peak. The inevitable impingement of different domains of the growing hydration products, which is a fundamental feature of nucleation and growth transformation, reduces the surface available for growth and readily explain the shift from accelerating to decelerating hydration rate [21].

2.1.4.2 Dicalcium silicate hydration

Similar to C_3S the reaction for the reaction of C_2S is:

$$C_2S + 4.3\ H \rightarrow C_{1.7}SH_{4.0} + 0.3\ CH$$

The reaction of C_2S is lower than C_3S. In fact the induction period is prolonged, and is followed by slow reaction until reaching a maximum value which is below of C_3S. Concerning the hydration products, the C-S-H is very similar to formed for C_3S and the quantity of CH is lower.

2.1.4.3 Hydration of calcium aluminates

The tricalcium silicate (C_3A) reacts with water affecting the rheological properties of cement pastes. C_3A has several different hydration reactions, depending on the sulfate presence. For the case of sulfate is absent, calcium aluminate hydrates will be formed, then we have:

$$C_3A + 6H \rightarrow C_3AH_6$$

The products cover the grains of C_3A, and its hydration occurs as a result of diffusion of ions, forming hexagonal hydrates based on the C-A-H system.

2.1.4.3.1 C_3A Hydration in the presence of Gypsum

The addition of gypsum radically modifies the C_3A hydration. This process has a long induction period followed by the crystallization of ettringite.

When sulfate is present, the ettringite is formed as:

$$C_3A + 3C\bar{S}H_2 + 26\ H \rightarrow C_6A\bar{S}_3H_{32} \quad \text{(Ettringite or Aft)}$$

As is known, C_3A reacts with water violently and in the presence of gypsum, ettringite is the only stable phase, covering the C_3A particles with a thin layer. The colloidal ettringite formed in the solution with Ca^{2+} ions causes more intensive retarded of hydration. At the shortage of SO^{-2}_4 ions in the solution close to ettringite, layer causes its transformation into monosulphate and its destruction [2]. Figure 2.3 shows the C_3A hydration in the presence of $CaSO_4$.

When the ettringite becomes unstable (due to sulfate depletion) the ettringite converts to monosulfoaluminate by:

$$2C_3A + C_6A\bar{S}_3H_{32} + 4H \rightarrow 3C_4A\bar{S}H_{12}$$ (Monosulphate or AFm)

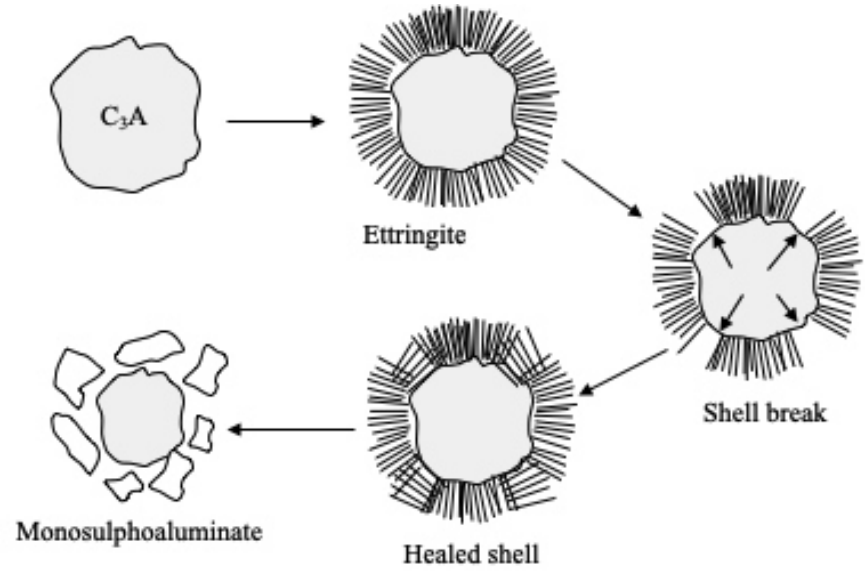

Figure 2.3 C_3A hydration in the presence of $CaSO_4$

2.1.4.4 Hydration of ferrite phase

This reaction is less well studied that those of the silicates. Similar that C_3A, the iron possibly substituting into the ettringite and monosulfoaluminate precipitating as an iron oxide (FH_3) gel by:

$$C_4AF + 10H \rightarrow C_3AH_6 + CH + FH_3$$

And for the reaction with sulfate, we have:

$$C_4AF + 3C\bar{S}H_2 + 30H \rightarrow C_6A\bar{S}_3H_{32} + CH + FH_3$$

Finally, the conversion to monosulfoaluminate phase, we have:

$$2C_4AF + C_6A\bar{S}_3H_{32} + 12H \rightarrow 3C_4A\bar{S}H_{12} + 2CH + 2FH_3$$

2.1.5 Properties of cement pastes

The properties of cement pastes are of interest due to their impact on the fresh concrete quality. Properties like consistency, workability, and setting time are related with rheological properties of cement paste. On the other hand, head of hardening, temperature rise and the chemical shrinkage are related with chemical composition of cement. If these properties are

known, it will be possible to select an adequate type of cement as well as the correct blend design of one concrete.

In the stage of early age, the rheological properties have an important effect that can be controlled by addition of superplasticizer, in order to modify the yield stress and plastic viscosity of the blend. At a later age, the development of strength depends on the quality of paste, so that factors like temperature evolution, drying shrinkage and swelling during wetting should be controlled [2].

2.1.5.1 Setting

At the moment that portland cement and water are mixed the hydration process start causing setting and hardening to the paste. The setting is the interval from the paste has plastic consistency with very low strength (Initial setting time) to the paste does not have a consistency handling due to the loss of plasticity (Final setting time). When a paste attains the stage of initial set it can no longer be properly handled and placed on the other hand, the final set corresponds to the stage at which hardening begins [3].

2.2 Rheology

The word rheology was defined in 1920 by professor Eugene Bingham at Lafayette College in Indiana USA and means the theory of deformation and flow of matter [26]. Basically the rheology studies the viscous behavior of fluids, suspensions, and solids.

2.2.1 Fundamentals

Figure 2.3 shows a diagram in order to define and explain the basic concepts of rheology. For this, it is consider one volume of fluid between two parallel surfaces, if a force is applied to the upper plate and an opposite force with the same magnitude in the lower plate, the fluid between surfaces is subject to shear [27].

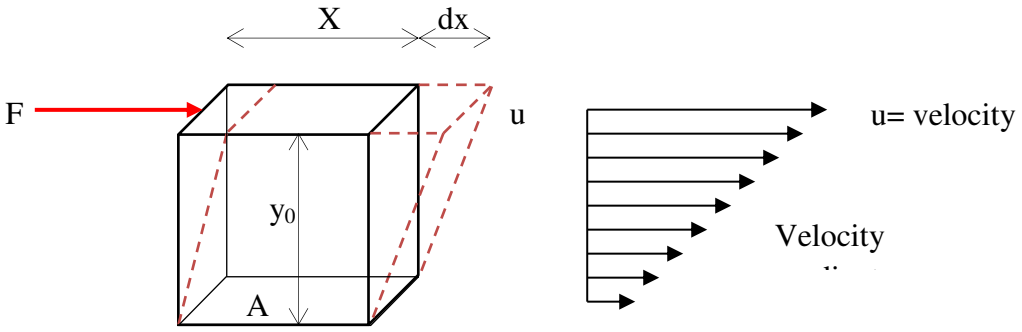

Figure 2.4 Flow of a liquid between two parallel plates (left). Fundamental definition of viscosity (right)

2.2.1.1 Shear stress

Stress is the result of a force that is applied over an area. The term shear stress is the result to applied one force opposite and parallel to another force but not in the same action line.

If stress in applied to elastic solid is compressed, elongated or shared and back to the original shape when the force is removed. In one fluid the shear stress produces that the individual layers of molecules move relative to one another, and the new position is to hold when shear stress is removed [27].

As is observed in Figure 2.3 the force applied uniformly across the area of parallel surface produce the shear stress which is transmitted over fluid defined by equation 1.

$$\boldsymbol{\tau_s} = \frac{\boldsymbol{F}}{\boldsymbol{A}} \; [=] \; \frac{N}{m^2} = Pa \qquad \text{Equation 1}$$

2.2.1.2 Shear rate

The shear rate is that value of velocity gradient of molecules and particles showed in Figure 2.3 (left). The geometry presented in the figure correspond to simple fluid where the velocity gradient is linear, therefore a linear velocity gradient applies only to simple fluids. To know the value of the shear rate we need to calculate the value of the velocity gradient of the point of interest. From Figure 2.3 (right) where the velocity gradient is linear we employ equation 2.

$$\dot{\boldsymbol{\gamma}} = \frac{\Delta \boldsymbol{u}}{\Delta \boldsymbol{y}} \; [=] \; \frac{\frac{cm}{sec}}{cm} = \frac{1}{s} = s^{-1} \qquad \text{Equation 2}$$

2.2.1.3 Viscosity

In order to define the viscosity, consider the Figure 2.3 and the relationship between shear stress and shear rate. That relationship is defined by the viscosity of the fluid, because for each applied shear stress the system keeps the equilibrium at a particular shear rate. The dynamic viscosity can be defined by equation 3.

$$\boldsymbol{\mu} = \frac{\boldsymbol{\tau_s}}{\dot{\boldsymbol{\gamma}}} \; [=] \; \frac{Pa}{s^{-1}} = Pa \cdot s \qquad \text{Equation 3}$$

The viscosity is the ratio of shear stress to shear rate at any applied shear rate. A high viscosity fluid will need more applied stress to achieve a particular shear rate than a low viscosity fluid.

2.2.2 Simple Newtonians fluids

Newtonian fluids are fluids that obey Newton's linear law of friction, represented by the scheme of Figure 2.3. When a tangential force is applied on the upper surface, this will be moved with velocity u, generating a laminar regime where the velocity of successive layers of liquid decreases when the distance from the surface sheared increase.

The shear stress applied is proportional to velocity gradient (u/y_0) represented by equation 4.

$$\boldsymbol{\tau_s} = \boldsymbol{\mu}\, \dot{\boldsymbol{\gamma}} \; [=] \; Pa \cdot s * s^{-1} = Pa \qquad \text{Equation 4}$$

Equation 4 define the behavior of Newtonian fluid because exhibit linear behavior (viscosity constant) that begins at the origin in stationary flow conditions and only is applied to describe laminar flow between two parallel plates [28].

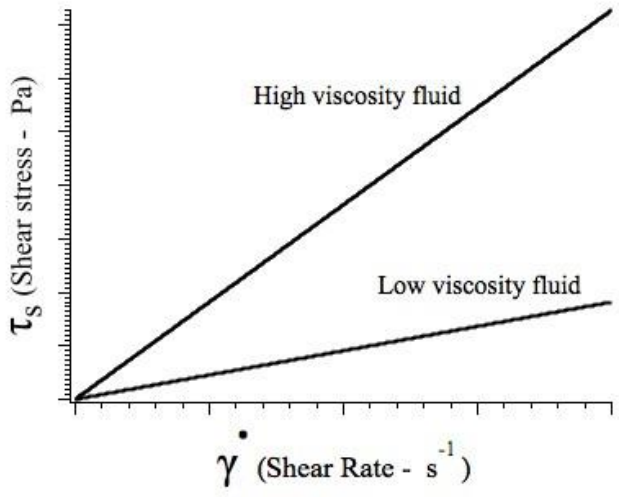

Figure 2.5 Rheograms of two simple fluids

Figure 2.4 shows a rheogram which the viscosity (μ) is the slope of flow curves. Viscosities of both the high and low are constants values that do not change as shear rate change and is clear that Newtonian fluids have constant and one viscosity as is observed in equation 4.

2.2.3 Non Newtonian fluids

The fluids that exhibit a deviation from the Newtonian behavior are known as Non-Newtonian fluids or complex fluids and the simple shear data $\tau_s - \dot{\gamma}$ do not pass through the origin and do not result in a linear relationship between them. For these fluids is common to call apparent viscosity, due to is not constant and is a function of τ_s or $\dot{\gamma}$ [29]. If the viscosity coefficient measured at same shear rate value, $\dot{\gamma}$.

In order to define simple mechanical properties to be used is necessary to consider the experiment of Figure 2.5. The figure shows a cylinder viscometer which a cylinder can rotate in a container about a vertical axis. It can be observed that annular space between the two cylinders' surface is filled with a liquid. The interior cylinder is subjected to torque M and the rotation occurs at constant angular velocity ω. The distance between the two cylindrical surfaces is defined by h and r represent the radius of the cylinder. It should be noted that h < r [30].

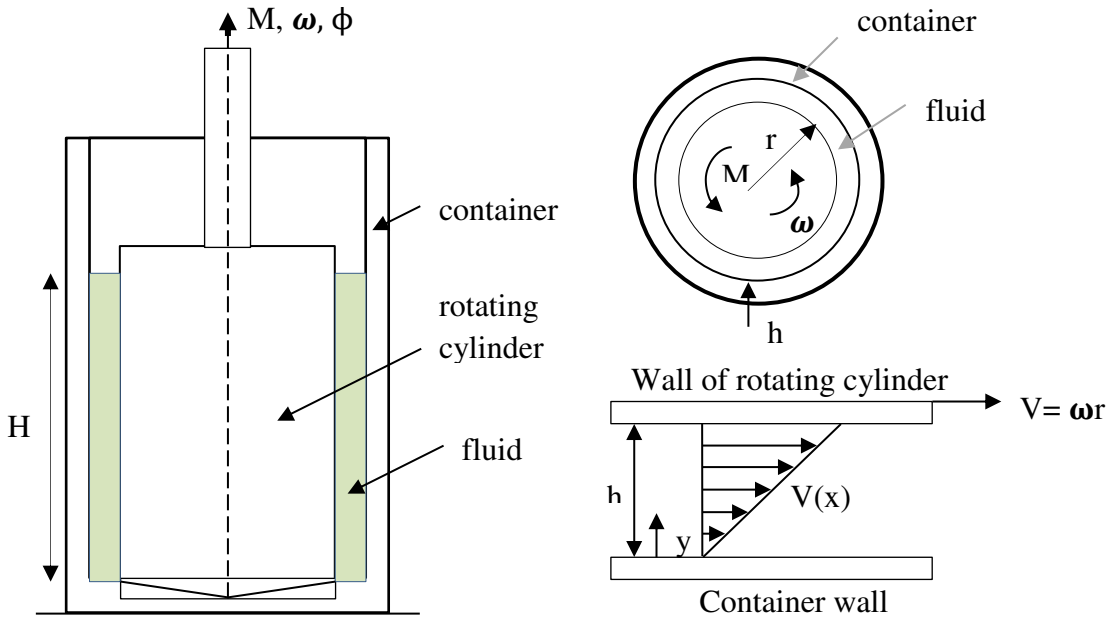

Figure 2.6 Simple shear flow into a cylinder viscometer

Firstly, we consider the velocity field in the experiment, given by: $v_x = \frac{v}{h}y, \quad v_y = v_z = 0$, and $v = \omega r$. During a short time interval dt, a volume of fluid with edges dx, dy and dz change its form by the shear strain d_γ by:

$$d_\gamma = \dot{\gamma} dt = \frac{dv_x}{d_y} dt = \frac{v}{h} dt = \frac{\omega r}{h} dt \qquad \text{Equation 5}$$

Called rate of shear strain, having the following equation.

$$\dot{\gamma} = \frac{dv_x}{dy} = \frac{v}{h} = \frac{r}{h}\omega \qquad \text{Equation 6}$$

The shear stress can be determined using the balance law of angular momentum applied to cylinder at constant angular velocity ω. The torque M is balanced by shear stress τ of the following way:

$$(\tau r) = (2\pi r H) = M \;\Rightarrow\; \tau = \frac{M}{2\pi r^2 H} \qquad \text{Equation 7}$$

By equation 5 and 6 is possible to obtain a relationship between the shear rate $\dot{\gamma}$ and shear stress τ, recoding the values of torque M and angular velocity ω.

In Non-Newtonian fluids in simple shear flow, the function of viscosity is:

$$\eta(\dot{\gamma}) = \frac{\tau}{\dot{\gamma}} \qquad \text{Equation 8}$$

Function 7 is called apparent viscosity, and the most common model for the viscosity function is given for the power law:

$$\eta(\dot{\gamma}) = K|\dot{\gamma}|^{n-1}$$ Equation 9

Where the parameters K and n depend of temperature

For the experiment of Figure 2.5 it will be include the elastic properties, this is that the test fluid in the container solidifies, and the torque M does not keep the constant angular velocity $\boldsymbol{\omega}$, but the cylinder will rotate an angle $\emptyset$. The rectilinear displacement of particles at the rotating cylinder will be $u = \phi r$ and the shear strain is defined by:

$$\gamma = \frac{u}{h} = \frac{r}{h}\phi$$ Equation 10

The materials are purely elastic if the shear stress is only a function of shear strain and for represent the linear relation is necessary introduce the shear modulus G and define the follow equation:

$$\tau = G\gamma$$ Equation 11

2.2.3.1 Time-independent rheology

These kind of fluid are characterized by the fact that the value of the rate of shear at a point in the fluid in the fluid is determined only by the corresponding value of shear stress and vice versa as is showed in equation 12, in other words, such fluids does not have memory of their past history [29].

$$\dot{\gamma} = f(\tau)$$ Equation 12

Depending upon the form of the equation there are the following possibilities which are showed in Figure 2.6:

- Shear-thinning or pseudo plastic behavior
- Visco-plastic behavior with or without shear-thinning behavior
- Shear-thickening dilatant behavior

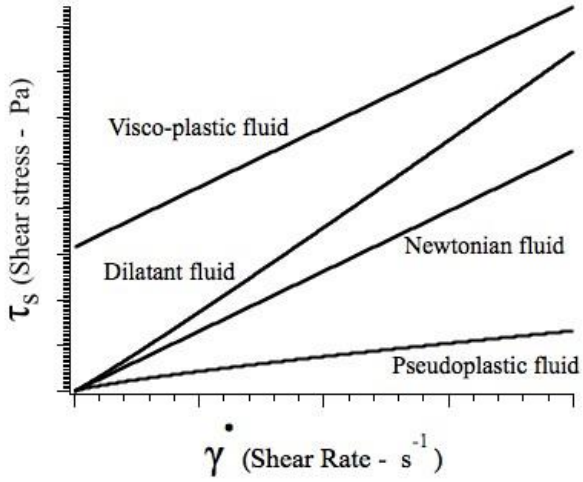

Figure 2.7 Flow curves for different types of Non-Newtonian fluids

2.2.3.2 Time-depend rheology

Many substances display complex flow characteristics, which cannot be represented by simple mathematical expressions and the apparent viscosity is not a function to applied shear stress τ or the shear rate $\dot{\gamma}$. Complex fluids like cement pastes are sheared at constant $\dot{\gamma}$ following a long period of rest its viscosity gradually decrease and its internal structure present broken down. At contrast, as the structure breaks down, the rate at which linkages can rebuild increase until a state of dynamic equilibrium is reaches. The time dependent fluids can be divided in two types depending upon the response to shear over period of time; Thixotropy and Rheopexy materials [31].

2.2.4 Thixotropy

Thixotropy can be observed when in an experiment the apparent viscosity under constant shear rate or shear stress decrease, followed by gradual recovery when the stress or shear rate has been removed. According to a general agreement in the scientific community, thixotropy is defined as the continuous decrease of viscosity with time when flow is applied to a sample that has been previously at rest and the subsequent recovery of viscosity in time when the flow is discontinued [32].

The thixotropy is strongly related with the change of microstructure of materials, where the driving force for microstructural changes is the equilibrium between break-down due to the flow stress and build-up due to in-flow collisions and Brownian motion of particles embedded in a solution [33-36].

Brownian motion is a result of the thermal agitation of atoms and molecules constantly bombarded that cause movement between them, and changed the microstructure which can be interpreted like alignment of fibers, distribution of particles in a suspension or drops in an emulsion and all they take a finite time to change their position due to the action of shearing or Brownian motion.

2.2.4.1 Mechanics of thixotropy

The mechanics of thixotropy especially in cementitious materials can be explained by [37]. Materials like fresh concrete are subject to high shear rates during its productions, transport in the mixing vehicle and placed in formworks at the constructions site. This can be represented in Figure 2.7.

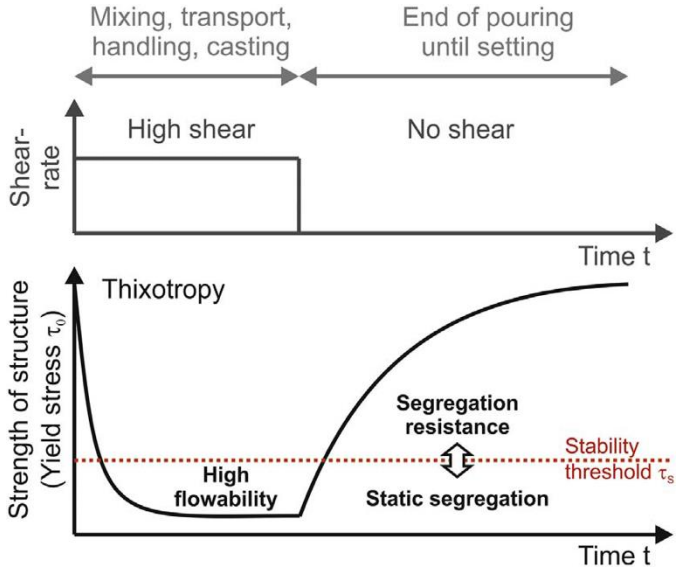

Figure 2.8 Thixotropy during processing of SCC [37]

At the beginning of process, the concrete presents low yield stress and viscosity due to high shear rate and segregation can occur. After when the blend is placed into formwork is no longer subjected to shear rate, in that moment yield stress and viscosity increase steadily within a few seconds avoiding segregation of the coarse aggregates.

Once cement particles are in contact with water an aggregation and flocculated structure is formed as a result of forces. These flocs are broken if the paste is subject to shearing due to the rupture of interparticle links reducing the viscosity of cement paste. At rest, the internal

structure tends to rebuild. The reconstruction of the structure is ascribed to the flocculation of the fine particles and colloidal interactions of the cement and additions as well as the first hydration products like ettringite and portlandite [38].

2.3 Colloidal suspensions

A mixture of solid particles in a liquid is a simple dispersion of solid elements, and is called suspension. There are several examples it, but we will focus on civil engineering materials like ceramics, concretes, mortars, asphalt and cement suspensions. The discussion about the rheology behavior of fluids was taken in account small molecules that compound it, but the nature of industry materials added to simple liquids elements bigger than the molecules of liquid. Of the above the behavior of these materials depends on the mutual interactions of the elements and their interactions with the molecules of liquid [39].

When a suspension have particles of size into the range from 10 nm to 1 μm, they become tendentious to the effects of thermal agitation by the molecules of the liquid, interacting at distance of the same order as their own size by attractive and repulsive forces. Suspensions with these characteristics are called colloidal suspensions [39].

2.3.1 Relation with yield stress and thixotropy

A sufficient quantity of particles can constitute a network of connections in a suspension, leads to behaviors. At rest, the suspension can show a solid structure but this can be broken by applying a force greater than some critical value, observing a yield stress in the suspension. This yield stress is a remarkable property in colloidal particles due to a small volume fraction of particles in a liquid can yield a mixture with a very high yield stress due to the particles exert mutual forces.

The relation of colloidal suspension with thixotropy can be explained by referring physical phenomenon resulting from the very small size of particles called Brownian motion. The thermal agitated liquid molecules transfer momentum to suspended solid particles during collisions. These collisions generate forces that a given time is related to the temperature of the system. The Brownian motion coupled with interaction forces lead to the growth of network that determinate the yield stress of a suspension.

2.3.2 Brownian motion

One particle immersed in a liquid is surrounded by a large number of molecules in thermal agitation, given the motion of the elements as is showed in Figure 2.8 (left). If the particle has inertial low, and its size is sufficiently small, the particle motion will be governed by a force of different magnitude and direction. The particle ends up following trajectory random through the liquid as is represented in Figure 2.8 (right), this is called Brownian motion. The displacement of the particle can be represented by r(t), which is a vector from the initial

position of a particle to its position at time t. This vector has a length equal to the distance traveled by the particle at the initial time of movement [39].

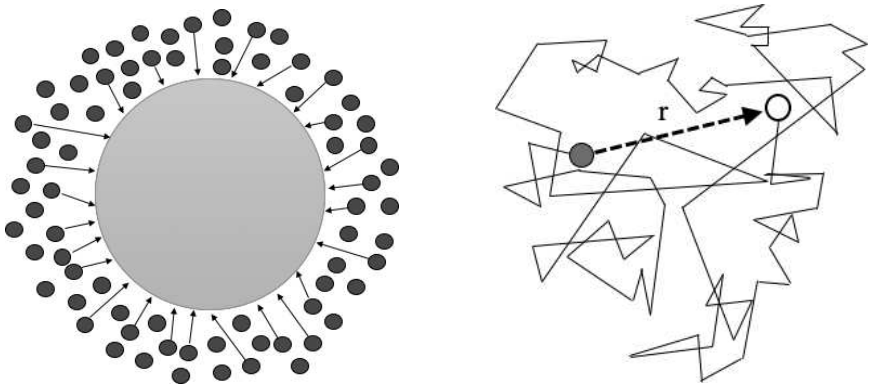

Figure 2.9 Molecules of a liquid colloiding with a colloidal particle (left) and Random trajectory by effect of Brownian motion (right)
[39]

2.3.3 Van der Waals Forces

In the different structures of molecules and their constitute atoms, there is a short-range attractive force between two molecules. One of these particles will behave as an instantaneous electric dipole, inducing an electric field in the neighboring atom which will in turn acquire a dipole moment, whereupon the two dipoles will attract one another. A colloidal particle is made up of a very large number of atoms interact each other.

Van der Waals force is always present between atoms and cannot be turned off, removed or eliminated because are only weak forces. If another attractive or repulsive force have been eliminated, Van der Waals force takes over [27].

One approximation for its calculus is considering the sum of the mutual interactions between pairs of atoms assuming that the interaction potential has the form $-C / r^6$. There are several equations to calculate the potential interactions; for a single atom where the particle is has a surface A and infinite thickness the potential can be found by:

$$U = \frac{KA}{12\pi h^2}$$ Equation 13

Where:

K.- Hamaker constant (K=$\pi^2\rho^2C$)

A.- Surface area

h.- Thickness

For two spherical particles with distance r = 2R+h between their center, we can use:

$$\Phi_a = -\frac{K}{6}\left(\frac{2R^2}{r^2-4R^2}+\frac{2R^2}{r^2}+ln\frac{r^2-4R^2}{r^2}\right) \quad \text{Equation 14}$$

Under the effect of Van der Waals interactions, two particles will be moving together and come into contact.

2.3.4 Attractive systems

In the case of attractive systems two particles move toward one another, they tend to position themselves at the distance corresponding to this minimum. This phenomenon is known as aggregation, and the particles will continually explore new positions by the effect of Brownian motion. Figure 2.9 shows structure formed by aggregation of particles. When clusters involving more than two particles successive aggregation can be formed, and those particles formed will continue to explore the surrounding space until finding another cluster and attach them. A weak attraction thus allows the particles to explore several clusters but the particles can easily explore low-density configurations until they find themselves jammed into a dense enough structure. On the other, hand if the attraction is strong, two particles will remain jammed into this random position forming a cluster. In the case of particles mixed by stirring and then left to aggregate, if there is not sedimentation, the cluster will be formed for gradually swell up to a critical size until it comes into contact with one another. They then form an infinite cluster by aggregation of fractal clusters reached a critical size which can be referred to as floccules.

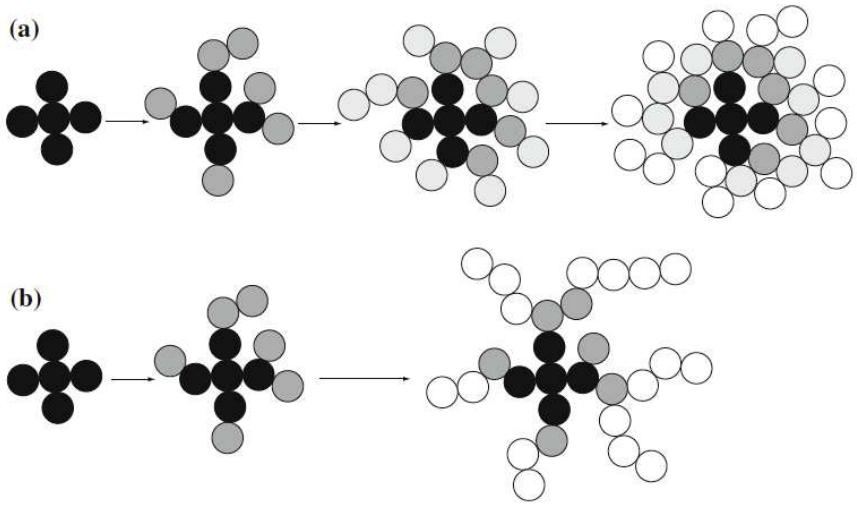

Figure 2.10 Structure formed by aggregation. a) weak attraction forming a closed structure. b) Strong attraction forming an open structure

2.3.4.1 Origin and kinetics of aggregation

Aggregation is an intrinsic step in precipitation, indeed in suspensions can be induced by adding electrolytes or polymers (coagulation and flocculation). Aggregation is the result of collisions and adhesion due to the motion of particles being the main cause the Brownian motion. Adhesion implies attractive interparticle force between two particles like Van der walls forces. In general, aggregation coincides with a process that affects growth and morphology of aggregates that depend on parameters as temperature, velocity gradient etc. [40].

The kinetics of aggregation are usually examined for monodisperse particles in the absence of nucleation, dissolution, and breakage. A cluster of mass m results from the aggregation of two sub-clusters with masses i and $j = m - i$.

2.4 Flocs and gel structure

One floc is a group of particles, associated with attractive forces. The particles that form a floc have weak forces like electrostatic and Van der Waal forces. Flocculated particles and gel structures are not chemically reacted so that flocculated structure in suspensions will break when they are subject to low shear rate intensities such as stirring, mixing or pumping [41]. As the flocculation process takes places, the particles form small flocs, and these small flocs grow into large 3-D gel structures.

2.4.1 Flocculation

Flocculation produces 3-D gel structures, containing large flocs connected by chains, being difficult to distinguish between flocs and chains. Figure 2.10 shows an example of the flocculated particle if this floc is subject to shear the particles can separate and travel individually, but when the system returns to initial state the particles can again flocculate. In the same figure, it can be observed the agglomeration of particles which during mixing or pumping will be difficult to break its structure. If the agglomeration is broken by milling, the particles are free to travel independently of another during shear, and when the shear is stopped, attractive forces can pull them together forming a floc different to the original formation.

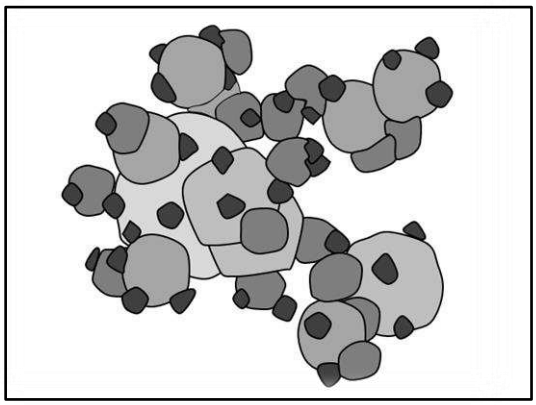

Figure 2.11 Floc formed by a group of particles

2.4.2 Gelation

Gel structure is characterized by 1) large continuous floc structures connected by flocculated chains and 2) continuous fluid channels within the structure. At the moment when all particles and flocs have formed large gel structure, the interparticle force can continue densifying and given strength of the structure expelling fluid into the channels. This process is known as syneresis. Figure 2.11 shows a suspension of particles; In the figure of top left all particles are independent of another followed by the formation of small flocs within the overall array of individual particles as is showed in the figure top right; The initial stage of growth of the floc structures is showed in figure bottom left. At this moment some flocs are still independent of the large structure but a significant quantity of particles has been incorporate into the growing structures; finally the complete structure is reach as is showed in figure bottom right, all particles and flocs are part of large single gel structure. An important property of flocculated suspension and gel structure is that all particles are tied into the structure and immobilized.

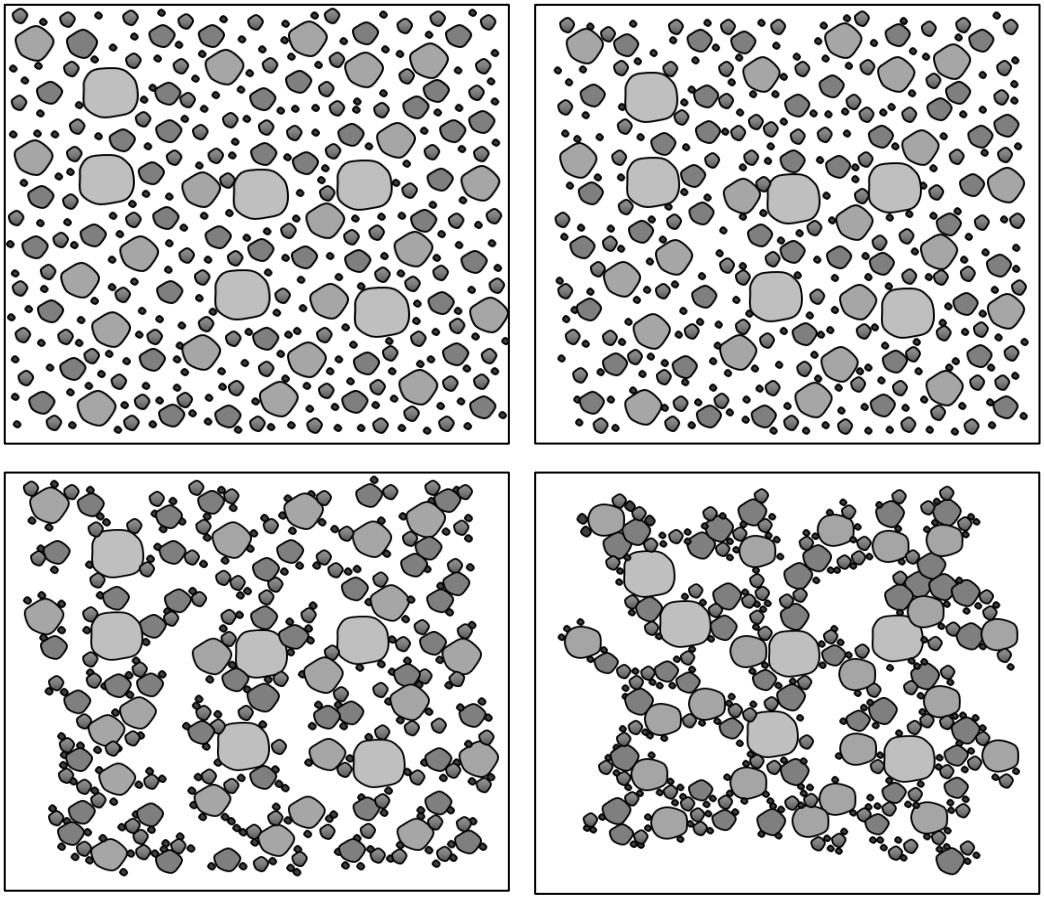

Figure 2.12 Gelation process

2.5 Characterization of colloidal suspension

The adjustment and monitoring of certain properties of colloidal suspensions is essential for adequate control of their functionality as well as the observation of their behavior. These controls require appropriate techniques for the determination of suspension properties such as particle morphology, hydrodynamics or specific interactions, surface area, interfacial properties, the concentration of particles, viscosity, and bulk properties of the dispersed phase [40].

2.5.1 Dynamic scattering DLS and DWS

The time-averaged signals from a scattering experiment are a novel tool to study the microstructure of colloidal suspensions. Dynamic scattering proves a temporal variations being a characterization method for colloidal suspensions.

Dynamic light scattering (DLS) technique allow to evaluating the fluctuation in scattered light caused by changes in the microstructure of the suspension. By DLS is possible to measure particle size, molecular weight, particle aggregation, phase transitions, and strength of colloidal gels [40,42]. As all techniques DLS has limits of applicability, one is that the concentration should be low enough or sufficiently high sample dilute to avoid strong multiple scattering because multiple scattering reduces the signal coherence. In contrast and for allowing strong multiple scattering diffusing wave spectroscopy (DWS) can be employed. The decay of the autocorrelation function is then related to the loss of coherence by a large number of scattered events. DWS gives the Brownian motion of a single particle as well as the mean free path of photo transport l^*, which is a function of particle concentration and suspension structure. DWS can be used to study the average diffusion coefficient, mean particle size, aggregation process and phase transition, and the most important contribution is of the study of microrheology of gels.

3 BACKROUND

In recent years, the research on industrial substances called multi-face have been development with more attention, because its rheological behavior does not follow the postulate of Newton about of linear relation between shear rate and shear stress, given place to non-Newtonian fluids or complex fluids, where the apparent viscosity is not constant and its behavior is not the only function of shear rate or shear stress, but is related to the kinetics of material [28,43,44,45].

The advances of rheological characterization have allowed to classifying the materials conformed its behavior, so it is possible distinguish materials purely viscous or time-independent, time-dependent materials, which can be divided in thixotropic and rheopexy and the viscoelastic materials [46,47]. This classification can be allowed to food, paints, biological flows, oils, slurries and portland cement pastes, this last object of study in this thesis.

The portland cement suspensions are non-linear rheological systems, where their characteristics are not depending on the shear rate or shear stress only, but also the. The thixotropic behavior of cement pastes has been studied by several researchers who have identified the physical and chemical parameters for its development, parameters from measurement protocol, mixing until the addition of supplementary cementitious materials and chemical admixtures that modify the hydration on blends [48-50]. Flocculation and coagulation have been studied as well as their relationship with thixotropy and shear thickening behavior due to these phenomes contribute to build-up of microstructure while viscosity is increasing at rest while setting is presented [51]. The coagulation is attributed mainly to the size of particles in cement and can be reduced it by use of superplasticizer admixtures. All this researches take into account the period when the suspension is critical for the casting and placing process [52].

3.1 Recent studies about thixotropy in cement suspensions

The research and studies about thixotropy have its origin at 1923 when the researches Schalek and Szegvari observed some iron oxide dispersions gels have the property of becoming in liquid sol by stirring slow, solidifying again after a period of time, developing a sol-gel transition [53]. Later it would be discovered that other materials had identical behavior and the studies continued until Freundlich proposed a viscosity model in stationary state in thixotropic gels, similar to the Bingham model and taken in account the basis of T. Peterfi studies [32]. In a thixotropic fluid when higher is shear rate the lower is the viscosity, and if the shear rate is decreasing progressively, the shear stress is lower than the registered at the beginning form a hysteresis cycle [28].

In recent years the research on thixotropy in cement suspensions has focused in the characterization of flow and deformation during setting and hardening, observing that the selection of rheometer is crucial to characterize adequately in order to have repeatability in

the measurements. It is also suggested, consider the set up in the experiments such as geometry, shear rates and type of measurement (rotational or oscillatory), because it has been proven the influence of sets in the rheometer as well as the type and time of mixing on the results of viscosity and yield stress in portland cement pastes [54,55]. Furthermore, some equations have been proposed to explain its behavior and its relation with the microstructural approach by rotational measurements ascribed this to coagulation rate and dispersion rate of the cement particles as published by [56,57].

One of the studies about of thixotropy in Portland cement pastes have been developed by [58]found that the thixotropic effect act at short timescales due to flocculation process, while at larger timescales the aging effects become significant. Afterwards Nicolas Roussel [59] presented a model for describing thixotropy on self-compacting concrete, where the main application of this research is the pressure of formwork and multilayer casting. In this work are mentioned the physical contribution due to the particle interaction forces as a consequence of the potential energy of each particle. While energy applied to the system does not exceed a given value the particle does not leave this state when the applied stress is stopped, the particle goes back to initial position showed elastic characteristics, however, if the energy applied to the system is higher, the particle leaves rest state and begin the flow.

These studies were supported with other research that had the aim to determine the origin of thixotropy in fresh cement pastes, so [60] presented one study defined two origins of thixotropy; The first origin corresponds to high critical deformation associated to colloidal interaction network between particles of cement. The second origin is associated to smallest critical strain due to the first hydrates, described it as practical thixotropy. As a contrast study and in order to simulate the real casting when a blended are initially in motion, the influence of clays on the rate of structural rebuilding after being broken down was studied [61], observing that the recovery after shear-induced breakdown in presence of clay is very rapid especially at early age and a longer resting time the hydration mechanism begin to dominate, corroborating the two origins described by Roussel.

On the other hand, the evaluation of structural build-up and its relationship with thixotropy, are crucial to understand the development of mechanical properties as well as the chemical contraction at final setting time. Controlling the structural build-up of concrete its processing technology will be at the heart of future progress, where the additive play an important role for digitalization of concrete industry [62]. The structural build-up experiments have shown the role of mineralogical composition of cement and its influence at initial periods of hydration [63]. Research as [64] studied the structural build-up of cement suspensions at rest and its relation with the thixotropy by dynamic rheometry (small amplitude oscillatory shear) analyzed the influence of water-to-cement ratio, cement type, fineness and presence of high range water reducing admixture. In this work, the shear modulus was determined and its increase is related directly with a capacity to form colloidal structure as well as the physical and chemical structuration. Of the same way in other study [65] studied the structural build-

up, now considering the alkali sulfate content and temperature of suspension. For this propose zeta potential and calorimetry test were carried out, finding that the Brownian collisions, the distance between dispersed particles and the intensity of cohesion controlled the percolation time. Although of this research the structural build-up of cement pastes has been evaluated comparing static yield stress test and small amplitude oscillatory shear test as is presented by [66]. In this study the static yield stress was dependent on the shear rate used in the test, lower shear rate resulted in higher yield stress ascribed this to the thixotropy effect and concluded that the uses of static yield stress test can be used to reflect thixotropic nature of structural build-up, as is observed in recent studies on mortars using dynamic and static yield stress [67]

Recent studies have been focused on the study the thixotropy of self-compacting concrete (SCC), due to in this kind of concretes is more common find the thixotropy phenomenon. The research carried out by [37] describing the thixotropic build-up based on interparticle interactions and hydration kinetics by the change of the components and quantified rheologically, at the same time superplasticizer adsorption, chemical bound water and maximum packing density were studied. In this study when solid fraction content increases the thixotropic structural build-up increase as well. Therefore, maximum packing density and coverage of particle surface both decreasing. As an highlighted the particle distance as a factor determinate on surface interactions and initial hydration of cement. Other studies have focused to take advantage of thixotropy properties in SCC, by its improve blend design and the use of additive manufacturing it has been enhanced its production and placing with several technologies achieve robust. [68,69].

3.2 The role of superplasticizer addition

In order to regulate the rheological properties by improving the dispersion of particles in the early hydration ages, a largest group of superplasticizers have been used. The main research is focused on the compatibility of additive with the variety of cements as well as its interaction with supplementary cementitious materials, and by a calculating of optimal concentrations quantify the effectiveness on rheology, furthermore the assessment of thixotropy and yield stress due to that additions [70-73].

Sulfonate-based superplasticizer is one group of high-range water reducers composed for the group of poly-β-naphthalene sulfonate but it can be found polymelamine sulfonates group. Synthetic organic polymers bearing carboxylates are used as the dispersing agent being more effective in the concrete industry as it has been showed in several studies. The mechanics explaining the dispersion of cement in presence of these admixtures are electrostatic force and steric hindrance effect being the key their ionic charge density [4,74,75].

The physical mechanism on concentrated cement pastes has been observed, where was found that its viscosity and yield stress decrease as result of plasticizer adsorption due to modification of flocculation having an impact of thixotropy behavior. This adsorption has

been studied both superplasticizer and viscosity agents observing the importance of surface of grains with the affinity of additives [76,77]

3.3 Studies of dynamics of suspensions

There are alternative techniques to study the rheology of complex materials by determination of the movement of particles embedded in solutions such as suspensions or emulsions [78], focused on determinate the Brownian motion, observing that the viscosity has an important role. Of the above, the mean square displacement has been measured with the aim to characterize and study the viscoelastic materials, for that, several tools based of light dispersion has been used to study phenomena as gelation, aggregation, flocculation, crystallization, and agglomeration of particles [79-81].

One of the most used optical tools classified as non-destructive analyzer is Multispeckle Diffusing Wave Spectroscopy (MS-DWS). MS-DWS is an advanced light scattering technique integrated by a laser source that is reflected on the sample. The particles are able to scatter the light in several times, detecting a speckle image that is the fingerprint of the dynamics in a specific time. By a camera as a detector, images of real-time are taken, representing the movement of particles that integrate the suspension [82]. One algorithm is designed in order to obtain the intensity of each image and its correlation with another boundary image, and it can be represented by intensity autocorrelation function during the time of analysis [83-85].

The applications of DWS have been varied to the research of several materials. In the case of gels, the process sol-gel has been analyzed; obtaining qualitative information of its transition as the structural changes, determining the elastic modulus and comparing the result with bulk rheometry find a good agreement between them [86]. The foams have been studied by the same technique analyzing the thickening and rearrangement of its molecules, being able to identify the change of dynamics as a function of rearrangement produce at the time [87]. Although, light propagation in foams and emulsions has been studied in order to probe the average bubble size, droplet size or the dispersive volume fraction, in these study it can be observed changes due to coarsening, flocculation or due to applied strains identifying local dynamics that govern their rheological behavior [88]. This dynamics of particles depends on particle size and temperature of the medium as has been observed in non-ergodic conditions [89].

3.4 Application of DWS on cement suspensions

Regarding research on cement suspension by DWS approach, there are few studies development. One of these studies has been published by [90] which monitor the development of viscoelastic properties on standard cement pastes of w/c ratios from 0.29 to 0.40, analyzing specially the storage and loss modulus, viscosity and elasticity, and their evolution for adding superplasticizer admixture on hydration kinetics. The parameters analyzed showed a

progressive increase with elapsed time and with addition of superplasticizer significantly decrease the values. In this publication, the mean square displacement is related with the hydration observing the change of curves over time, but the thixotropic effect (structural build-up) is not discussed.

Afterward of that research [91] analyzed the effect of colloidal polymers on the rheological properties and cement hydration. The authors used diffusing wave spectroscopy with the aim to understand the effects of polymers on fresh cement pastes. With this technique, it has been possible to identify the quick formation of the flocculated structure of cement grains and the delayed of that formation with a high dosage of polymer.

4 JUSTIFICATION, HYPOTESIS Y OBJECTIVES

4.1 Justification

The concentrated portland cement suspensions are the base in the processing of slurries, grouts, mortars and concretes, being the most important construction materials mainly because of its low cost and strength. After their mixing, these materials can be pumped, sprayed, casted and now even printed with additive manufacturing, therefore, the control of their formulation, rheological properties and dynamics of its particles, is crucial in cementitious materials. The yield-stress is an important parameter to take in account into flow properties. Indeed, the higher the yield-stress of cementitious materials the lower is the capacity of being pumped, and an insufficient yield-stress can lead to a phase separation between water, cement, and aggregates. Recent procedures to evaluate flow properties consist of simple tests like slump, L-box, V-funnel. However, these tests do not directly measure the rheological properties and more specifically, do not estimate the thixotropy. The thixotropy commonly can be observed in pumping and self-levelling applications. The required for pumping pressure is directly proportional to the viscosity that dependence on the shear rate. For self-levelling applications, the yield-stress has to be low enough to pour the materials and create a flat surface and avoid sedimentation. In both cases, the thixotropy build-up of yield-stress and the viscosity is of particular importance on the reduction of pressure in formwork, and the segregation strength of constitutive materials.

On the other hand, from the point of view of flow properties, cement pastes exhibit chemical thixotropy due to chemical reaction of cement particles, and physical thixotropy which to attractive behavior is due cement particles. This leads to its agglomeration of the paste and therefore, its change of viscosity over time. This thixotropy controls the time which a cement paste can be subject to flow, and thus, affects the pumping and self-levelling applications of cementitious materials. Furthermore, the rheological properties of cementitious materials can be controlled with plasticizer and stabilizer additives, adsorbed it on the surface on fine particles and their contributions to flow properties of several blends, hence, they should be considered during the processing of any cementitious material.

Therefore, an understanding of thixotropy and dynamics of particles embedded in an aqueous phase is crucial to correlate the agglomeration of particles along the setting and the beginning of hardening of cement suspensions, identifying physical and chemical process, taking into account solid volume fraction (or water-cement ratio) and chemical admixtures like high range water reducing admixture and viscosity modifying admixture contents.

4.2 Hypothesis

The analysis of thixotropy and dynamic properties of white portland suspensions makes it possible to determinate the physical and chemical evolutions of the hydration kinetics during setting time, identifying the influence of water-cement ratio, high range water reducing admixture concentration and viscosity modifying.

4.3 Objectives

4.3.1 General Objective

To analyze the structural build-up thixotropy and the particle dynamics of white portland cement-based concentrate suspensions, as a function of high range water reducing admixture (HRWRA) concentrations, water-cement ratio (w/c) and with the addition of viscosity modifying admixture (VM)

4.3.2 Specific Objectives

- To obtain the physical and chemical parameters of white portland cement (WPC) in study.
- To design a mixing protocol of suspensions, defining mixing time, speed and sequence of components additions.
- To monitor the heat release due to hydration reaction during time and its variation with an increase of concentration of HRWRA, water-cement ratio, and the incorporation of VM.
- To determinate the initial and final setting time and compressive strength at 24 h, and its variation with the increase of concentration of HRWRA, water-cement ratio, and the incorporation of VM.
- To characterize rheologically the structural build-up thixotropy of suspensions to water-cement ratio 0.25, 0.34, 0.40, and 0.46, using concentrations of 0.04%, 0.120% and 0.360% of HWRA additive, and 0.360% of HRWRA with 0.41% of VM, to shear rate of 0.01, 0.025, 0.1, 0.25, 1 and 6 s^{-1}.
- To propose empirically a mathematical function that describes the changes of viscosity over time, and the variation of its terms due to the fit in the experimental blends.
- To study the dynamics and particle aggregation of suspensions with water to cement ratio of 0.25, 0.34, 0.40, and 0.46 without admixtures, and using concentrations of 0.04%, 0.120% and 0.360% of HWRA additive, and 0.360% of HRWRA with 0.41% of VM.

5 MATERIALS

5.1 Description of materials

In this chapter, the materials used in the thesis are described, in order to know the characteristics of cement and the additives employed in the research. All materials are commercially available.

5.1.1 White Portland Cement

To ascertain the rheological properties and the MS DWS analysis, pastes were prepared with portland cement type I [6] or CPC 30R B, according to with the Mexican standards [8]. A white portland cement has been selected with the aim to prepare suspensions as less absorbent possible, considering the C_3A content and the specific surface area as important factors on rheological behavior in the cement suspensions [34].

5.1.2 High Range Water Reducing Admixture.

A polycarboxylate ether – based high range water reducing admixture (HRWRA) was employed in the mixtures. The superplasticizer was provided by Sika technology, commercially called Sikament® SP MN. The specific gravity of the HRWRA is 1.19, cataloged as type A and F for standards [92]. The Sikament® is an efficient blended superplasticizer which allows reducing water contents in several mixes, getting to increase the strength due to reducing of water, increase the workability, permeability, durability and enhance the appearance of elements. The dosage rate according with the maker is between 0.13 to 1 L / 100 kg of total cementitious material.

5.1.3 Viscosity Modifying Admixture

The viscosity modifying admixture (VMA) corn starch based called stabilizer as well, was employed in the mixtures with high content of HRWRA. The additive was provided by Sika technology, commercially called Sika® Stabilizer – 4R. The specific gravity of the VMA is 1.01, cataloged as type S for standards [92]. The Sika® Stabilizer – 4R improves stability and segregation resistance, which enhances to surface quality. It is suitable to improve flow, higher segregation resistance, migration of air, fluctuation of water content and faster consolidation of the mixes. The recommended dosage is 65 – 455 ml / 100 kg of cementitious materials.

5.2 Experimental techniques of characterization

The white Portland cement was characterized with the aim of know the chemical composition and the physical parameters that influence the rheological properties during the experiments. The experimental techniques are described in the following part.

5.2.1 Physical characterization of white Portland cement

5.2.1.1 Specific surface area BET method

Specific surface area is defined as the surface area per unit of mass, expressed in square centimeters per gram (cm^2/g) or square meters per kilogram (m^2/kg). The specific surface area is a function of particle size, shape of the grains and imperfections. In cement pastes the surface area is an important parameter and it controls the hydration reactions of individual components of portland cement, especially for the calcium silicates.

One of the best know method based on physical adsorption is the so called BET, founded on the work of Brunauer, Emmett, and Teller [93] based on physical adsorption, in other words the interaction of a gas with a solid surface. This technique assumes that the gas molecules are strongly attracted and adsorbed on a surface of particles and also that the sorbent molecules have access to the walls of the pores. This process depends of n gas pressure, therefore when the relative pressure increases the degree of gas adsorption increases as well.

For this research, the specific surface area was determinate by BET method (Figure 5.1). The sample was dried and placed into a desiccator. The mass of the sample introduced to the measurement system was 0.2169 g and Nitrogen gas was employed for the test. The isotherm of test was determined in order to calculate the specific surface area of white portland cement.

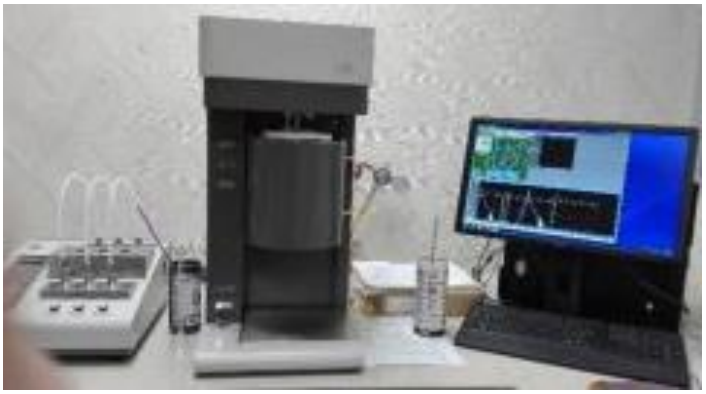

Figure 5.1 Gas physisorption equipment

5.2.1.2 Particle size distribution by laser ray diffraction

The laser diffraction measures particle size distribution and is based in the angular variation of intensity of light scattered that passes through a dispersed particulate sample. The scattering intensity data is analyzed to calculate the size of the particles for creating the spatial distribution of scattered light called scattering pattern [94]. Laser diffraction uses Mie theory of light scattering assuming a volume equivalent sphere model. The application of the theory

requires the knowledge of the optical parameters like refractive index and its imaginary component, which are relatively easy to find from published data.

Laser diffraction is a widely technique used for materials from hundreds of nanometers up to several millimeters as the case of cement Portland particles. The technique has the advantage of rapid measurements, repeatability and the monitoring and control the particle dispersion process.

The particle size distribution of white portland cement (PSD) was determined by MICROTRAC S3500 equipment (Figure 5.2). The sample was analyzed immersed in isopropyl alcohol, with an ultrasonic time of 60 s in order to avoid possible agglomerations and measure time of 15 s. For measurement, a sample of cement powder having a mass about to 0.1 g was introduced into the deposit of around 0.5 L. The optical transmission coefficient employed for the test was 0.971.

Figure 5.2 Particle size distribution analyzer by laser diffraction equipment

5.2.1.3 Density

The density is defined as the mass per unit volume of the solids in hydraulic cement. The density of white portland cement was determined as is specified in [95]. For this procedure, the Le Chatelier flask is used to obtain a volume of cement particles immersed in a solution free of water as is showed in Figure 5.3 (left). The amount of cement required was 64 g, introducing this amount in small increments at the same temperature as the liquid in order to have an adequate value of volume. Two tests were carried out by the same operator, without variation of more than 0.03 in the results. The knowledge of the density of white portland cement in important to calculate solid volume fraction on suspensions studied, which is indicative of the concentration of solids in the samples analyzed.

5.2.1.4 Normal consistency

The normal consistency is the amount of water required to prepare hydraulic cement pastes for different tests. [96]. 650 g of cement has been mixed with a measured quantity of water following the mixing protocol described in the procedure for mixing pastes of practice C305. When the pastes are mixed, one portion is inserted into the vicat ring in order to put the plunger in contact with the surface of paste as is showed in Figure 5.3 (right). The paste will be of normal consistency when the road settles to a point 10 ± 1 mm below the original surface in 30 s. The normal consistency was determined for white portland cement in study in order to have the water content for setting time test.

Figure 5.3 Density determination (left) and normal consistency (right) of white portland cement

5.2.1.5 Setting time by Vicat Needle

The setting times characterize the stiffening of a concentrate cement suspension, characterized by an initial setting and final setting time. Once a cement suspension achieves the stage of initial setting time it cannot be handled and placed in formwork because the concentrated suspension has a semi-plastic state. When the suspension achieves the final setting time, the hardening process has started. According to several authors in the stage of initial setting time, the crystallization of ettringite is the hydration product that contribute in this time, and the final setting time occurs before of the accelerator period on the calorimetry curve [15,97].

For this thesis, the setting times have been determined by Vicat apparatus on a concentrated cement suspension in normal consistency as established the standard test method [98]. The test specimen was quickly formed and placed into of a conical ring (Figure 5.4 left). The test was carried out in a moist room in order to have a constant temperature. One needle of 1 mm diameter was employed for penetration 30 min after molding and every 15 min until

penetration of 25 mm or less is obtained (initial setting time) and when the needle on the surface does not leave a mark in the paste (final setting time) The apparatus is showed in Figure 5.4 (right).

Figure 5.4 Conical ring with cement paste (left) and apparatus of setting time test (right)

5.2.2 Chemical characterization of white Portland cement

5.2.2.1 X ray fluorescence

X-ray fluorescence (XRF) spectrometry is a non-destructive analytical technique that gives elemental information of several kinds of materials, mainly in industry applications [99]. Materials like cement, glass, iron, steel etc. can be analyzed by this technique. The XRF is the phenomenon according to which a material is exposed to x-rays of high energy, and these x-ray strikes an atom in the sample. The energy is absorbed by the atom and if the energy is high enough, a core electron is ejected out of its atomic orbital. An electron from an outer shell will occupy the orbital in order to fill the hole left. The transition gives an x-ray characteristic energy that can be detected by fluorescence detector. The energy necessary to eject a electron is characteristic of each element [100].

There are two spectrometer systems: wavelength dispersive systems (WDXRF) and energy dispersive systems (EDXRF) where the difference is in the detection system.

The chemical composition of white Portland cement was determined by X ray fluoresces by dispersive energy (ED-XRF). The PANalytical equipment Epsilon3-XL model (Figure 5.5 right) was used to analyze the sample. The main parts of the spectrometer are the radiation source, the sample, and the detection system, where the x-ray irradiates the sample directly, and the florescence coming from the sample is measured with an energy dispersive detector.

For the analysis, pellets of white cement powder were carried out keeping the size of cement particles from manufacturer. A hydraulic machine was employed to press the particles and to compact the sample (Figure 5.5 left) ensuring uniform density on the analysis area.

Figure 5.5 Hydraulic machine for pellets (left) and X ray spectrometer of dispersive energy (right)

5.2.2.2 X ray diffraction

This technique employs X-ray, which is photons with energy from 125 eV to 125 keV and a wavelength of 0.01 – 10 nm. Diffraction occurs when the light is scattered by a periodic array with long-range order, producing constructive interference at specific angles [101]. The X-ray diffraction is used analytically for the identification of compounds (present phases in the material) and for giving information of constitutive individual compounds [102].

The basis of diffraction can be explained using Bragg's law, related it to interspacing between atomic planes called d-spacing. By Bragg's law the interplanar spacing can be determined by measuring the angle between the incident and diffracted directions of the radiation (2θ) by following expression: [103]:

$$2d\ sin\theta = \lambda \qquad \text{Equation 13}$$

The mineral phases present in white portland cement were studied by X-ray diffraction. A Bruker AXS D8 Advance diffractometer was used (Figure 5.6) employed a radiation of CuKα ($\boldsymbol{\lambda}_{RX}$=1.5418 Å). The interval of analyzing was between 10 to 70 degrees 2θ and step size of 0.5 and increments of 0.05 degrees. The interpretation of the peaks was carried out by EVA version 11.0.0.3 software.

Figure 5.6 X - ray diffractometer

5.2.2.3 Loss ignition

The lost on ignition test consists of strongly heating a sample of material at a specific temperature with the aim to allow the volatile substance escape until its mass has a constant weigh, in the case of portland cement, the loss represented the total moisture and CO_2 in the cement. For this test the procedure of ASTM C 114 was followed, using two samples of 1 g weigh in two porcelain crucibles. Previously to ignition, the crucibles were carried to constant mass by cycles of heating to 950 ± 50 ºC in order to determine the mass of crucibles free of some contaminants (Figure 5.7 left). The sample in a tared crucible was ignited to 950 ± 50 ºC (Figure 5.7 right) with a minimum of 15 min for the initial heating period and periods of 5 min for the subsequent heating. When the mass of the sample was constant after several periods of ignition, it was taken as the mass free of volatile substance.

The main contribution of this test to the project was ensuring that the white portland cement did not have some degree of hydration, allowing to prepare the suspensions homogeneously.

Figure 5.7 Crucible for test (left) and ignition of sample to 950º C (right)

6 EXPERIMENTAL

6.1 Introduction

The experimental methodology of this thesis has been divided into three parts. The first part was focused on rheological characterization by Rheometry; measurements of flow curve $\sigma(\dot{\gamma})$, viscosity $\eta(\dot{\gamma})$ and interval thixotropic $\eta(t)$ have bee carried out, all measurements as a function of water-cement ratio, high range water reducing admixture concentration (HRWRA), viscosity modifying admixture (VMA) addition, and shear rate. This first study has been complemented with the second part of the thesis, which focused on measurements of the local dynamics. Intensity autocorrelation function of back scattered light in the multiple scattering regime have been determined, and quantitative data have been obtained. These experiments have been carried out with the aim of research agglomeration and aggregation of particles into the White portland cement suspensions at microstructural build-up stage. With the aim to contrast the rheological measurements and analysis of local dynamics, a third step has been developed in this thesis focused at the monitoring of the hydration kinetics of suspensions in study; Measurements of heat release due to exothermic hydration reaction have been carried out by semi-adiabatic calorimetry. On the other hand, compressive strength development has been measured by ultrasonic reflection. Both tests were carried out immediately after of mixing process until 24 h of age. Into the same step, some blends have been selected to observe the development of microstructure at several ages by scanning electron microscopy (SEM), finally, flexural test on rectangular specimens of 30 h age have been carried out, the aim of which is to correlate the development of dynamic rebuild-up of suspensions with its strength in hardening stage.

6.2 Experimental Design

Two experimental designs have been selected to carry out all measurements considered in the methodology. The first design corresponds to the rheological characterization and the thixotropy measurements, where the variables studied were the water-cement ratio, three high range water reducing admixture (HRWRA) concentrations and their combination with a viscosity modifying admixture (VMA), furthermore of applied shear rates. With the aim to study an interval between slurries and pastes which are suspensions commonly used into the construction industry and as a first variable, four water-cement ratios have been selected: 0.25, 0.34, 0.40 and 0.46 respectively. The influence of HRWRA on thixotropy behavior in the water-cement ratios described above was defined as a second variable. Three percentages of HRWRA concentration were established, the first one was 0.120% that is the optimal concentration obtained by Rheometry; one concentration above and one below were selected to study their influence on thixotropy, 0.360% and 0.04 % respectively. The influence of VMA on thixotropy behavior was analyzed; firstly its optimal concentration has been obtained with the combination of the high concentration of HRWRA (0.360%). Its optimal concentration was 0.41% and it has been included in the experimental design. Those variables

were used in tests of heat release and compressive strength in order to observe their correlations. Finally, and as a third variable, six shear rates have been selected; 0.01 s^{-1}, 0.025 s^{-1}, 0.1 s^{-1}, 0.25 s^{-1}, 1 s^{-1} y 6 s^{-1}. Figure 6.1 shows the scheme of the first experimental design carried out in this research.

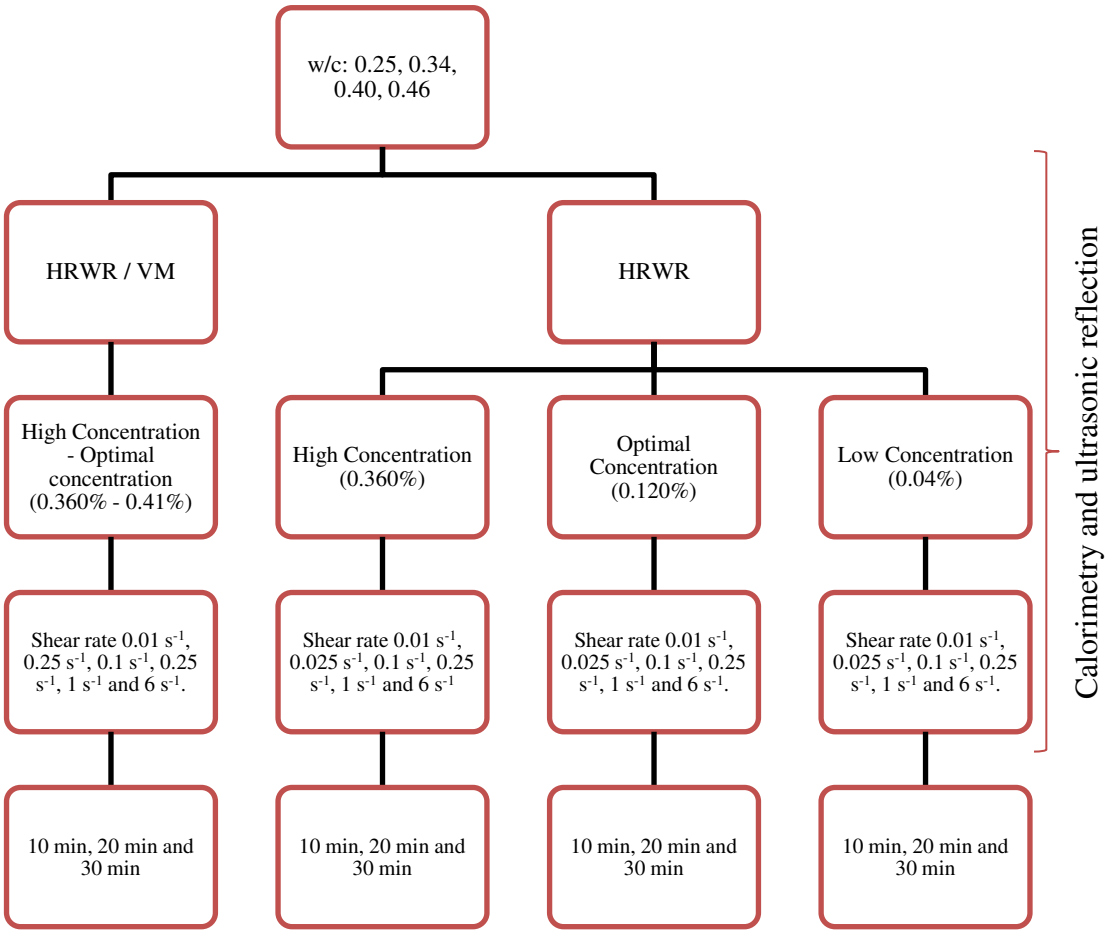

Figure 6.1 First experimental schematic of thesis

The second experimental design corresponds of the particle dynamics measurements on white portland cement suspensions. Water-cement ratio, HRWRA concentration, and its combination of VMA were the variables studied. For this case, suspensions without additives were evaluated, selecting water-cement ratios of 0.25, 0.265, 0.28, 0.30, 0.31, 0.32, 0.34, 0.36, 0.40 and 0.46. For these water-cement ratios, flexural strength test by three-point system has been carried out, as well as, the analyze of microstructure into several time by scanning electron microscopy (SEM). The above in order to correlate the results of dynamics at the early age and its final strength.

For suspensions with additives, the concentrations described at the first experimental design (0.04%, 0.120%, 0.360% of HRWRA and 0.360% of HRWRA combined with 0.41% de VMA) have been maintained, as well as, the water-cement ratios (0.25, 0.34, 0.40, 0.46). We use the same variables in order to compare the thixotropic measurements by rheometer and the dynamics of suspensions in this study. Figure 6.2 shows the scheme of the second experimental design.

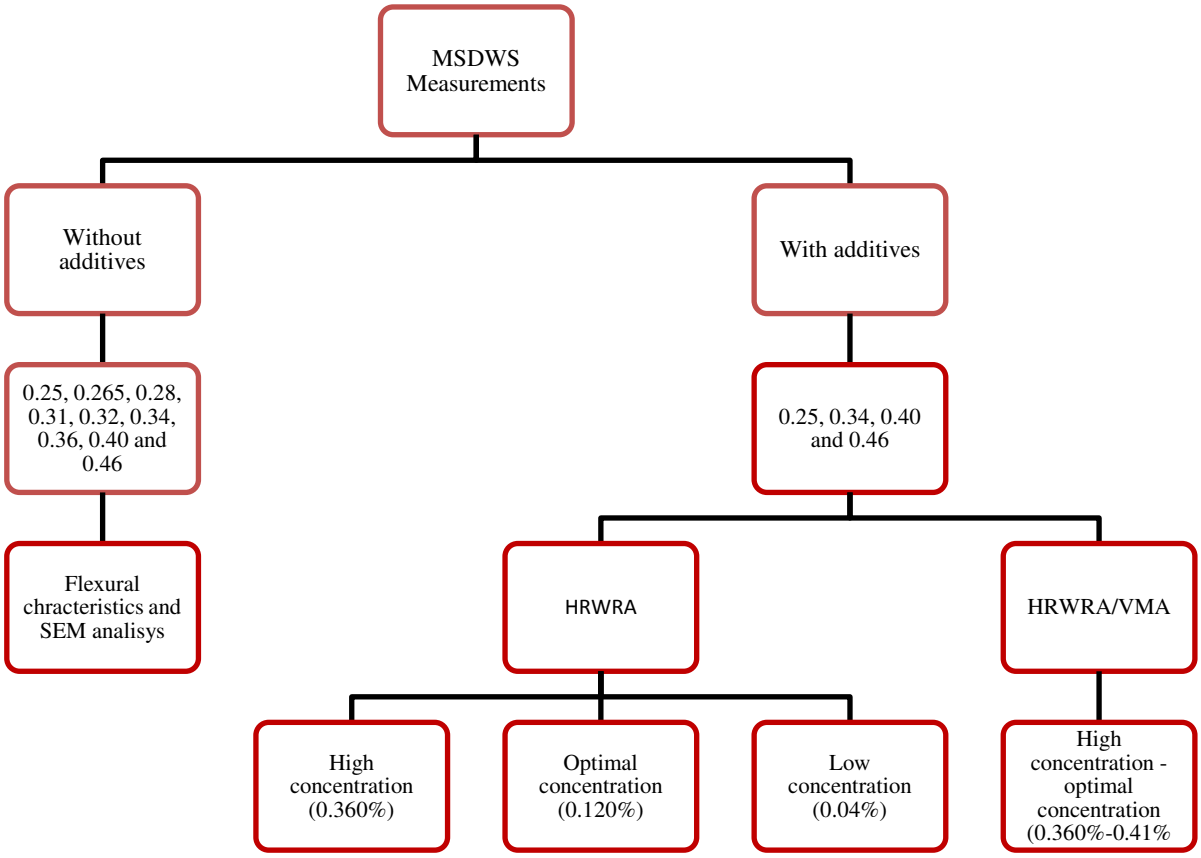

Figure 6.2 Second experimental schematic of thesis

6.3 Mixture proportions

Table 6.1 shows the mixing proportions of suspensions studied in the first experimental design, corresponding to thixotropy analysis by Rheometry, semi-adiabatic calorimetry, and compressive strength by ultrasonic reflection tests. On the other hand, Table 6.2 shows the mixing proportions of the second experimental design, with which the MSDWS measurements on suspensions with and without additives were carried out. The volume of each sample was 150 ml of cement suspension in order to have a representative sample of suspension.

Table 6.1 Mixture proportion of white portland cement suspensions; Thixotropy test

w/c (by mass)	w/c (by vol.)	Cement (g)	Water (g)	HRWRA (ml)			VMA (ml)
				0.04 %	**0.120 %**	**0.360 %**	**0.41%**
0.25	0.75	280	70	0.112	0.336	1.008	1.148
0.34	1.01	250	85	0.100	0.300	0.900	1.025
0.40	1.20	230	92	0.092	0.276	0.828	0.943
0.46	1.38	210	96.6	0.084	0.252	0.756	0.861

Table 6.2 Mixture proportions of white portland cement suspensions; MS-DWS test

w/c (by mass)	w/c (by vol.)	Cement (g)	Water (g)	HRWRA (ml)			VMA (ml)
				0.04 %	**0.120 %**	**0.360 %**	**0.41%**
0.25	0.75	280	70	0.112	0.336	1.008	1.148
0.265	0.79	280	74.2	-	-	-	-
0.28	0.84	270	75.6	-	-	-	-
0.30	0.90	270	81	-	-	-	-
0.31	0.93	260	80.6	-	-	-	-
0.32	0.96	260	83.2	-	-	-	-
0.34	1.02	250	85	0.100	0.300	0.900	1.025
0.36	1.08	240	86.4	-	-	-	-
0.40	1.20	230	92	0.092	0.276	0.828	0.943
0.46	1.38	210	96.6	0.084	0.252	0.756	0.861

6.4 Mixing protocol

The method used for mixing suspensions has an important influence not only on the rheological properties but also in the microstructural development and the hydration kinetics of pastes in fresh state as well [104]. It was observed that increasing the mixing speed increases the hydration kinetics and the content of alkalis into pore solution. [105]. A mixing

protocol has been established where the time, the mixing speed and the sequence of components addition was fixed, with a minimal quantity of a suspension of 200 ml.

A mixer Heidolph model RZR 2041 with a stirring paddle of propeller geometry of 4 cm diameter was used. A stirring nonabsorbent glass was used to prepare the suspensions. The stirring paddle creates a radial agitation and ensures the homogenizing of the suspension. Figure 6.3 shows the equipment and its several parts.

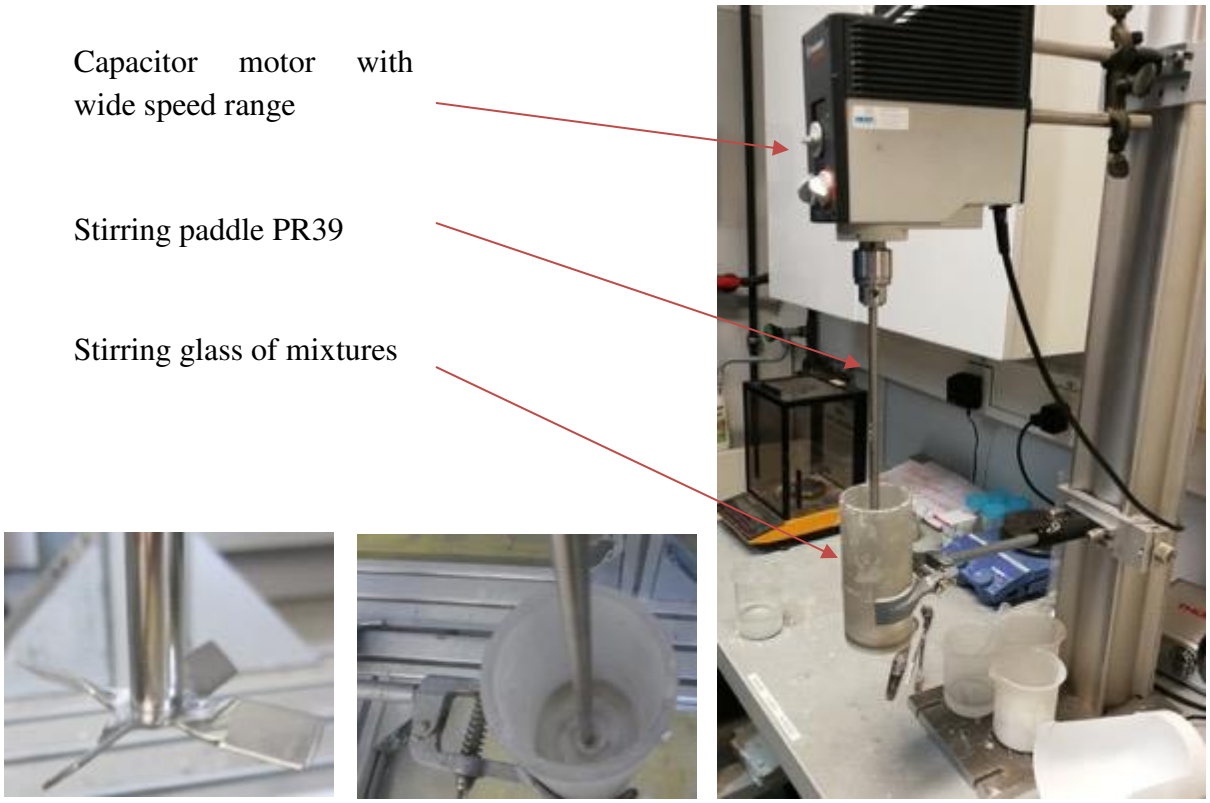

Figure 6.3 Mixing machine and its several parts

The mixing protocol consists of three steps of one minute (three minutes in total) at 500 rpm speed, (i) the water is mixed with the progressive addition of the additive and half of the amount of cement (ii) the second half of the cement is progressively introduced in the mixer and (iii) all the components are mixed together. Figure 6.4 shows the sequence of this protocol.

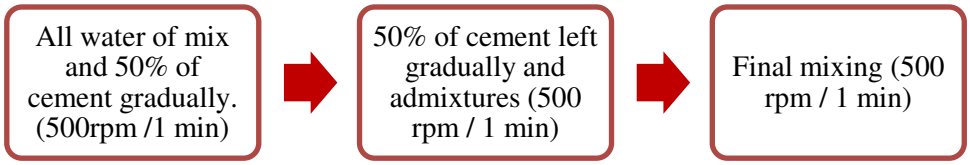

Figure 6.4 Protocol of mixing

6.5 Experimental analysis techniques

6.5.1 Rheometry

The pastes analyzed were loaded into a MCR 301 Anton Paar stress imposed rheometer (Figure 6.5) equipped with a helicoidal geometry designed for the rheological measurements of a cement pastes as described in [49], the rheometer tool was calibrated per procedure described in [106].

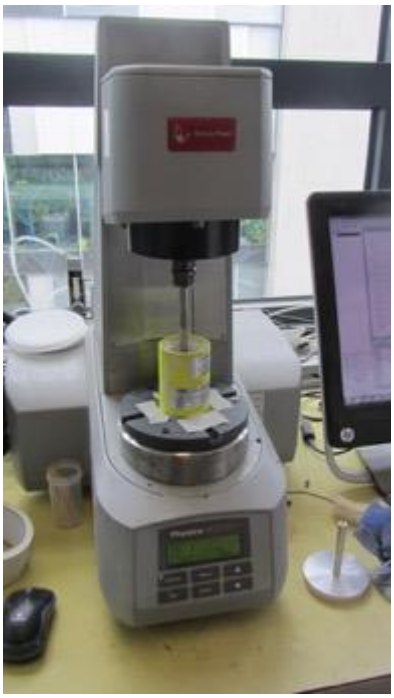

Figure 6.5 Rheometer used in rheological measurements

6.5.1.1 Flow and viscosity test

For the measurements of flowability of each suspension in this study the flow and viscosity curves have been obtained by the following protocol: After the mixing the suspension is

loaded in the cell. A pre-shear of 60 s at 200 s^{-1} is applied, the shear stress σ is measured as a function of the shear rate $\dot{\gamma}$ from 200 s^{-1} to 0.1 s^{-1} with 25 points even distributed in logarithmic scale, in order to analyze the variation of stress during the rebuild-up of suspensions after a intensive sheared, identifying the variability of stress due to different w/c ratio, HRWRA and VM incorporated.

6.5.1.2 Interval thixotropic test

The measurements of structural rebuild-up (thixotropic) after a short period of high shear on the suspensions studied have been carried out in three steps: In a first step we considered the time of rest between the instant after end of mixing of suspensions and the flow of the suspension into the cup. Second step corresponds to the structural break down of suspensions by high shear and finally, the third step measures the rebuild-up of suspension as a function of time.

For the step one we estimate the time during the placing of suspension into cup was of 1 minute approximately. In step two the high shear rate has been established to 400 s^{-1} during 30 s, this part of the protocol know to break structure. Finally, in step three the rebuild-up of suspensions is measured on each one of suspension established in experimental design, considering six shear rate of analysis which are 0.01 s^{-1}, 0.025 s^{-1}, 0.1 s^{-1}, 0.25 s^{-1}, 1 s^{-1} and 6 s^{-1} into a period of 600 s. Three interval of 600 s each one has been carried out in order to observe the behavior of suspensions over time.

6.5.2 Semi-adiabatic calorimetry

Semi-adiabatic measurements were made with a noncommercial device used in several researches [107, 49, 108]. The equipment has 8 individual cells with one temperature sensor of type PT 100B for the record the temperature history of a fresh sample (120 g proxy) poured into a calibrated isolated container (Figure 6.6). The quantitative evolution of heat generated during chemical reactions was calculated by considering the temperature rise of paste as well as the heat lost to the environment by the equation 14.

$$Q(t) = \rho V C_p [T(t) - T_e] + kA \int_0^t [T(t) - T_e]\, dt \qquad \text{Equation 14}$$

Where Q(t) is the cumulative heat, T_e the exterior temperature in Kelvin, T(t) the temperature of the sample in Kelvin, ρ cement volume fraction, A the area of the contact surface between the sample and the cell, V the sample volume, C_p the specific heat capacity of the paste and k

the thermal transfer coefficient of the box, which is determined by the monitoring of the temperature decay of a heated non-reactive specimen placed in the calorimeter.

Figure 6.6 Semiadiavatic calorimetry equipment

As is showed in Figure 6.7 the heat rate gives the fingerprint of chemical reaction during setting and hardening of pastes, in other words gives the strength evolution of the material.

The heat rate was measured on all suspensions studied in this thesis, the aims were to have information about the change of kinetics due to variation of the volume fraction of cement and the presence of admixtures mentioned above.

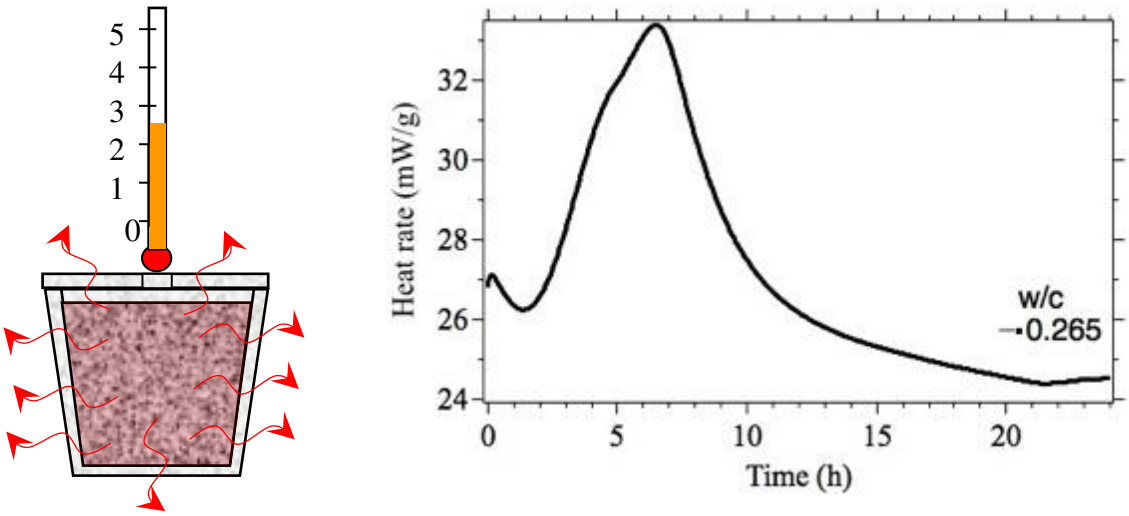

Figure 6.7 Heat rate in samples of cement (left) and heat evolution over time (right)

6.5.3 Compressive Strength by Ultrasonic Reflection

The monitoring of compressive strength during setting and hardening is crucial to assess the quality of cement-based materials. For this project, a non-destructive method, based on monitoring the reflection coefficient of the ultrasound waves at the interface was used. The system is based on ultrasound pulse echo reflectometry (UPER) technique, which by propagation of ultrasound waves inside the sample assesses the acoustic properties. A noncommercial instrument was used with ultrasonic shear sensor employed to follow the evolution of the shear wave as a function of time (Figure 6.8). The monitoring allows to measure the shear modulus G^*, and its relation with the compressive strength σ [107,109].

Figure 6.8 Ultrasonic reflection equipment

The experimental set-up consisted of a transducer and a Plexiglas waveguide. At the end of the guide, the cement-based material was placed as is showed in Figure 6.9. At the beginning of the experiment, the ultrasound bursts are transmitted inside the waveguide in contact with air without paste. The acoustic impedance of the Plexiglas is z_1 and is much higher than the acoustic impedance of the air z_a, and the reflection coefficient is:

$$r = \frac{z_a - z_1}{z_a + z_1} \approx -1 \qquad \text{Equation 15}$$

Of the above the amplitude of the wave A_i at the cement paste/Plexiglas interface was equal to the sum of the amplitude reflected A_r and transmitted A_t, therefore the reflection coefficient can be linked to the acoustic impedance of the following way:

$$r = \frac{A_r}{A_i} = \frac{z_a - z_1}{z_a + z_1} \approx -1 \qquad \text{Equation 16}$$

For determine the complex shear modulus G^*, the equation 17 can be used, considering the value of density of cement paste sample ρ:

$$G^* = \frac{z_2^2}{\rho} = \frac{z_1^2}{\rho}\left(\frac{1-r}{1+r}\right)^2 \qquad \text{Equation 17}$$

Once obtained the values of G* were converted to strength (MPa) by the following consideration:

$$\sigma = Ed_0 \qquad \text{Equation 18}$$

The equation 18 is based on the assumption of a constant critical strain d_0, considering a compressive strength as a maximum of the linear stress-strain relation. Finally, the value of G^* from the ultrasonic measurements converted to Young's modulus E by Poisson ratio gives the term E used in equation 19:

$$E = 2G(1+v) \qquad \text{Equation 19}$$

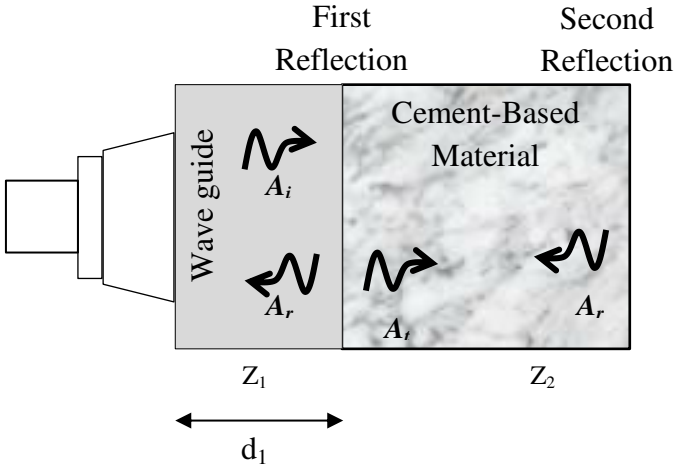

Figure 6.9 Experimental setup: Incident, transmitted and reflected waves

[109]

6.5.4 Multispeckle diffusing-wave spectroscopy (MSDWS)

Multiple scattering measurements based in multi-speckle diffusing wave spectroscopy technique (MS-DWS) is a light scattering technique suitable for concentrated and opaque media, based on the multiple scattering of photons in concentrated media such as colloidal suspensions, allowing to measure dynamics, structure and viscoelastic properties [110, 111]. With this technique it is possible to collect a large number of speckles by a camera as a detector to average fluctuations (Figure 6.10) [86]. The MSDWS has a very high spectral resolution in fact, is sensitive to the displacement of the particles in the sample having a precision of the order to one nanometer [87, 112].

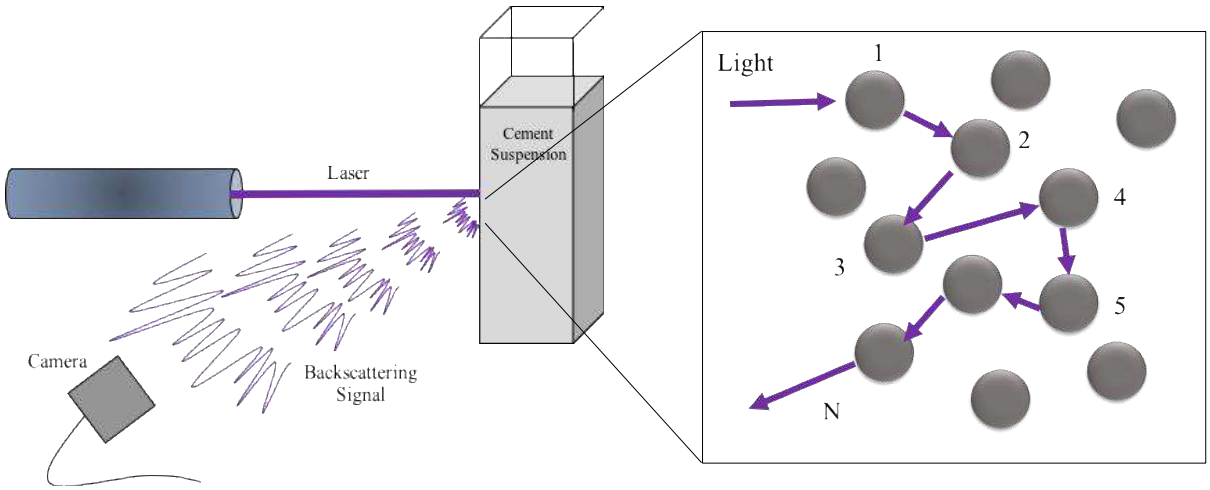

Figure 6.10 Schematic diagram of MS-DWS equipment

6.5.4.1 Background

The basic idea of diffusing wave spectroscopy consists to illuminate a diffusive sample with a coherent beam of light from a laser and to measure the temporal fluctuations of the resulting speckle pattern of scattered light. The DWS is very similar to dynamic light scattering technique (DLS): both entails the detection of the intensity of a single speckle spot of the scattered light and the measurement of its temporal fluctuations. In both techniques, these fluctuations are characterized by the temporal autocorrelation function as a representation of the dynamics of the scattered medium. The DWS approaches the problem of multiple scattering from different limit, this is, the light does not undergo only one or even a small number of scattering events, but instead is scattered a very large number of times, being the direction of the light random and by statistical approximation the the propagation and the effect of the dynamics can be analyzed [113].

The temporal autocorrelation function entails a fundamental approximation it is concerning the light propagation through the scattering medium and each photon is scattered a very large number of times and its path is described by as a random walk. There is no approximation concerning the dynamics of the scatters. It can be Brownian or non-Brownian. The diffusion approximation is used to describe the propagation of light through a medium laying the basis for describing the transport of light with very widely applicability. It should be mentioned that the light propagation is parameterized by the diffusion coefficient of light $D_1=vl^*/3$, where v is the speed of light and l^* is the transport mean free path in the medium, defined as the length that a photon must travel before its direction is randomized. This length is larger than the scattering mean free path, l, that is the length that the photon must travel before it's scattered a single time.

The main condition for using the diffusion approximation is that samples strongly scatter light. Samples should have a white or milk-like appearance, in other words, the sample must be sufficiently opaque that a negligible amount of unscattered light is transmitted through the sample.

On the other hand, the use of diffusion propagation ensures that the scattering wavevector, which relates the incident and detected light, has relevance on the result of correlation function because of a large number of scattering events. As a consequence, there are two basic experimental geometries: The backscattering geometry and transmission geometry, respectively. In backscattering geometry, the light is incident on one side of the sample and the scattered light is detected from the same side. While in transmission geometry the light is incident on one side of the sample and the scattered light transmitted through the sample is collected. A schematic representation of both geometries is showed in Figure 6.11.

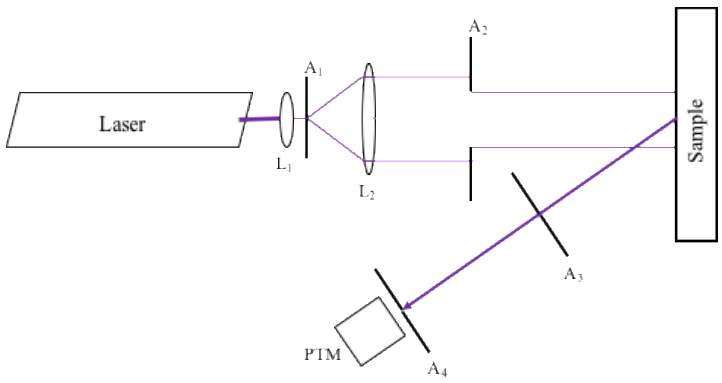

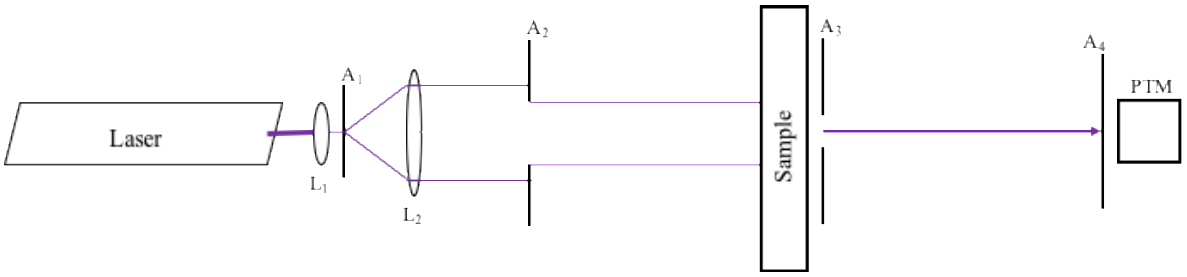

Figure 6.11 Experimental geometries in diffusion propagation Top: Backscattering geometry. Bottom: Transmission geometry

One of the most important applications of DWS is the measure of particle motion on very short length scale. The intensity fluctuation measured with DWS arise when the pathlength of the scattered light changes by one wavelength due to the cumulative motion of a very large number of scatterers. Using DWS, it is possible to measure the motion of micrometer-sized particles on length scales as small as a few Ångströms. Another application of DWS lies in the possibility to study dynamic events that are spatially or temporally rare.

6.5.4.2 Fundamentals

In order to discuss and interpret the results obtained with DWS experiments the calculation of temporal autocorrelation function of the intensity fluctuations of the scattered light is explained. Firstly, the light propagation through the very highly scattering medium is approximated as a diffusive process to the aim to determine all different paths that a photon can take and the probability that a photon will follow any given path. We need to consider that a long path involves many scattering events and each scattering event is approximated by an average of scattering events. Now we replace the sum over the individual scattering events by a sum over the same number of scattering events and this allow us to calculate the contribution of individual paths to the correlation function.

In order to illustrate this approach, consider the transmission geometry of Figure 6.10 again, where the laser is incident on one side of the sample and the signal is collected from the other side. For this case, any photon incident on one side of the sample can follow a large number of possible paths involving many scattering events and it can be described as random walk. The propagation of light can be calculated by the diffusion equation and it allows determining the distribution of different lengths. The total correlation function can be calculated by summing over the contributions of all paths, whose distribute depends on the geometry of the experiment.

6.5.4.2.1 Single and multiple scattering

For a conventional dynamic light scattering experiment laser light with incident wavevector, k_0 illuminates the sample, and the concentration of colloidal particles is scattered. The light that is scattered through an angle θ with wavevector ks is detected in the far field. The scattered field at the detector is E_0, and then the total field is the superposition of scattered fields from particles, expressed by equation 20:

$$E(t) = \sum_{i=1}^{N} E_0 \, exp[iq \cdot r_i(t)] \qquad \text{Equation 20}$$

Where:

q. - scattering wavevector (k_s-k_0)

$r_i(t)$. - Position of i^{th} particle

N. - Number of scattering event

As the particles in the scattering volume move, the phase of scattered field from each particle change caused the scattering intensity to fluctuate in time. This fluctuation can be characterized by their temporal autocorrelation function [114] defined by equation 21 and 22:

$$g_1(t) = \frac{\langle E(t)E(0)\rangle}{\langle |E| \rangle^2} \qquad \text{Equation 21}$$

$$g_2(t) = \beta \left(\frac{\langle I(t)I(0)\rangle}{\langle I \rangle^2} - 1 \right) \qquad \text{Equation 22}$$

In equation 23, β is a constant determinate of collection optics and based on Siegert relation one has.

$$g_2(t) = 1 + \beta q_1^2(t) \qquad \text{Equation 23}$$

Where β depends on the collected optics

On the other hand substituting the terms, considering that $\Delta r(t) \equiv r(t) - r(0)$, and take into account that for simple diffusion $\langle \Delta r^2(t) \rangle = 6Dt$, we obtain:

$$g_1(t) = \exp(-q^2 Dt) \qquad \text{Equation 24}$$

In this case the autocorrelation function decays exponentially with a time constant

$$\tau = \frac{1}{Dq^2}. \qquad \text{Equation 25}$$

In the multiple scattering regimes, two length scales characterize light scattering and transport: the mean free path *l* and the transport mean free path *l**. The mean free path can be obtained by: $l = \frac{1}{\rho\sigma}$, where ρ is the number density of particles and σ is the total scattering of cross-section; The transport mean free path *l** is the length scale over which the direction of light propagation is randomized and can be obtained by $l^* = \frac{l}{\langle 1 - cos\theta \rangle}$, where θ is the scattering angle and ⟨ ⟩ indicates an ensemble average over many scattering events. Both parameters can be determined experimentally by measuring of transmission coefficient through a suspension of thickness L. There are two conditions for scattered light, if $L \lesssim l$, then $T \approx \exp(-L/l)$ and most of the transmitted light is unscattered light. If $L \gg l^*$, then $T \approx l^*/L$ and essentially none of the transmitted light is unscattered. When $L \gg l^*$, the system is considered to be in the highly multiple scattering limit.

6.5.4.2.2 Autocorrelation function for multiply scattered light

In order to obtain an expression for the field autocorrelation function in highly multiple scattering limit, we need to consider an experiment in transmission geometry where light of laser is incident on one side of the sample of thickness $L \gg l^*$, and scattered light is collected on the opposite side. For this case, a single photon passing through the sample with n scattering events and its phase depends on the total path length s. A schematic representation can be observed in Figure 6.12.

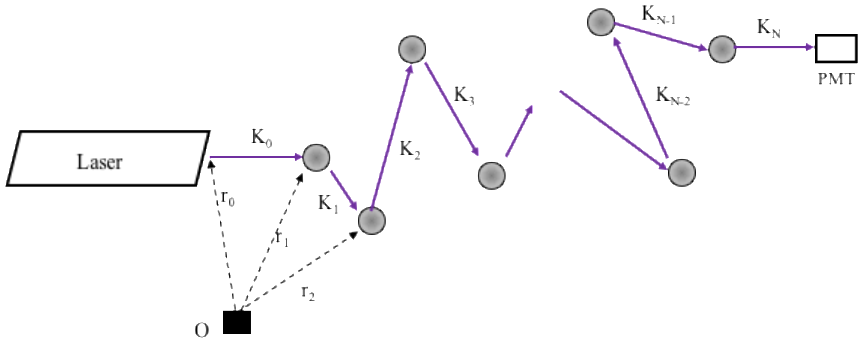

Figure 6.12 Schematic representation of single photon during scattering event

The total path length in N times can be calculated by

$$s = \sum_{i=0}^{N} |r_{i+1} - r_i| = \sum_{i=0}^{N} \left(\frac{k_i}{|k_i|}\right) \cdot (r_{i+1} - r_i) \qquad \text{Equation 26}$$

Where:

K_i. - Wavevector of the light after I scattering events

r_i. - Position of particle i for i≤1≤n

r_0. – Position of source laser

r_{N+1}. –Position of the detector

N. – The total number of scattering events

For the calculation of phase shift ϕ (t) of the photon after passing of laser, we can use the following equation:

$$\phi(t) = k_0 s(t) = \sum_{i=0}^{N} k_i(t) \cdot [r_{i+1}(t)\ \ r_i(t)] \qquad \text{Equation 27}$$

The fields are superposed in order to calculate the total field by follow equation:

$$E(t) = \sum_{P} E_p e^{i\emptyset_p(t)} \qquad \text{Equation 28}$$

Where:

$\sum_P$. – Sum over paths

E_p. – Amplitude of the field from p

The field autocorrelation function then writes:

$$g_{(i)}(t) \equiv \left(\frac{\langle E(0)E^*(t)\rangle}{\langle |E|^2\rangle}\right) = \frac{1}{\langle I\rangle}\langle(\sum_{p} E_p e^{i\emptyset p(0)})(\sum_{p'} E^*_{p'} e^{-i\emptyset p'(t)})\rangle \qquad \text{Equation 29}$$

Where $\langle I\rangle$ is the total average scattered intensity at detector. It must be considered that p≠p' term practically independent and do not contribute to the average so that:

$$g_{(1)}(t) = \sum_{P} \frac{\langle I_P\rangle}{\langle I\rangle}\langle e^{i[\emptyset_p(0)-\emptyset_p(t)]}\rangle \qquad \text{Equation 30}$$

For this experiment it is important to obtain an expression that describes the change of phase of the scattered light from a particle motion. We have the following.

$$\Delta\emptyset_p(t) = \sum_{i=1}^{N} q_i \cdot \Delta_{ri}(t) \qquad \text{Equation 31}$$

In this equation the magnitude q must be related with the angle θ by:

$$q = 2k_0 sin\frac{\theta}{2}$$ Equation 32

By the central limit theorem it is possible to evaluate the average over the phase factor in equation 30 and we have:

$$\langle \Delta \emptyset_p^2(t) \rangle = \frac{2}{3} k_0^2 \langle \Delta r^2(t) \rangle \frac{s}{l^*}$$ Equation 33

For diffusing colloidal particles, $\langle \Delta r^2(t) \rangle = 6Dt$ and we have

$$\langle \Delta \emptyset_p^2(t) \rangle = 4k_0^2 Dt \frac{s}{l^*}$$ Equation 34

From the equation defined above we replace the fraction of scattered intensity in path p, $\frac{\langle I_p \rangle}{\langle I \rangle}$, with the fraction of scattered intensity I paths of length s, P(s) and using for diffusive motion we have:

$$g_{(1)}(t) = \sum_s P(s) exp\left(-2k_0^2 Dt \frac{s}{l^*}\right)$$ Equation 35

With this expression the calculation of the autocorrelation function is reduced to the determination of the path-length distribution function P(s) through the sample P(s) depends on the geometry of the experiment in the continuum limit becomes:

$$g_{(1)}(t) = \int_0^\infty P(s) e^{-\left(\frac{2t}{\tau}\right)\frac{s}{l^*}} ds$$ Equation 36

Where:

$\tau = (k_0^2 D)^{-1}$ (Assumed particle motion)

The equation 36 is the basis for the calculation of autocorrelation function in diffusing wave spectroscopy (DWS).

6.5.4.2.3 Backscattering experiments

One geometry used regularly in DWS is the backscattering geometry. The advantage of this geometry is the access on one side of the sample, and another most important advantage is that it does not require the knowledge of transport mean free path, a term used in the calculation of autocorrelation function [115].

In this geometry the laser beam is expanded so that it illuminates an area on the incident face that is much wider than l^*, thus the light is collected from a small area near of the center of illumination. The thickness of the sample is L and incident face is z=0 (the same condition for transmission geometry). For this geometry, the distribution of path length depends on the value of z_0. Therefore by a planar source at $z=z_0$, we can use the solution of $\overline{U}(p,z)$ and we have:

$$g_1(t) = \frac{exp\left[-\frac{z_0}{l^*}\sqrt{\frac{6t}{\tau}}\right]}{+\frac{2}{3}\sqrt{\frac{6t}{\tau}}} \qquad \text{Equation 37}$$

Long paths decay quickly and lead to relatively short length scale motion. It should be mentioned, that the initial slope of $g_1(t)$ is infinity, reflecting the contribution of infinitely long paths. At longer times the decay of the autocorrelation function comes from shorter paths.

6.5.4.3 Experimental set up

For all experiments, the sample was illuminated using polarized light from an argon/krypton laser operating at a wavelength of $\lambda =$ 406.7 nm in back-scattering geometry. The laser beam is expanded to a diameter of approximately 2 mm and is incident on the sample cell of polymethyl methacrylate (PMMA) of 10 mm of thickness (Figure 6.13). The multiply

scattered light has been collected by a high velocity camera BASLER model ac1300-200um, with PYTON semiconductor with a capacity of taking 203 pictures per second to 1.3 MP of resolution.

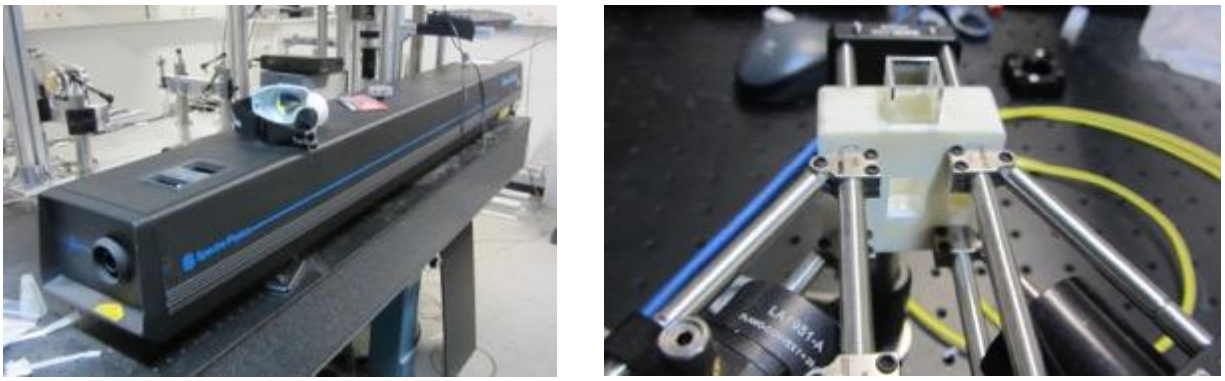

Figure 6.13 Argon/Krypton laser beam (left) and PMMA sampler cell (right)

6.5.4.3.1 Optics of experiment

The schematic of optics has been dividing into two parts. The first part is related to the incident of laser light on the sample. As is showed in Figure 6.14, when the laser comes from the beam, is redirecting by one mirror to the filter to reduce the incoming intensity. After the laser pass the filter, a set of lens L1 and L2 forming a 5 x telescope is placed. Finally, the laser is incident on the sample as it is set in 6.5.4.3.

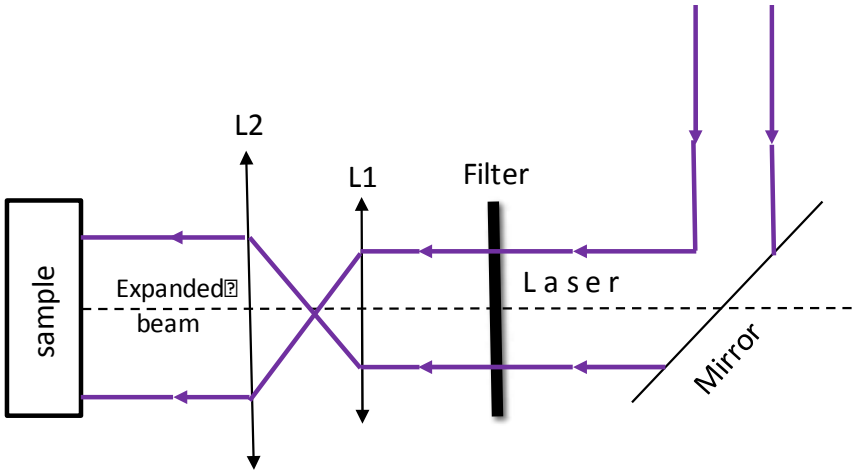

Figure 6.14 Scheme of incident laser light on the sample

The second part (Figure 6.15) is related to the light diffusion. This light is focused on a diaphragm with help to a convergent lens L3. The function of the diaphragm is to diffract the light and subsequently control the speckle size which after is collected by the camera. The speckle size is controlled by the opening of the diaphragm and by its distance with the camera. In all experiments, the area of speckle was around 10 pixels.

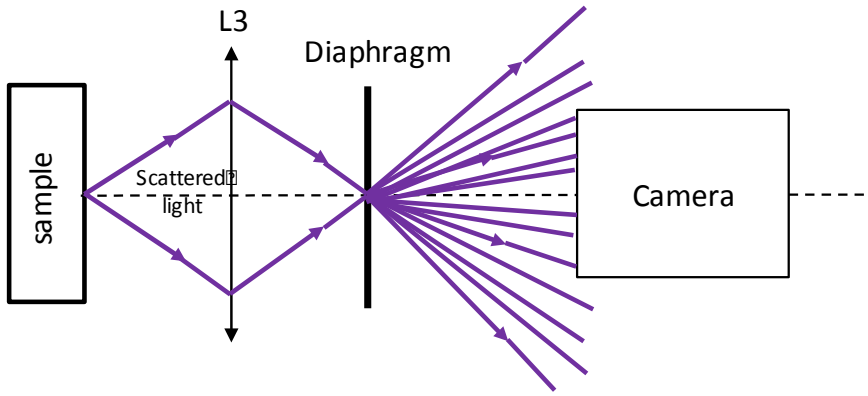

Figure 6.15 Light diffusion on camera

The schematic of Figure 6.16 shows the experimental setup optics used in this thesis

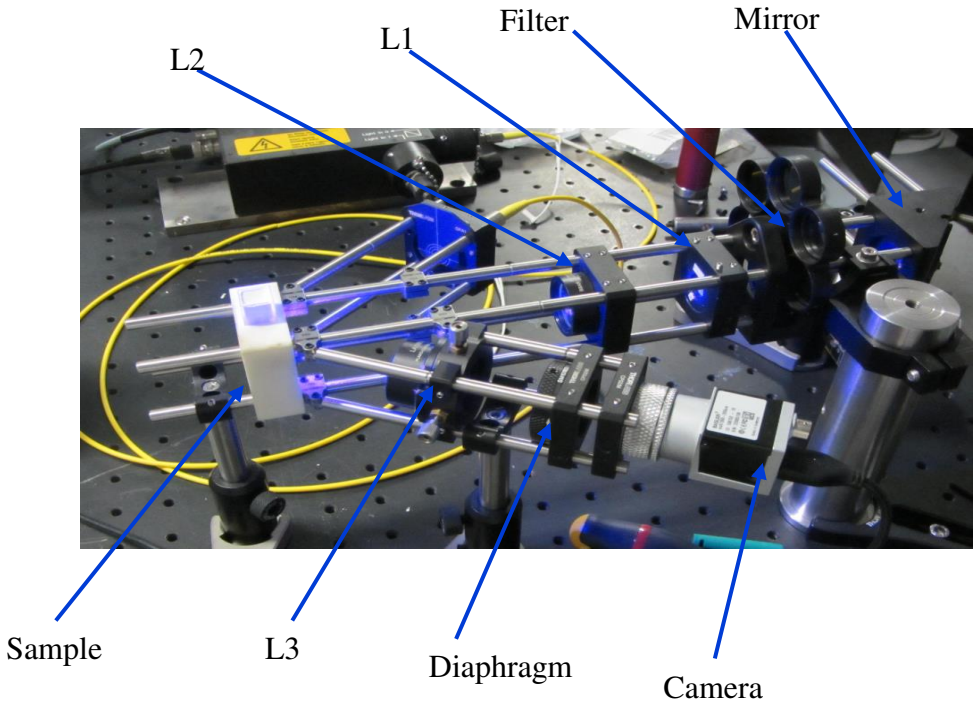

Figure 6.16 Setup optics used in experimental analyzed

6.5.4.4 Data acquisition

In all experiments, the speckle images obtained over time were it recorded and stored in an external hard drive by a program of PYTHON, in which is possible to choose the recording parameters of speckles. Figure 6.17 below shows the interface of program employed.

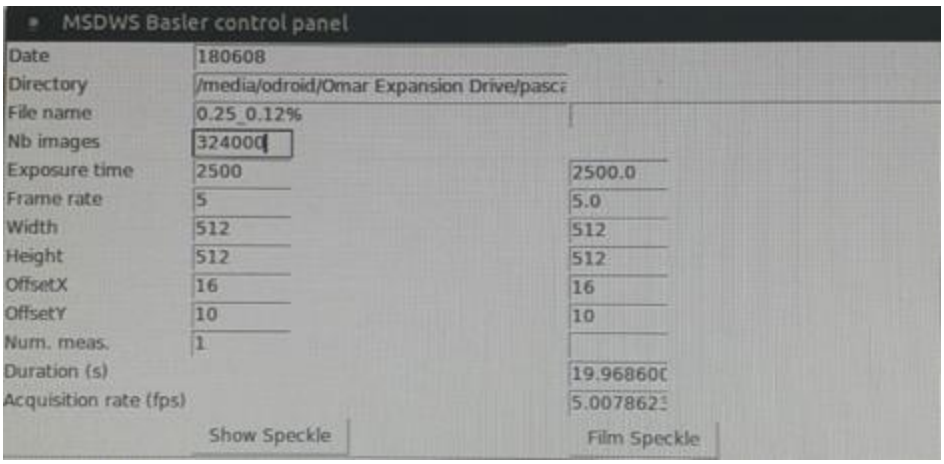

Figure 6.17 Interface of program for data acquisitions

The interface allows creating a file with the date of experiment and choosing the directory to store the files (speckle images). The nomenclature of the experiment can be added as well. The parameters "Frame rate" and "Nb images" allow knowing the analysis time of the diffusion light. For the experiments of this project, the frame rate was an interval between 5 and 10 fps in order to store significant information on the dynamics during experiments. The Nb images are equivalent of time of the experiment, in other words, the higher the number of images, the higher is the time of experiment. For this project, two Nb intervals images have been employed, the first one correspond to intervals from 15 min, 30 min, 45 min 60 min, 90 min and after 90 min, intervals of 60 min until 14 h. the second interval takes the number of images necessary to reach between 13 h to 15 h of experiments without interruption.

Regarding width and height of the images, the program adjusts the resolution of images taken by the camera. The size of images for this project has been 128x128 and 512x512 respectively, the size selected was a function of the time duration of the experiment due to the storage necessary for the images record.

Concerning the position of analysis, the function offset is used to focus a window of resolution 512x512 or 128x128 on a large window (maximum resolution of the image recording for camera), in general, this function was not changed for experiments because it

had a good position for taking the speckle images. A representation of this description can be observed in Figure 6.18.

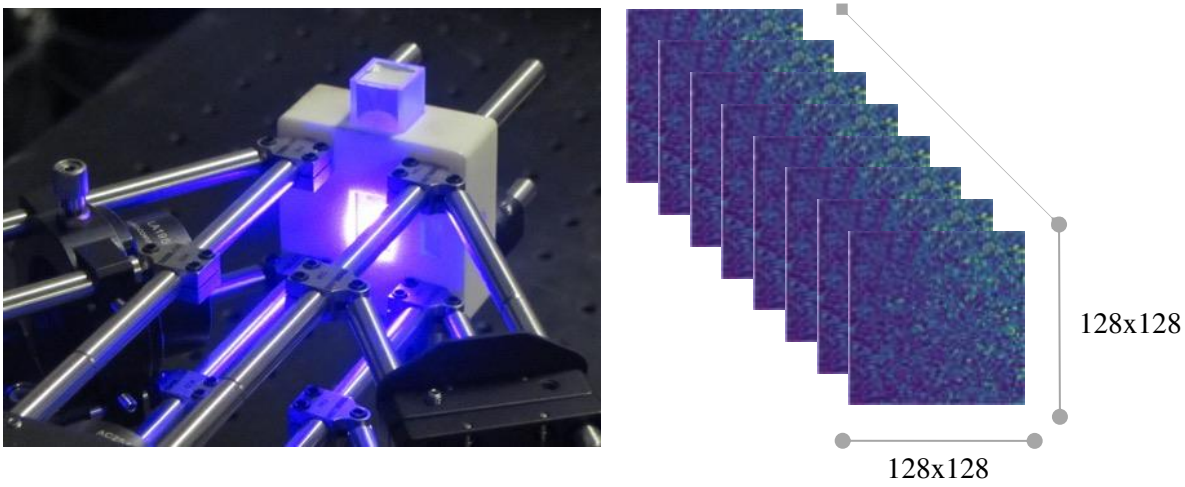

Figure 6.18 Example of speckle images during experiment

To carry out the measurements of diffusion in good condition the camera and optics of equipment must be adjustment, because previously to staring the measurements the speckle image recorded by camera needs to be correct, that is to say, the images obtained by camera must be homogenous in intensity, on the contrary, the recorder images will not be characteristic of the studied suspension. Figure 6.19 left, showed a speckle image that fits the criteria of homogeneity.

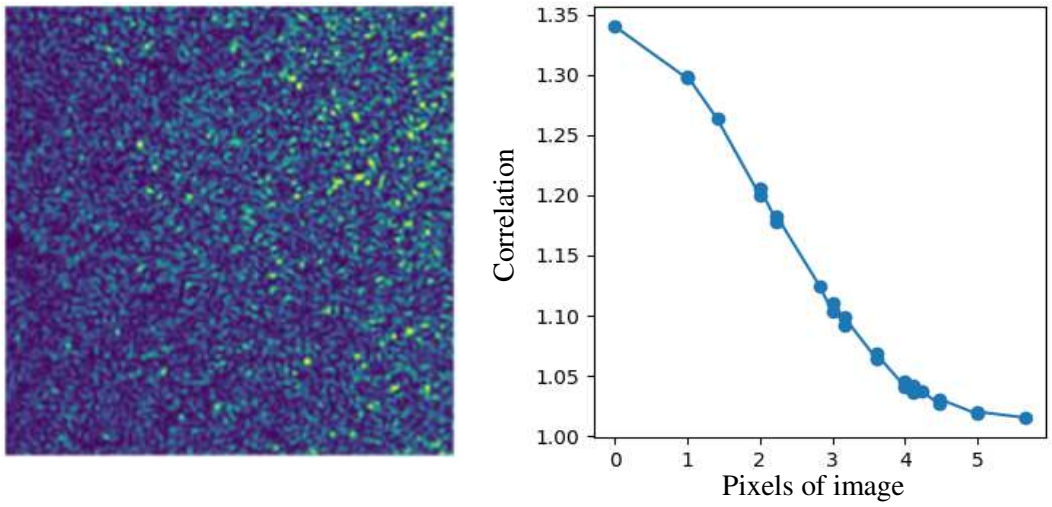

Figure 6.19 Speckle images (left) and correlation of pixels from speckle images (right)

The linear dimension s of a speckle is gives by [116]:

$$s = \frac{d\lambda}{a}$$ Equation 38

Where:

d.- Distance between the diaphragm and camera

λ.- wavelenght og light

a.- diameter of the diaphragm

Adjusting "d" and "a" the size of speckle can be controlled and the spatial intensity autocorrelation function can be measure by:

$$C(p) = \frac{\langle I_i \, I_{i+p} \rangle_i}{\langle I_i^2 \rangle_i}$$ Equation 39

Where:

I_i.- is the intensity of scattered light at pixel i

I_{i+p}.- is the intensity of light p pixel away

The correlation function C(p) is obtained by averaging of all pixels, and as is showed in Figure 6.19 right the C(p). The speckle size was defined as the distance which the intensity profile remains spatially correlated. In Figure 6.19 $s \simeq 3$, which corresponds to a speckle area $\simeq 10$.

6.5.4.5 Intensity autocorrelation function

In this part, the calculation of autocorrelation function will be explained, which taken account the descriptions of [116, 117]. The autocorrelation function is a statistical tool denoted by g_2 (t) and express the following: Firstly, the intensity is obtained from each image, because each recorded image is compound of a set of pixels with different intensities, we have calculated for each image the mean value of pixels composing the speckle image and a reference image

has been set for correlated with other. If several images are correlated to the reference image, it is possible to plot g_2 as a function of time, and knowing the number of images taken by the camera every second (frame rate) we can determine the time of scattering experiment.

The autocorrelation function is obtained by the following equation:

$$g_2\,(t_0, t) = \frac{\langle I_i(t_0) I_i(t + t_0\rangle_i}{\langle I_i(t_0)\rangle_i \langle I_i(t + t_0)\rangle^i} \qquad \text{Equation 40}$$

Where $\langle \ldots \rangle$ mean the average over the pixels of the acquired image.

The equation means that the correlation function $g_2(t_0, t)$ is determined multiplying two frames, one of time t_0 and other at time t_0+t together pixel by pixel, summing the results from all pixels, and dividing by the number of pixels.

6.5.4.6 Multiple correlation function determination

As it was said, the resulting images are saved in an external hard drive for their analysis. By PYTHON program the function of correlations in intensity have been studied as a function of time. For this purpose, two programs were created in order to analyze the large number of recorded images by the camera and plot over time the intensity autocorrelation function values g_2. The analyzing time, depend of setup parameters of camera and the number of images taken in one second. The first program has the aim to listing the data from correlation in a large matrix, and efficiently determines the location of interest intervals. The second program allows tracing the correlation values in the matrix as a function of time.

Figure 6.20, shows the operation of the first program. This program cuts the set of images at several intervals of the same size and therefore at the same time. This method is used to trace the correlation function for each interval and is plot it as a function of the experimental time. The program associates a new reference image to each interval, in other words, the reference image is varied over the total time of measurement. The reference image is correlated with all images one after the other contained in their intervals.

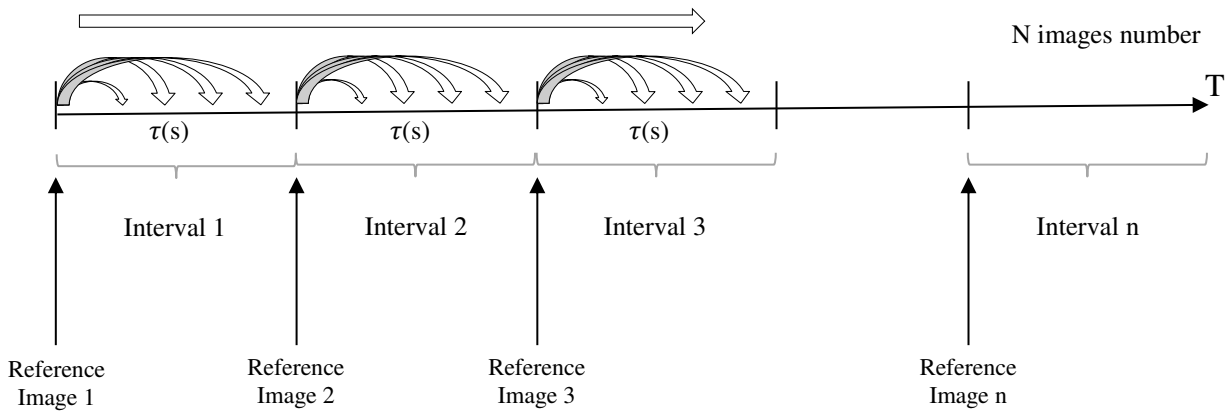

Figure 6.20 Division of interval in first program

In the schema is possible to identify two different time variables: The total time of the measurement T (seconds) and the correlation time τ (seconds) between the reference image and one image in its characteristic interval.

We have used this feature to build a large matrix and store the correlation values between two images with dimensions T – using equation 38.

Concerning to the structure of the matrix, Figure 6.21 shows its construction, and basically the structure can be observed as a superposition of all intervals until the total duration of the experiment.

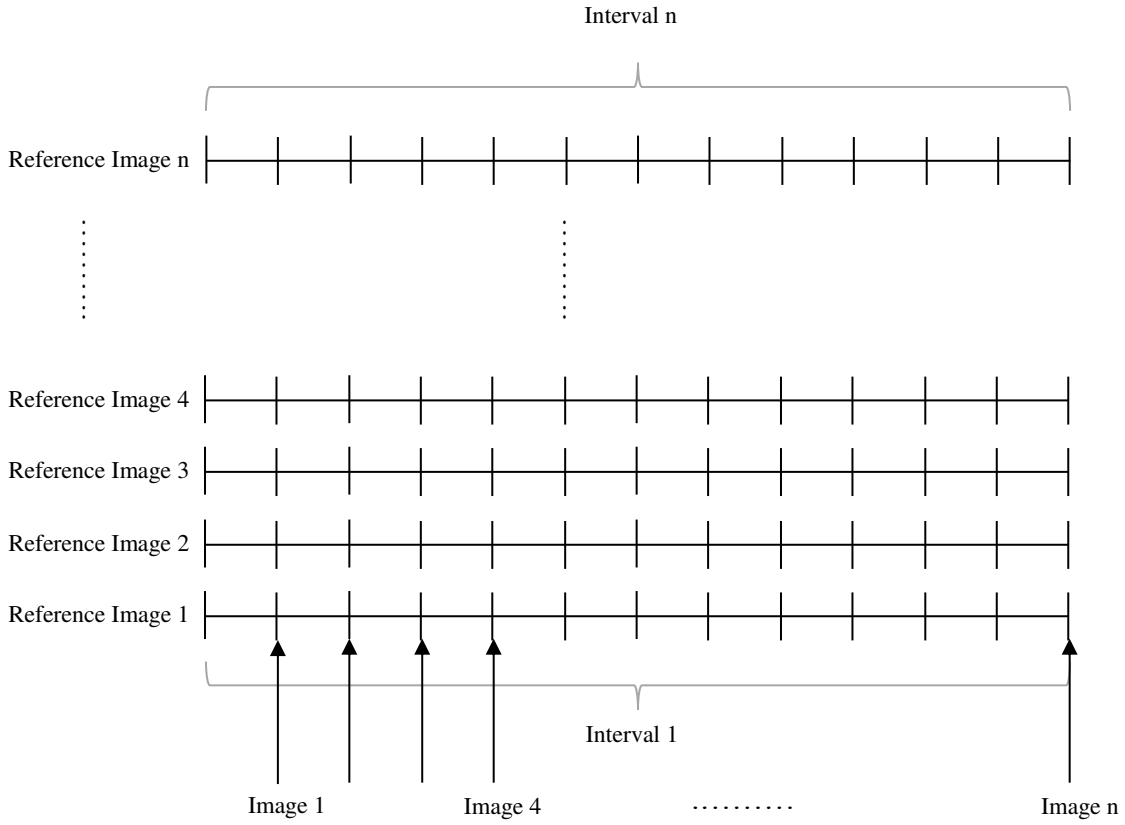

Figure 6.21 Structure of matrix and superposition of intervals

It is possible to change the size of each interval, considering the following parameters into the matrix. This can be illustrating on Figure 6.22.

- Change of reference image every 10 images
- Cutting the total images in several intervals of 3000 images
- Correlating the reference images and image of characteristic interval every two images.

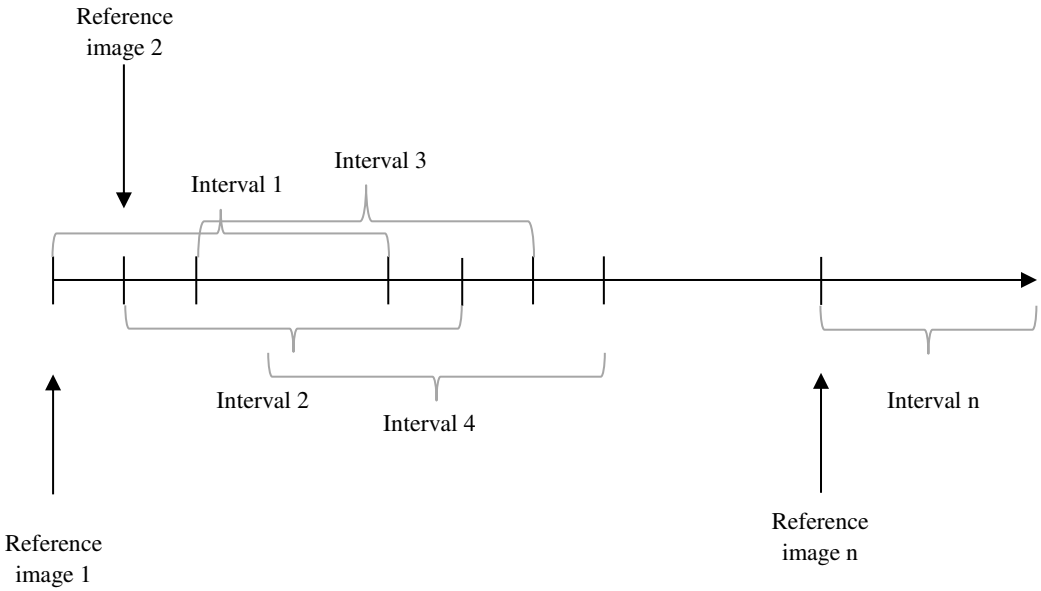

Figure 6.22 Interchange of reference images and interval position

6.5.5 Flexural strength by three-point loading system

The flexural strength means the stress in a material just before it yields in a flexure test. Some materials experiment a range of stress across in depth, having both compressive and tensile stress during experimental bent. The flexural properties are important in materials because they are directly related to of the microstructure and defects during its processing or in the case of cementitious materials, the development of hydration products, internal micro-cracks or any each defect during setting and hardening.

In this thesis, the flexural stress at break was determined on pastes analyzed in MSDWS studies. The test was performed according to the procedure provided in [118]. Bars of a rectangular cross section of 0.5 x 1.0 x 12 inch (in order to have a support span-to-depth ratio of 16:1) were made. This bars rest on two supports and were loaded midway between the supports as is showed in Figure 6.22 (left). The strain rate in the test was 0.1 mm/min until rupture, testing three specimens for each mixture (Figure 6.23 right). The calculation of stress was determinate by:

$$\sigma_f = \frac{3PL}{2bd^2} \qquad \text{Equation 41}$$

Where:

σ_f= Stress in the outer fibers at midpoint, MPa.

P= Load at a given point on the load-deflection curve, N.

L= Support span, mm.

b= Width of beam tested, mm.

d= Depth of beam tested, mm.

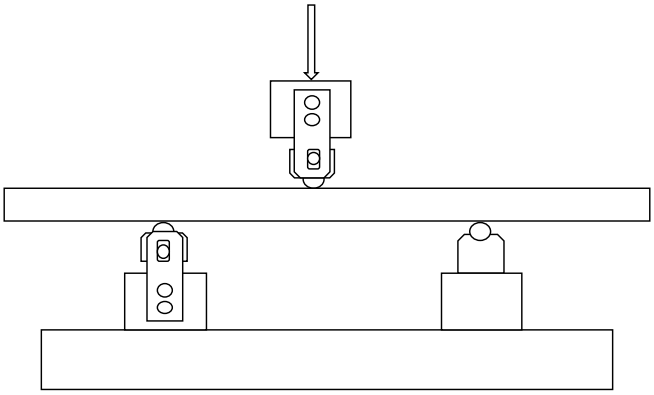

Figure 6.23 Flexural strength test; left: Supports of the sample; right: Test

7 RESULTS AND DISCUSSION

7.1 Characterization of WPC

7.1.1 Chemical and physical properties

Table 7.1 Present the results of the chemical analyses conducted on white portland cement (WPC). According to the composition, the WPC contains a high rate of CaO, and low rate of iron oxide due to the minerals used for the processing of this kind of cement has a low contents of iron as was described in 2.1.2.1. Composition showed in table 7.1 is similar to presented by authors whom have worked with white portland cement [119, 120].

In the same table are showed the phases of WPC, which through Bogue's equation have been calculated. As it can observe the minimal phase presented is C_4AF, due to the low content of iron oxide discussed above. The other phases presented are similar with phase compositions of different white portland cements studied in literature.

Other parameters showed in table 7.1 are loss on ignition with value of 1.5, being for below of permissible value of max 3% [6] and has been demonstrated that the cement were not some degree of hydration during its use in this study. The initial and final setting time are showed in the table 7.1 as well, having 0 hours 56 minutes for initial setting and 3 hours 7 minutes for final setting. These times were determined by Vicat apparatus on cement pastes with normal consistency (26.2 %) showed in the table as well, being the values of setting on pastes without additives to an optimal content of water for hydration, and so compare them with results of setting in ultrasonic reflection test.

One of the more important parameter in the WPC is its density, with one value of 2.99 g/cm^3 as is showed in table 7.1. The density was crucial in calculating of quantity of paste and solid volume fraction of each one of blends analyzed.

Finally, the specific surface area of WPC has a value of 1491 m^2/kg, as expected; this high value is due to the method employed for its determination (BET) as is observed in some research [65]. This value is important due to the high specific surface means that the cement will react quickly, therefore, this value should be have standard like is obtained in this cement.

Table 7.1 Physical and chemical parameters of white portland cement

Component	Weight (%)
Calcium oxide(CaO)	64.90
Silicon dioxide (SiO_2)	24.03
Aluminum dioxide Al_2O_3	4.88
Sulfur trioxide (SO_3)	1.62
Iron oxide (Fe_2O_3)	0.20
Magnesium oxide (MgO)	0.58
Sodium oxide (Na_2O)	0.16
Potassium oxide (K_2O)	0.36
C_3S	43.82
C_2S	35.92
C_3A	12.59
C_4AF	0.61
Lost on ignition (LOI) (%)	1.5
Initial setting time (h:min)	0:56
Final setting time (h:min)	3:07
Normal consistency (%)	26.2
Density (g/cm^3)	2.99
Specific surface area BET (m^2/kg)	1491

7.1.2 Mineralogical phases of WPC

Figure 7.1 shows the result of X ray diffraction of the WPC. As is observed, the predominant phases of cement are tricalcium silicate (C_3S) and dicalcium silicate (C_2S), both conform between 70% – 80% of components [121]. A significant content of tricalcium aluminate (C_3A) is observed as well, being important its content due to its fast reactions with water and gypsum to form ettringite, controlling the setting time and therefore the rheological properties into the system [97]. As it can be observed there is not presence of ferrite phase, due to the low content of iron did not allow identifying it during the test. Similar diffractograms has been published for white portland cement composition [13].

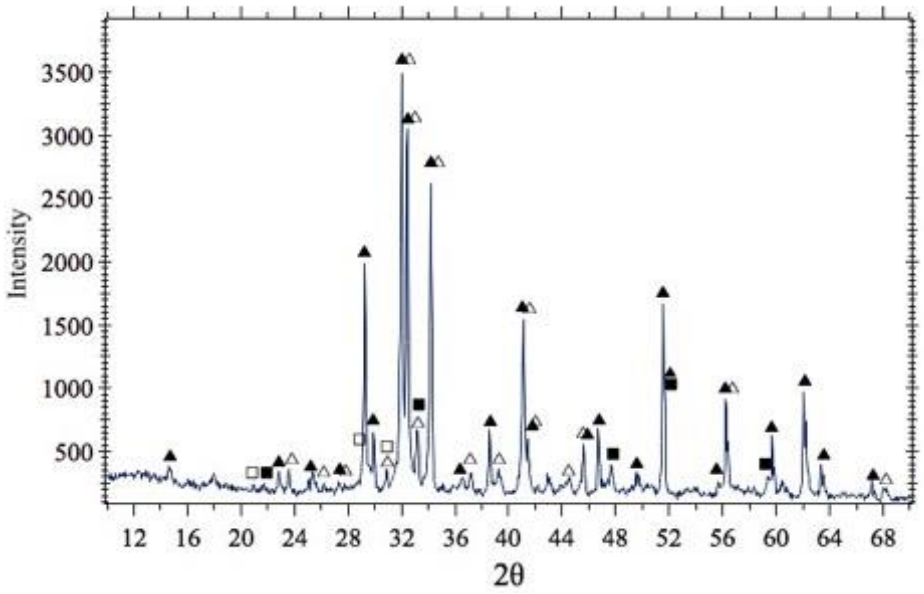

Figure 7.1 XRD analysis of white Portland cement: ▲ C3S-Alite, ∆ C2S-Belite, □ C3A-Tricalcium aluminate, □ CaSO4- Calcium Sulfate

7.1.3 Laser diffraction granulometry and morphology of WPC

The average particle size distribution obtained for white Portland cement sample is plotted as a probability density function (Figure 7.2 a)) and as uniformity function of the cement particles (Figure 7.2 b)). The distribution of cement in study is quite similar to another reported by several authors [122]. The cement presents sizes about of 5% < 2 μm, the average size of particles of WPC was 24.04 μm and its standard deviation 17.21 μm. The asymmetric of curve a) has a value of 0.326 and means that the coarse particles have a minimal influence on the distribution due to the form of the distribution is approximately same that the normal distribution of the bell.

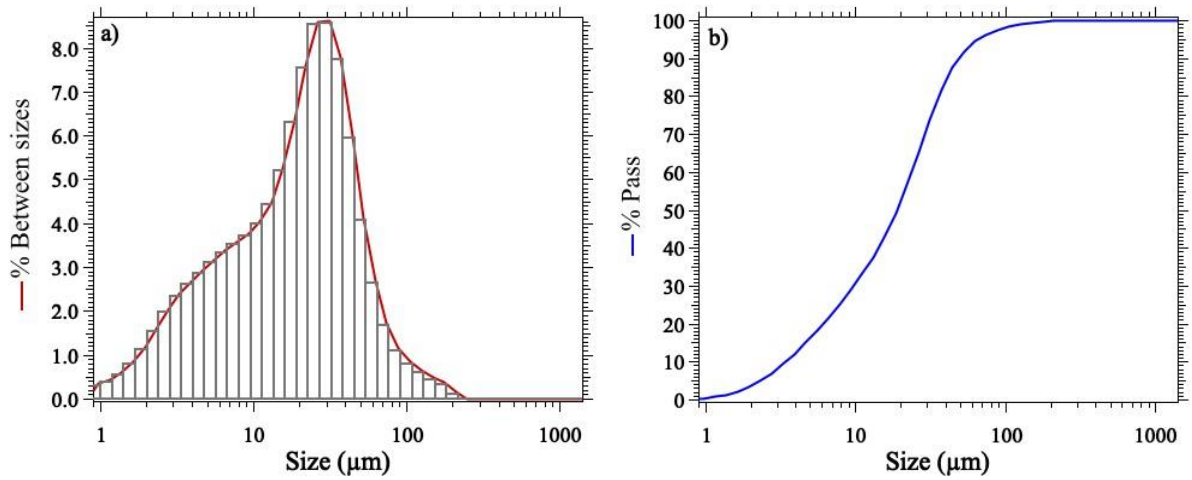

Figure 7.2 The particle size distribution of white portland cement measured using laser diffraction analyzer a) probability density function b) cumulative volume

7.1.4 Scanning electron microscopy (SEM) and elemental analysis by X ray (Energy dispersive spectroscopy, EDS)

Additionally, to those results, micrographics of WPC were obtained and are showed in Figure 7.2 and 7.3. These micrographics show angular particles and can be observed several size of them, as is showed in scale of micrographics the particles have sizes from 2 µm to 25 µm approximately. The aim of these micrographics is to observe the shape of particles and by energy dispersive spectroscopy to identify the elemental composition of the grains. From the Figures can be observed presence of Ca as majority component followed of Si and Al that combined with the Oxygen form the silicates of the cement. Other components like Mg and S can be observed, having compatibility with FRX composition present above.

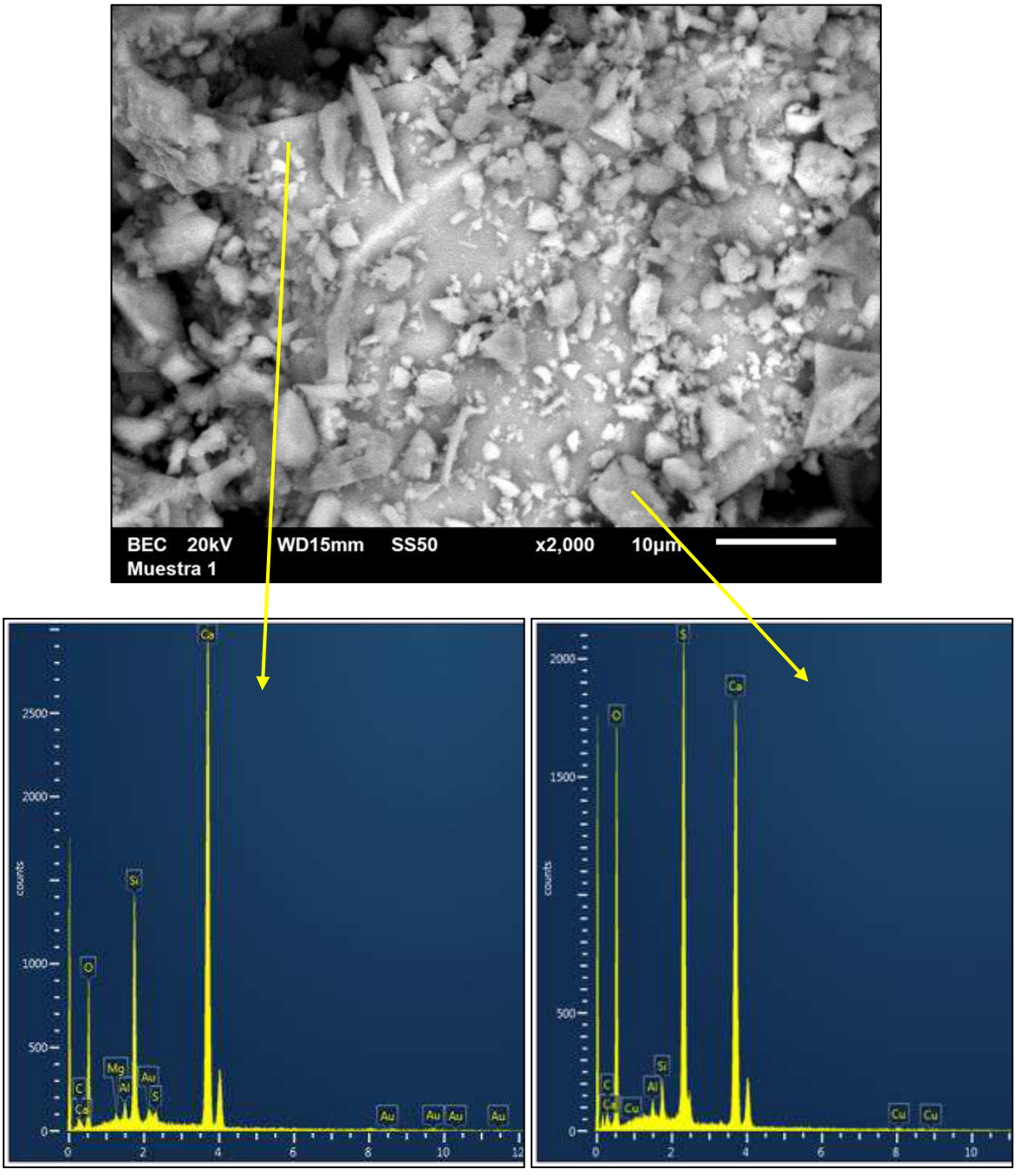

Figure 7.3 Micrographic to x 2,00 of WPC and its elemental composition

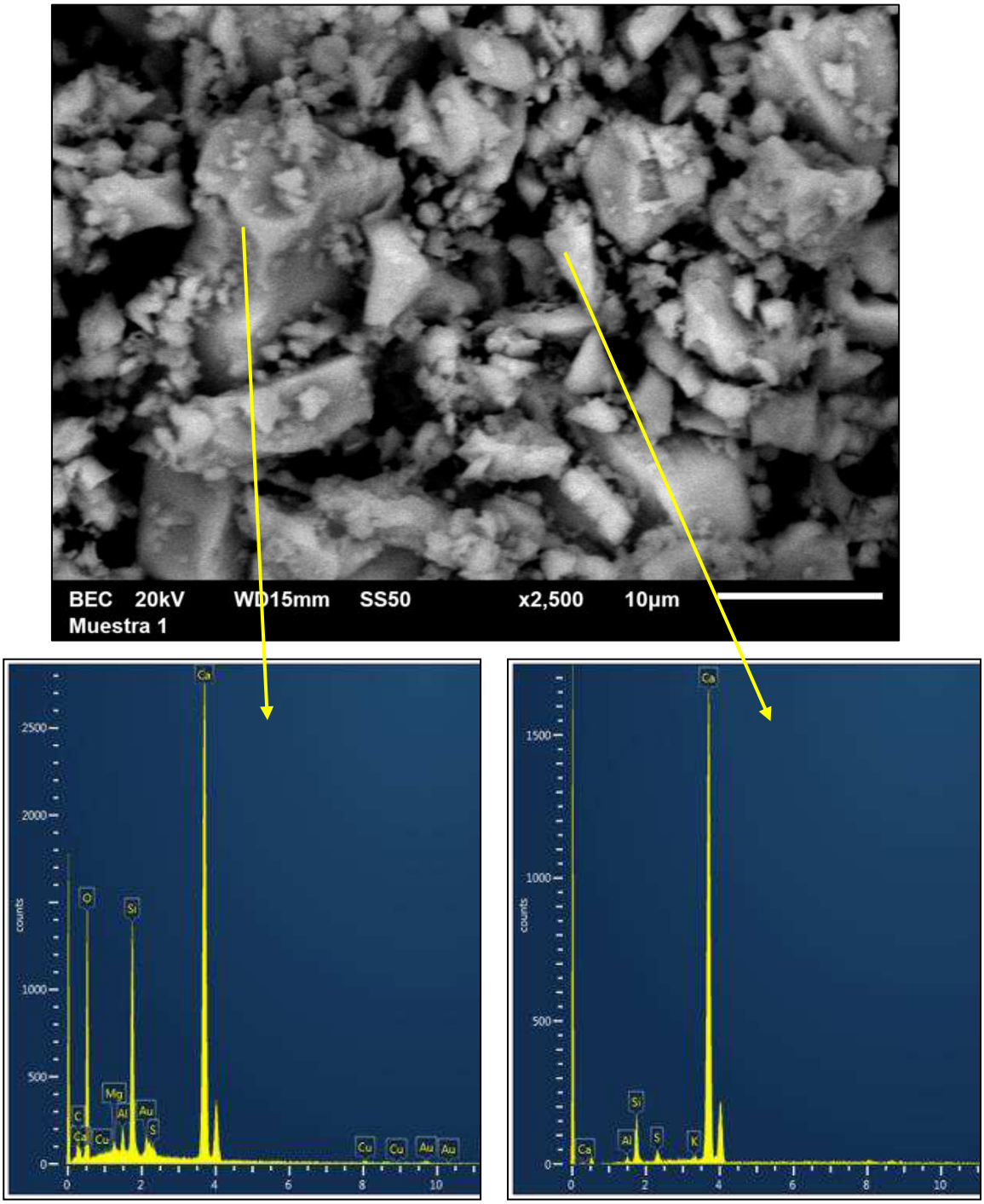

Figure 7.4 Micrographic to x 2,500 of WPC and its elemental composition

7.1.5 Concentration of additives

7.1.5.1 Optimal concentration of High Range Water Reducing Admixtures (HRWRA)

Figure 7.5 shows the determination of optimal concentration of high range water reducing admixture (HRWRA) on a suspension of 250 g of cement with water to cement ratio of 0.33. By flow curves (shear rate – shear stress) the influence of additive on shear stress was determined into a interval of shear rate from 0.1 s^{-1} to 300 s^{-1}. It can observed that the stress necessary for reach determinate shear rate change with the concentration of additive until a boundary saturation point, where the value of stress is constant. In other words, the yield stress change due to the addition of HRWRA, being possible obtain a higher flow maintaining the same content of cement and water. A given yield stress at 0.5 s^{-1} was taken in order to plot its variability due to change of concentration of additive, for this case Figure 7.5 (left) shows the variability of yield stress at concentration from 0 to 0.75 ml, selecting 0.30 ml as start of saturation of additive on the paste as is observed in Figure 7.6 (right). For calculating the optimal percentage the 0.30 ml of plasticizer was divided for 250 g of cement, in order to determinate the value respect to weigh of cement, and multiply for 100 to obtain the percentage. 0.120% was the optimal concentration of plasticizer used in this project.

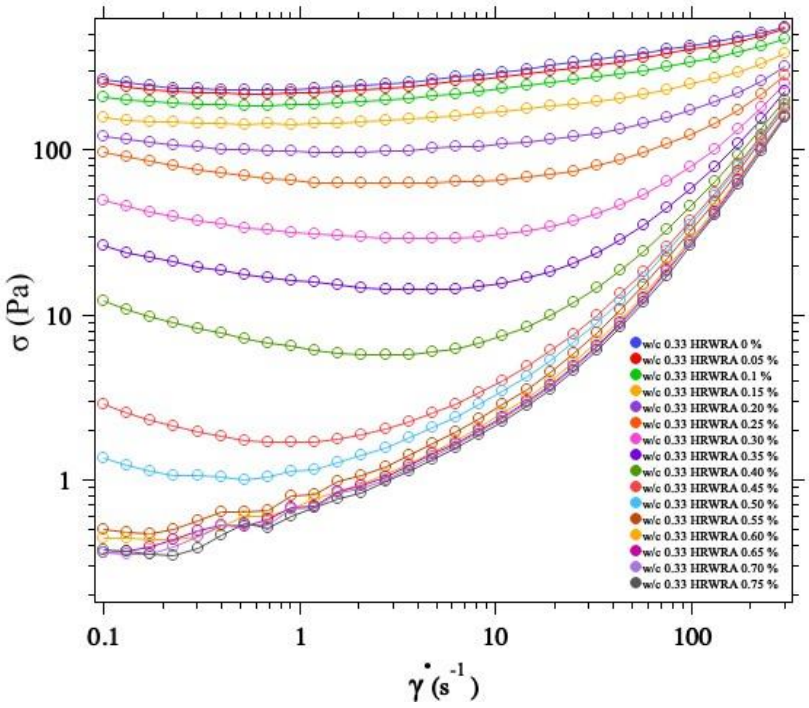

Figure 7.5 Flow curves of suspensions w/c = 0.33 at several concentration of HRWRA

HRWRA Concentration	Yield at 0.5 s^{-1}	HRWRA Concentration	Yield at 0.5 s^{-1}
0	232	0.40	7.19
0.05	219	0.45	1.71
0.10	186	0.50	1.00
0.15	143	0.55	0.635
0.20	99.9	0.60	0.600
0.25	69.7	0.65	0.524
0.30	33.9	0.70	0.529
0.35	17.7	0.75	0.537

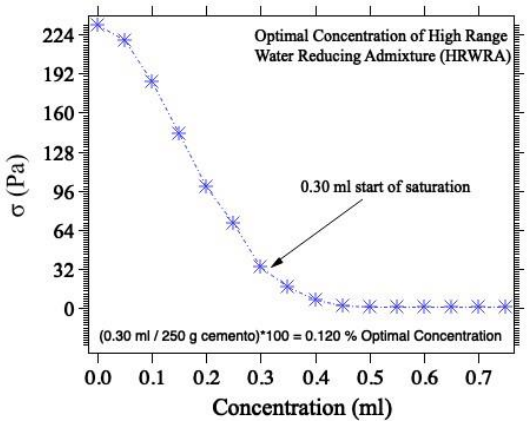

Figure 7.6 Values of yield stress at 0.5 s^{-1} (left) and saturation point of HRWRA (right)

7.1.5.2 Optimal concentration of Viscosity Modifying (VM)

The optimal concentration of viscosity modifying admixture (VM) was determined following the same methodology described in 7.1.5.1. For this additive a high concentration of HRWRA previously described in 6.2 was selected with value of 0.360%, flow curves (shear rate – shear stress) were measure at several concentrations of viscosity modifying as is showed in Figure 7.7.

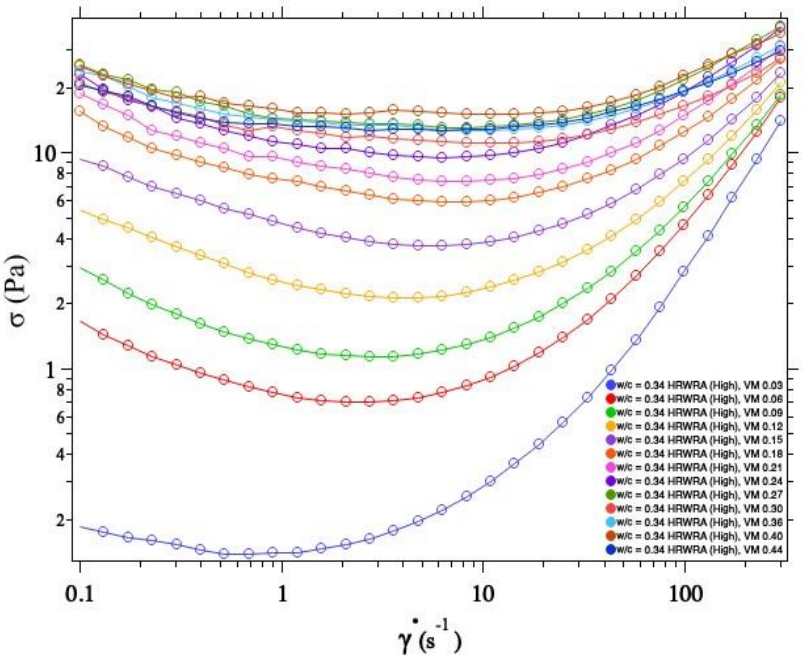

Figure 7.7 Flow curves of suspension w/c = 0.33 with high concentration of HRWRA (0.360%) at several concentration of VM

For this case the shear stress increased due to addition of stabilizer (VMA) even when the stabilizer was added, as it can be observed in Figure 7.8. In the same way, the saturation point was identified and taken the value of cement used in the suspension, the optimal concentration was determined.

VM Concentration	Yield at 0.9 s^{-1}	VM Concentration	Yield at 0.9 s^{-1}
0.03	0.1392	0.24	11.27
0.06	0.7746	0.27	14.42
0.09	1.293	0.30	13.16
0.12	2.587	0.36	14.19
0.15	4.842	0.40	15.98
0.18	7.617	0.44	13.69
0.21	9.577		

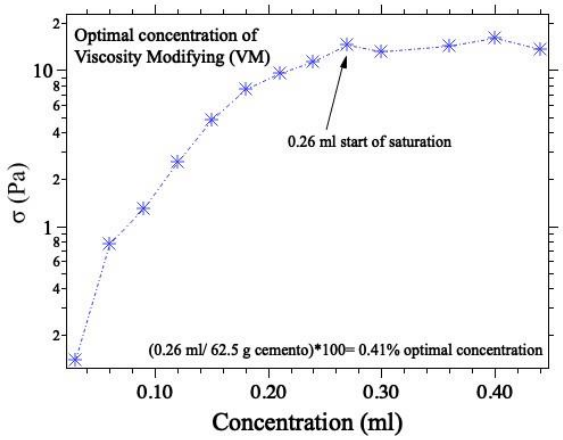

Figure 7.8 Values of yield stress at 0.9 s-1 (left) and saturation point of VMA (right)

7.2 Experimental Results

7.2.1 Flow and viscosity of cement paste in study

7.2.1.1 Shear rate – Shear Stress ratio

The thixotropic behavior of the suspensions are observed by the increase of the shear-stress, σ, as a function of shear-rate, $\dot{\gamma}$, as shown in the graphic of Figure 7.9: thixotropy is responsible for the increase in shear stress after a critical shear rate in between 1 and 10 s^{-1}, corresponding to the minimum observed stress. This behavior can be observed for the entire w/c ratio tested with concentration from 0.04% to 0.360% of HRWRA, while for pastes with 0.360% HRWRA and 0.41% VM the critical shear rate is between 10 and 40 s^{-1}, observing the stability conferred to the paste by VM additive. The higher is the w/c ratio and the lower is the shear-stress but instead of having a plateau of shear stress at the lower range of shear rate, an increase of the shear stress is observed in the 240 s of the experience. When the shear-stress σ is plotted as a function of the shear-rate (Figure 7.8), one can observe an increase of the shear-stress with a decrease of the shear-rate for the low value of shear-rate. This is an illustration of a thixotropic behavior because the sample recovers with time and the shear-rate is not high enough to perturbate the microstructure of the cement paste [49]

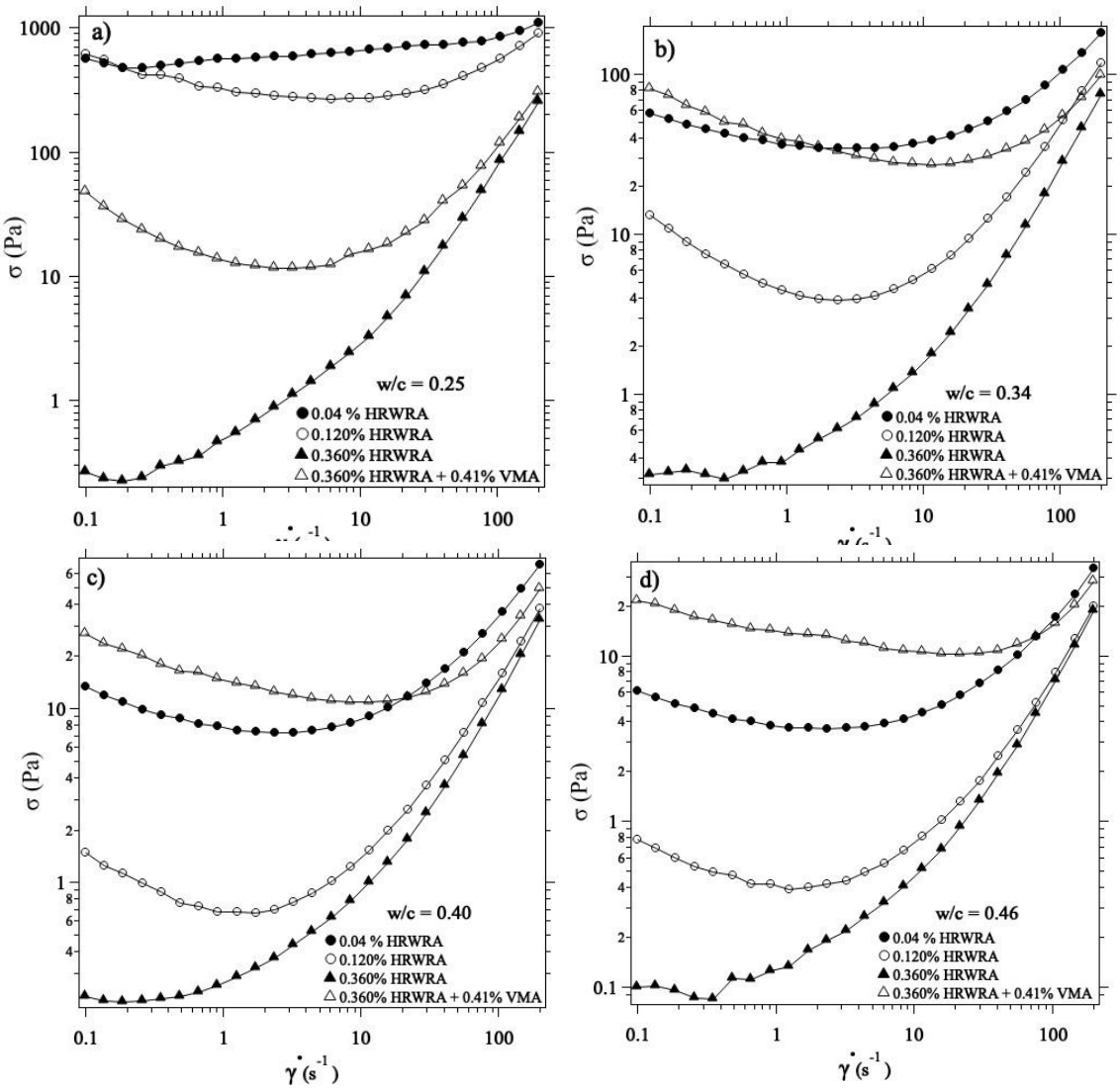

Figure 7.9 a) Shear-stress as a function of the shear-rate for a cement suspension at a fixed w/c = 0.25 and changing HRWRA concentration of 0.04% ●, 0.120% ○ and 0.360% ▲. The last measure has also been testes with an addition of 0.41% of VMA △. All the curves were obtained with the same concentrations of HRWRA but with different water to cement ratio. b) w/c = 0.34, c) w/c = 0.40, Bottom right: w/c = 0.46.

7.2.1.2 Shear rate – Viscosity ratio

The rheological curves using the shear-rate sweep protocol are plotted in Figure 7.10, where the viscosity η is plotted as a function of the shear-rate $\dot{\gamma}$. As expected, the higher the concentration of HRWRA, the lower is the viscosity at low-shear rate. The yield stress σ_0, is dependent upon the concentration of suspended particles and this is true for all the w/c tested in this study. It can also be observed that the higher is the plasticizer concentration, the lower

is the critical shear-rate $\dot{\gamma}^c$ for which the slope of $\eta(\dot{\gamma})$ starts to increase. This is equivalent to say that the microstructure responsible for the yield-stress can be broken at a lower shear-rate [123] this behavior can be explained by the weakening of the interparticle interactions when the concentration of HRWRA increases. An increase of the viscosity for shear-rate higher than 10 s^{-1} for the samples at two highest w/c is observed. This is an artefact due to the formation of a vortex increasing the measured torque and therefore articitially increasing the calculated viscosity. The addition of a stabilizer increases the sample viscosity for all the range of shear rate, moreover the critical shear-rate $\dot{\gamma}^c$ is also higher. Again, this behavior can be explained by the modification of the interparticle interactions

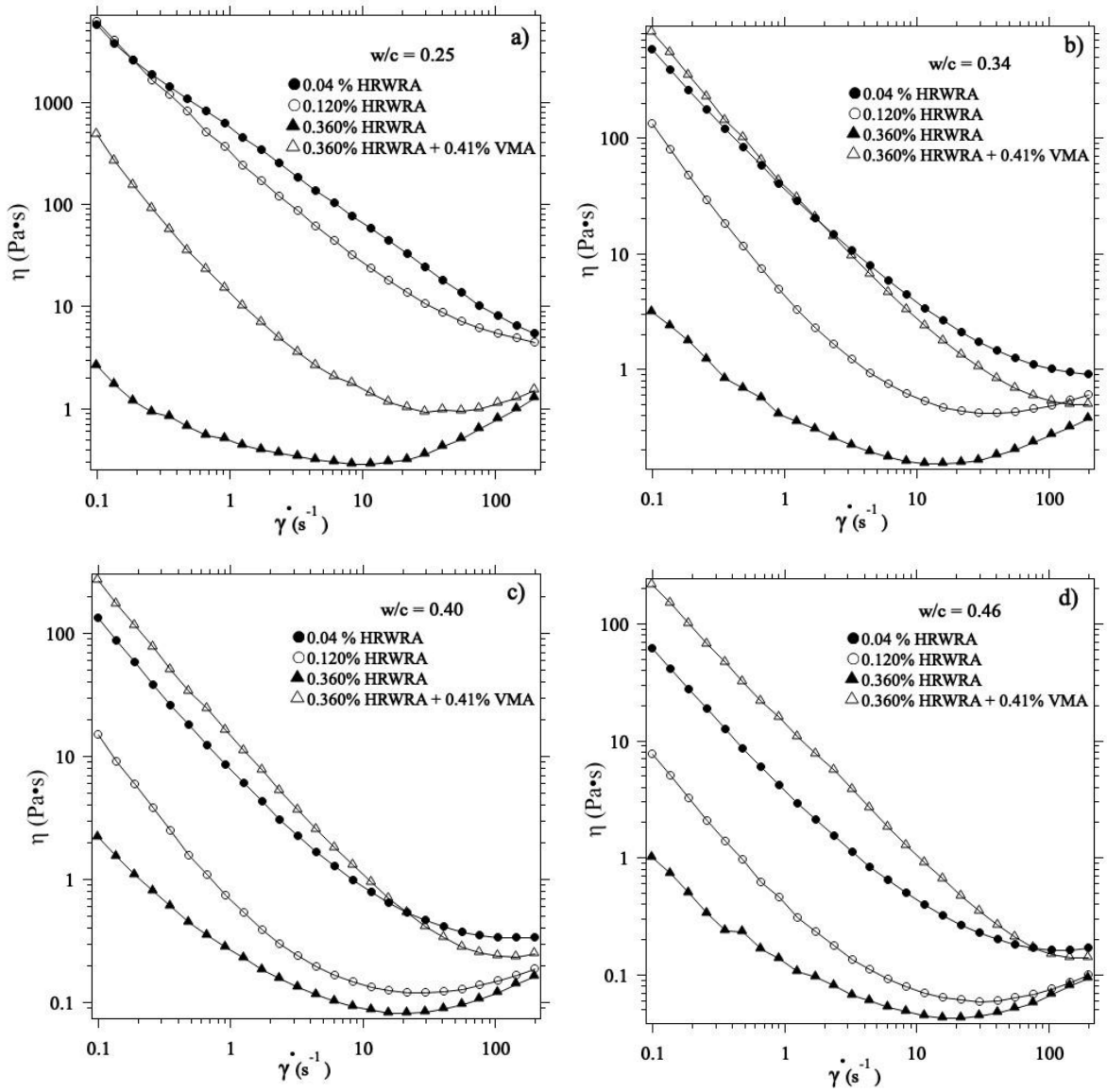

Figure 7.10 a) Viscosity as a function of the shear-rate from 200 s-1 to 0.1 s-1for a cement suspension at a fixed w/c = 0.25 and changing HRWRA concentration of 0.04% ●, 0.120% ○ and 0.360% ▲. The last measure has also been testes with an addition of 0.41% of VMA △. All the curves were obtained with the same concentrations of HRWRA but with different water to cement ratio. b) w/c = 0.34, c) w/c = 0.40, d) w/c = 0.46.

7.2.2 Rebuild up interval thixotropic

7.2.2.1 Time – Viscosity ratio

The thixotropic behavior of the paste is quantified using a protocol where the paste is first submitted to an initial pre-shear, after which, the paste is sheared at a constant rate in decreasing increments while observing the change in viscosity as a function of time. After the shear-rate sweep, the second step of the protocol is performed, and the sample is first sheared at high shear-rate and then allows recovering at a much lower shear-rate. Therefore, it enables the study of the recovery of the cement particles network under several flow conditions which could result in a competition between build-up and rupture of the microstructure. Just after the cessation of the strong pre-shear, the suspension starts to recover with the time as it can be observed in the graphic of Figure 7.11

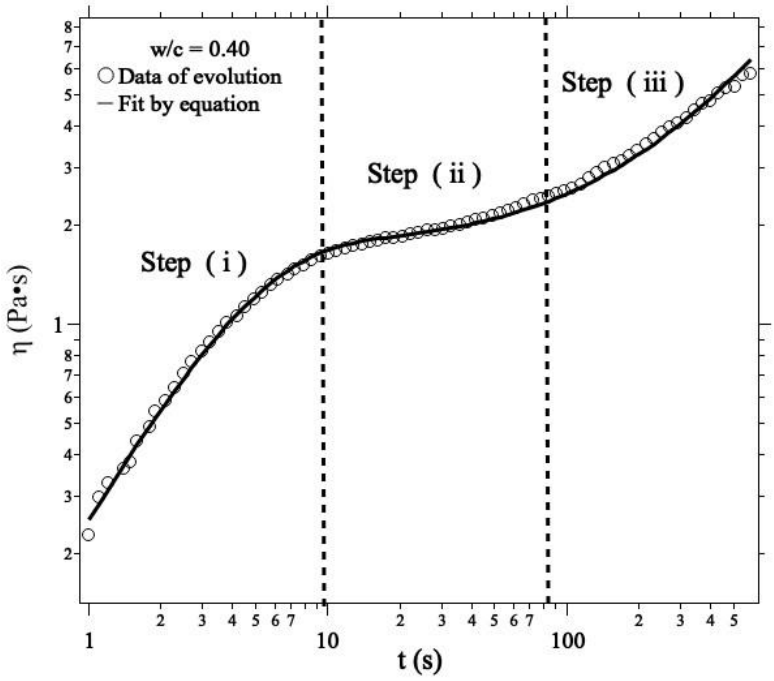

Figure 7.11 Time evolution of the viscosity of a cement paste at a w/c = 0.40 with a concentration of HRWRA equal to 0.120% and a recovery shear-rate $\dot{\gamma}$ = 0.25 s-1 ○ and the fit following the equation 41 —

7.2.2.2 Empirical fit law proposal

The increase of the viscosity with time of the Figure 7.10 can be described by three successive steps:

i. Just after the decrease of the shear-rate, the viscosity increases quickly until this increase slows down and
ii. Reaches a plateau which can be more or less long depending of the experimental conditions, followed with
iii. A second viscosity increases with time.

This time evolution of the viscosity can be fitted with the equation 42 which takes into account the different steps with 5 fitting parameters, each parameter controls the adjustment of the curve in a different shear rate region, and the overall flow curve adjustment is performed by a Levenberg-Marquardt adjustment algorithm. An example of the associated fit is represented in the graphic of Figure 7.12

$$\eta(t) = \eta_0 \left(1 - e^{\left(\frac{-t}{\tau_1}\right)^{\beta}}\right)\left(1 + \left(\frac{t}{\tau_2}\right)^{\alpha}\right) \qquad \text{Equation 42}$$

The step (i) shows an initial increases of the viscosity which can be described by equation 43, where η_0 is the value of the viscosity at the plateau in the intermediate regime of the viscosity, τ_1 is the exponential time constant and β is a mathematical constant which indicates the broadness of the time distribution: if β = 1, then only one time constant exists in the system.

$$\lim_{t \ll \tau_1} \eta(t) = \eta_0 \left(1 - e\left(\frac{-t}{\tau_1}\right)^{\beta}\right) \qquad \text{Equation 43}$$

The final increase, corresponding to the step (iii), can be approximated by the equation 44, where η_0 the same viscosity plateau is used in equation 42 and 43, τ_2 can be seen as a beginning of this third phase and α is the power-law exponent of the relationship between viscosity and time.

$$\lim_{t \gg \tau_2} \eta(t) = \eta_0 \left(\frac{t}{\tau_2}\right)^{\alpha} \qquad \text{Equation 44}$$

The complex relationship for viscosity recovery successfully fits most of the experiments as it can be checked on Figure 7.12, but in some case, the first time scale is so small than the fit can

be limited to the simplified expression $\eta(t) = \eta_0 \left(1 + \left(\frac{t}{\tau_2}\right)^{\alpha}\right)$. When $\tau_1 < t < \tau_2$ $\eta(t) \sim \eta_0$ and it corresponds to step (ii).

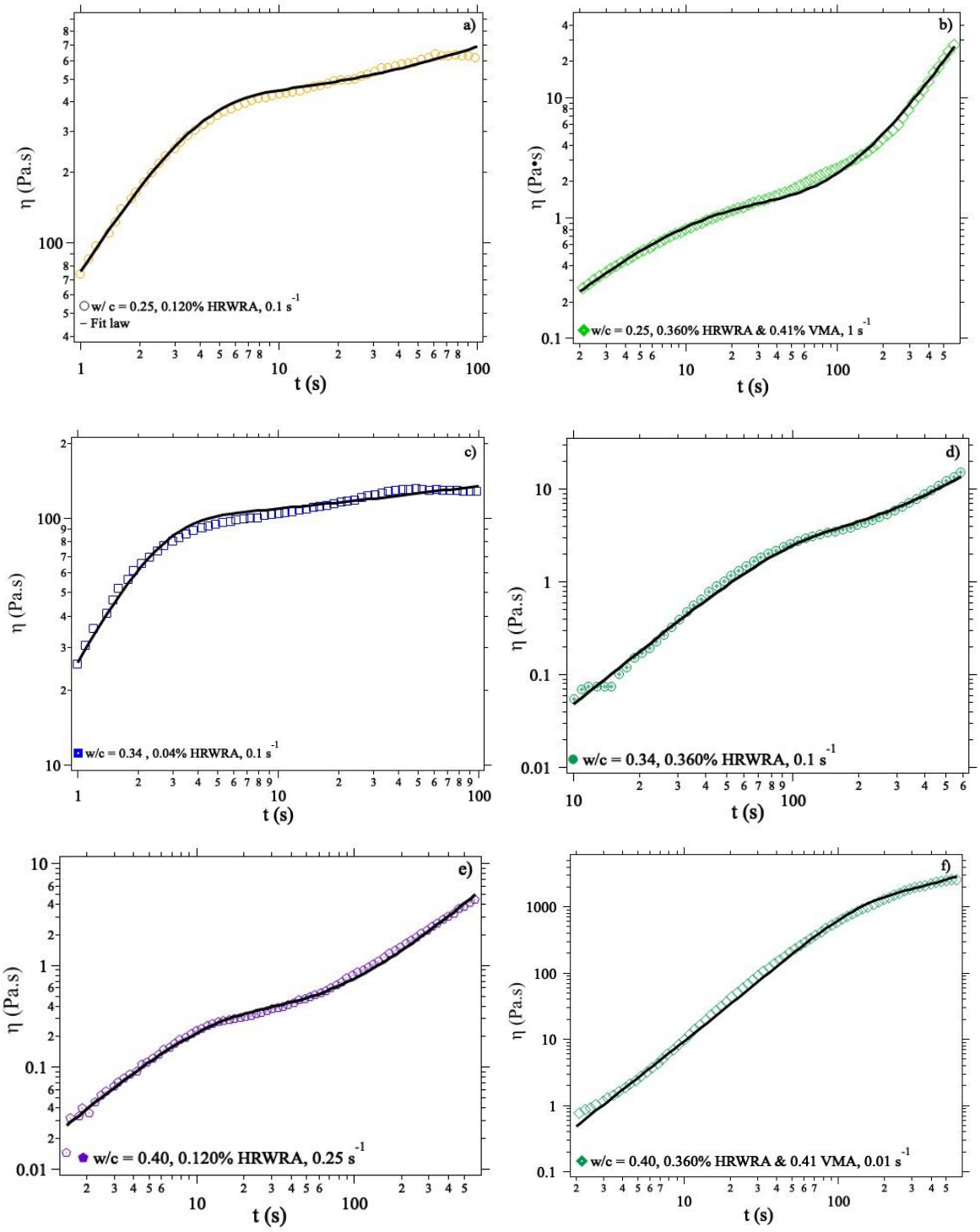

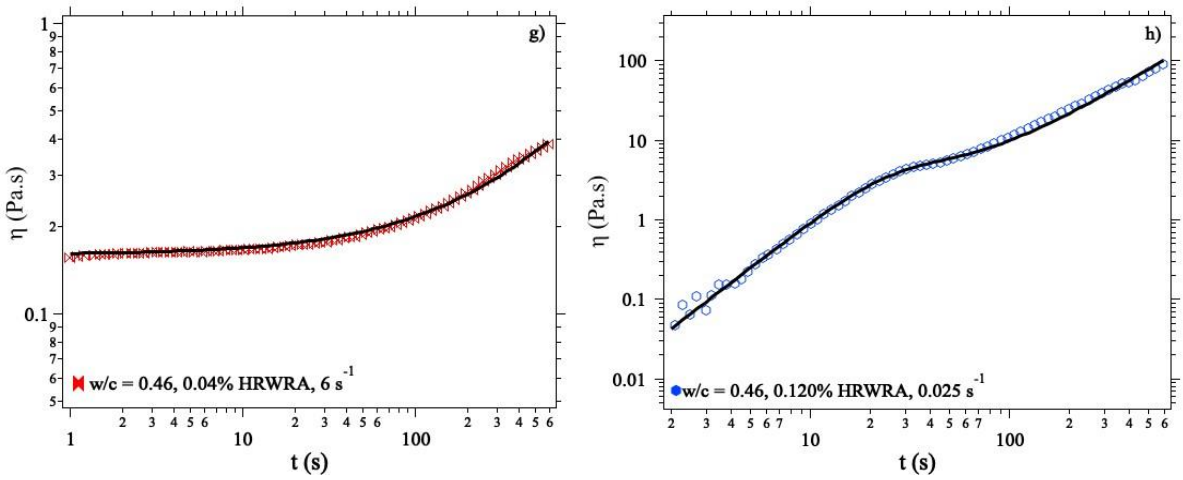

Figure 7.12 Time evolution of the viscosity of a cement paste at a) w/c = 0.25, with a concentration of HRWRA equal to 0.120% and a recovery shear rate $\dot{\gamma} = 0.1\ s^{-1}$, b) w/c = 0.25, with a concentration of HRWRA equal to 0.360% with addition of 0.41% of VMA and a recovery shear rate $\dot{\gamma} = 1\ s^{-1}$, c) w/c = 0.34, with a concentration of HRWRA equal to 0.04% and a recovery shear rate $\dot{\gamma} = 0.1\ s^{-1}$, d) w/c = 0.34, with a concentration of HRWRA equal to 0.360% and a recovery shear rate $\dot{\gamma} = 0.1\ s^{-1}$, e) w/c = 0.40, with a concentration of HRWRA equal to 0.120% and a recovery shear rate $\dot{\gamma} = 0.25\ s^{-1}$, f) w/c = 0.40, with a concentration of HRWRA equal to 0.360% with addition of 0.41% of VMA and a recovery shear rate $\dot{\gamma} = 0.01\ s^{-1}$, g) w/c = 0.46, with a concentration of HRWRA equal to 0.04% and a recovery shear rate $\dot{\gamma} = 6\ s^{-1}$, h) w/c = 0.46, with a concentration of HRWRA equal to 0.120% and a recovery shear rate $\dot{\gamma} = 0.025\ s^{-1}$ all pastes have the fit following the equation 41 ▬.

7.2.2.2.1 η_0 behavior

As it can be seen on the graphics of Figure 7.13, the fit parameter η_0 is depending on the recovery shear rate $\dot{\gamma}_r$, but more interestingly it evolves in a similar way than the rheological curve. This similarity can be explained by the fact than $\eta\left(\dot{\gamma}_r\right)$ is the plateau value of the fit and therefore acts as a pseudo-steady-state value on a similar way than the value of $\eta\left(\dot{\gamma}\right)$. The value difference can be explained by the fact that in the first case, the sample is pre-sheared at a higher shear-rate and the fact that the value of the viscosity η and η_0 are not measured at the same time. Thixotropy depends on shear history and time [124].

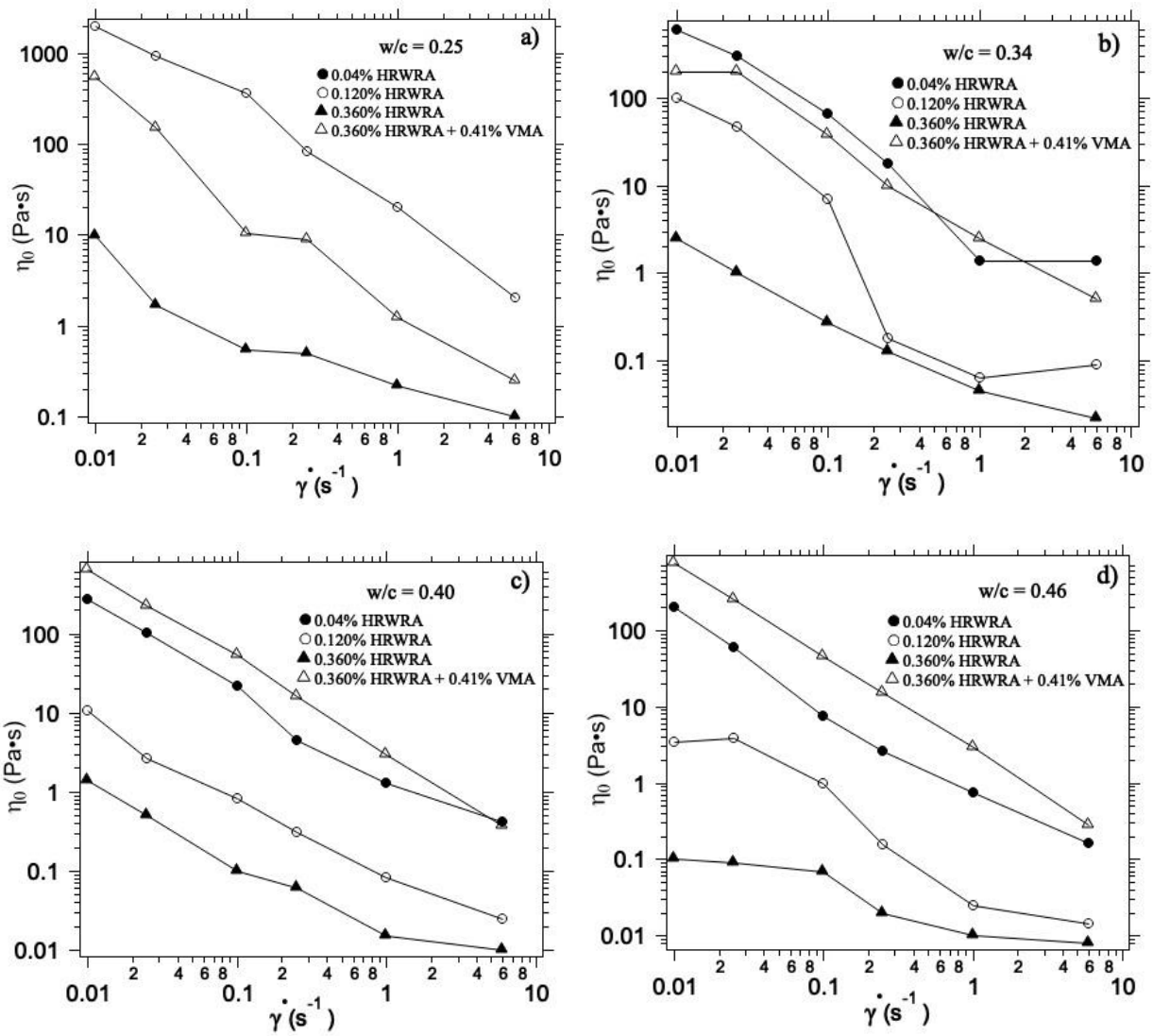

Figure 7.13 a) evolution of the fitting parameter η_0 from equation 41 as a function of the recovery shear-rate of 0.01 s-1, 0.025 s-1, 0.1 s-1, 0.25 s-1, 1 s-1 and 6 s-1 for a cement paste at a fixed w/c = 0.25 and changing HRWRA concentration of 0.04% ●, 0.120% ○, and 0.360%▲. The last paste has also been tested with an addition of 0.41% of VMA △. All the curves are obtained with the same concentrations of HRWRA but with different water to cement ratio. b) w/c = 0.34. c) w/c = 0.40. d) w/c = 0.46.

7.2.2.2.2 α behavior

Looking at the long-term thixotropy, the fit parameter α is plotted as a function of the shear-rate for all the experiments represented in Figure 7.14, and one can realize than for most of the experiments, α ≈ 1. It means that the viscosity evolves linearly with time for a timescale

$t \gg \tau_2$. The linear evolution of η (t) has already been studied in [125] and has been attributed to the early hydrates formed between cement grains, developing a network connected by CSH bridges. Therefore, the long-term evolution of the thixotropy may be attributed to the precipitation of the hydrates at the surface of the cement particles, and may consequently be the result of the chemical reaction occurring in the suspension during the dormant period. In order to prove this assumption, similar experiments have been carried out with a suspension of quartz with a similar particle size distribution than the cement, which does not react but also displays attractive interaction. As it can be observed on the data of the right chart of Figure 7.15, there are important differences between the recovery of a cement paste and a quartz flour paste: for the quartz flour experiment the recovery of the viscosity can be approximated by the simplified equation 2 which does not take into account the linear increase of the viscosity at long-time. Thus, the second motor of the thixotropy may be due to the reactivity of the cement particles.

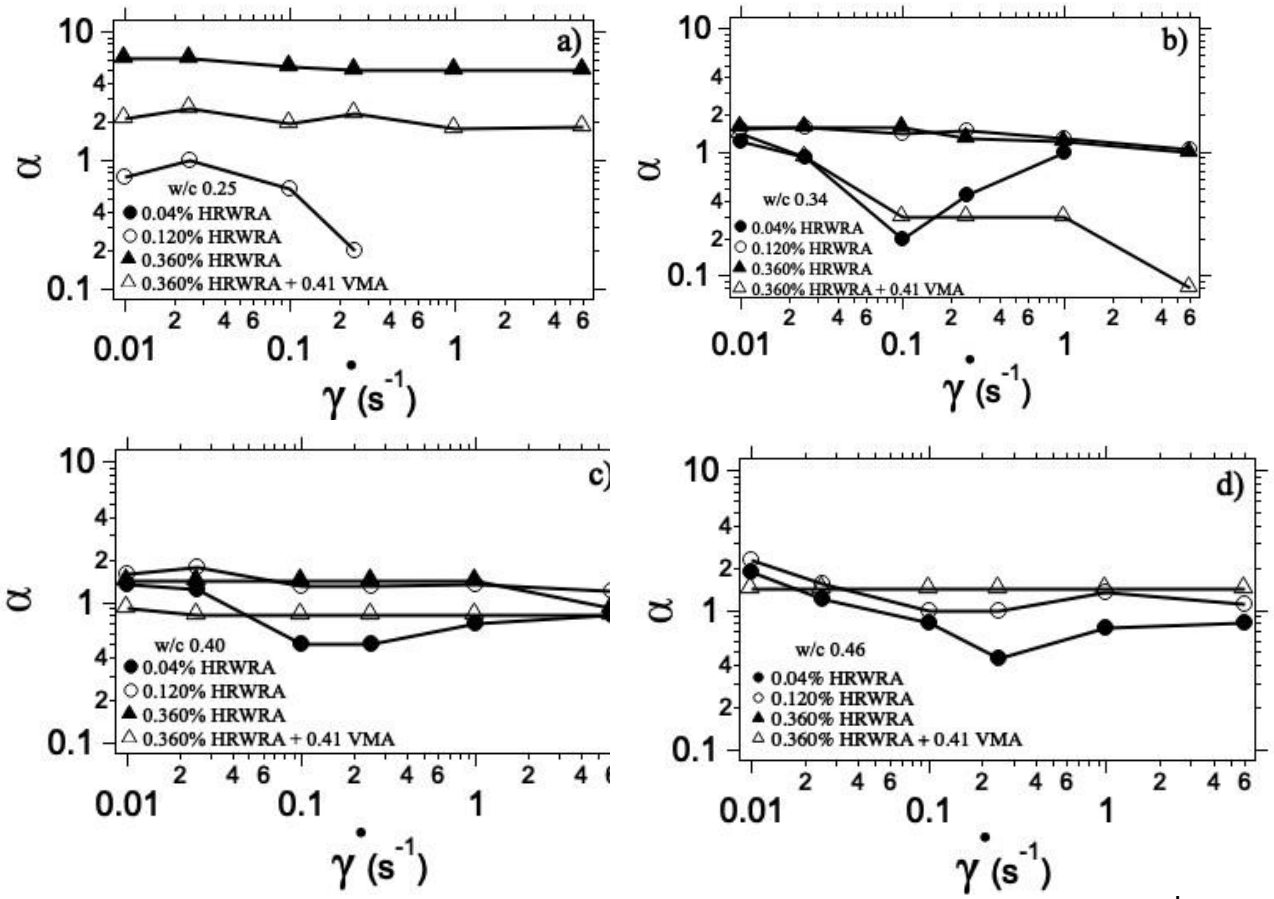

Figure 7.14 a) Value of the fit parameter α as a function of the recovery shear-rate $\dot{\gamma}_r$ for the cement paste at a w/c = 0.25 and changing HRWRA concentration of 0.04% ●, 0.120% ○, and 0.360% ▲. The last paste has also been tested with an addition of 0.41% of VMA △. b) w/c = 0.34. c) w/c = 0.40. d) w/c = 0.46.

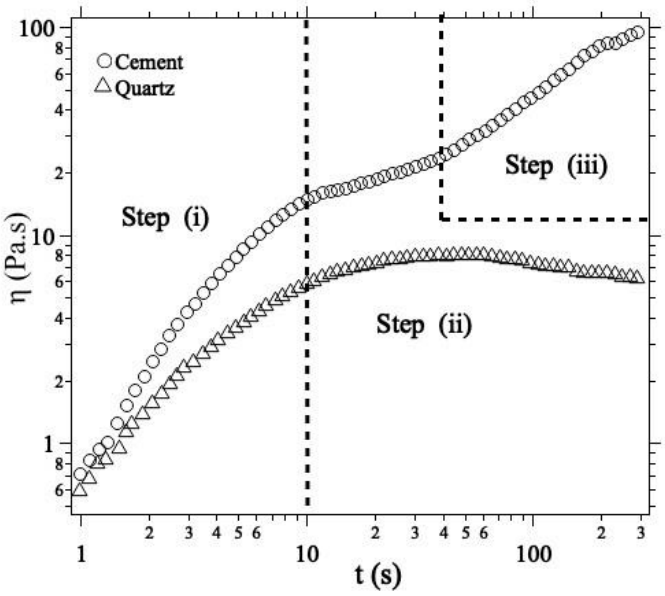

Figure 7.15 Time evolution of the viscosity of a cement paste at w/c = 0.34 with a concentration of HRWRA equal to 0.08% and a recovery shear-rate $\dot{\gamma}$ 0.1s^{-1} (upper curve ○) and the time evolution of the viscosity of a quartz flour paste at a w/q = 0.40 without HRWRA and a recovery shear-rate $\dot{\gamma}$ = 0.1 s^{-1} (bottom curve △).

7.2.2.2.3 β behavior

In all the experiments the values of τ_2 range in time values interval between 100 and 200 s. No correlation with the recovery shear-rate or the additive concentrations has been determined. The fact that τ_2 is almost constant in all experiments could be a hint that it is only related to the material chemistry. In a similar way, the value of β obtained using the fit described in Equation 41 is represented in the graphics of Figure 7.16 as a function of the shear-rate for different HRWRA concentrations and water contents. For all the w/c, the values of β are close to 1 but in some cases, the necessity of a parameter β≠1 is needed in order to correctly fit the data. As discussed previously, β≠1 means there is more than one time constant in the system due to the change of amplitude of exponential function.

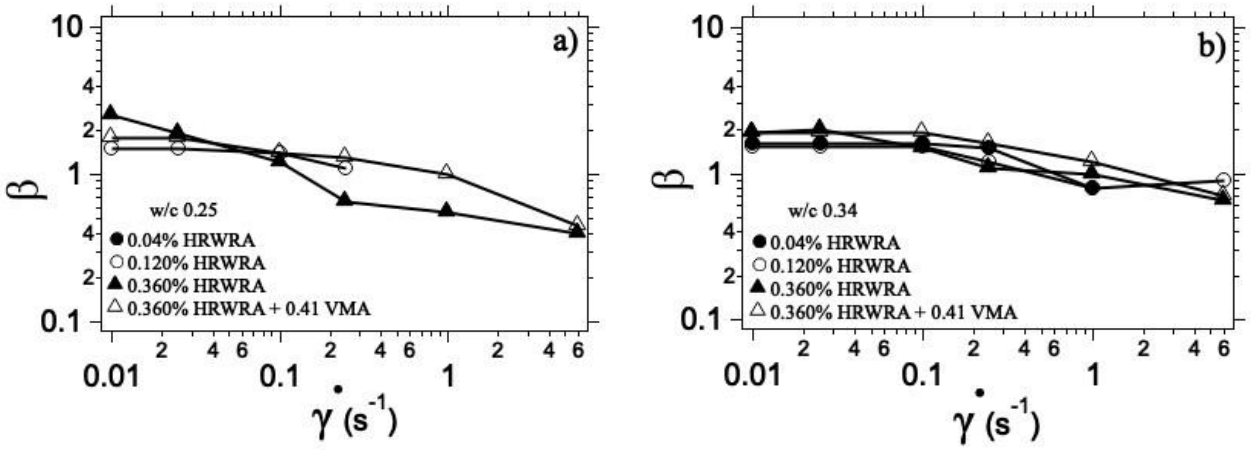

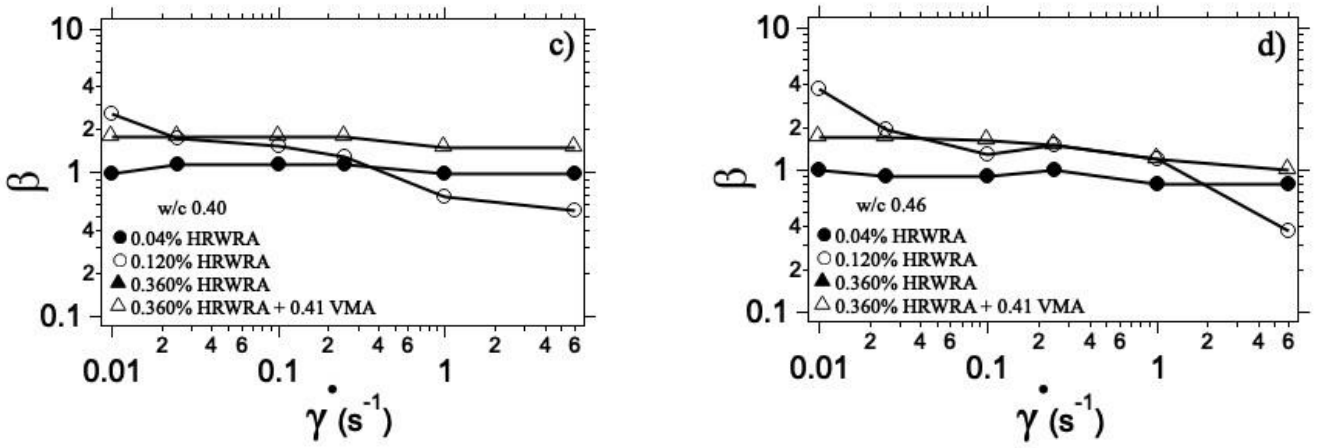

Figure 7.16 a) Value of the fit parameter β as a function of the recovery shear-rate $\dot{\gamma}_r$ for the cement pastes at a w/c = 0.25 and changing HRWRA concentration of 0.04% ●, 0.120% ○, and 0.360% ▲. The last paste has also been tested with an addition of 0.41% of VMA △. b) w/c = 0.34. c) w/c = 0.40. d) w/c = 0.46.

In order to take into account both the value of β and τ_1 that means the physical aging and its amplitude for the first kinetic due to the interaction and flocculation of particles of cement, a new parameter $\tilde{\tau}$ described in equation 4 has been computed and it is mathematically assumed this parameter allows to compare the broad spectrum in relaxation time (β+1) described in [126].

$$\langle\tilde{\tau}\rangle = \int_0^{\infty} e^{\left(\frac{t}{\tau_1}\right)^{\beta}} dt = \frac{\tau_1}{\beta}\Gamma\left(\frac{1}{\beta}\right) \qquad \text{Equation 45}$$

The values of $\tilde{\tau}$ have been plotted as the function of the shear-rate for the 4 w/c and the 4 different HRWRA concentrations in the graphics of Figure 7.17. The parameter $\tilde{\tau}$ does not seem to be dependent of both the w/c ratio and all superplasticizer concentrations tested but $\tilde{\tau}$ is highly dependent on the shear-rate, and one can remark a power-law relationship with the shear-rate: $\tilde{\tau} \propto \dot{\gamma}^{-q}$. The power-law exponent q is strongly dependent of the superplasticizer concentration: q decreases when the superplasticizer concentration increases. When a VMA is added to the suspension, q increases.

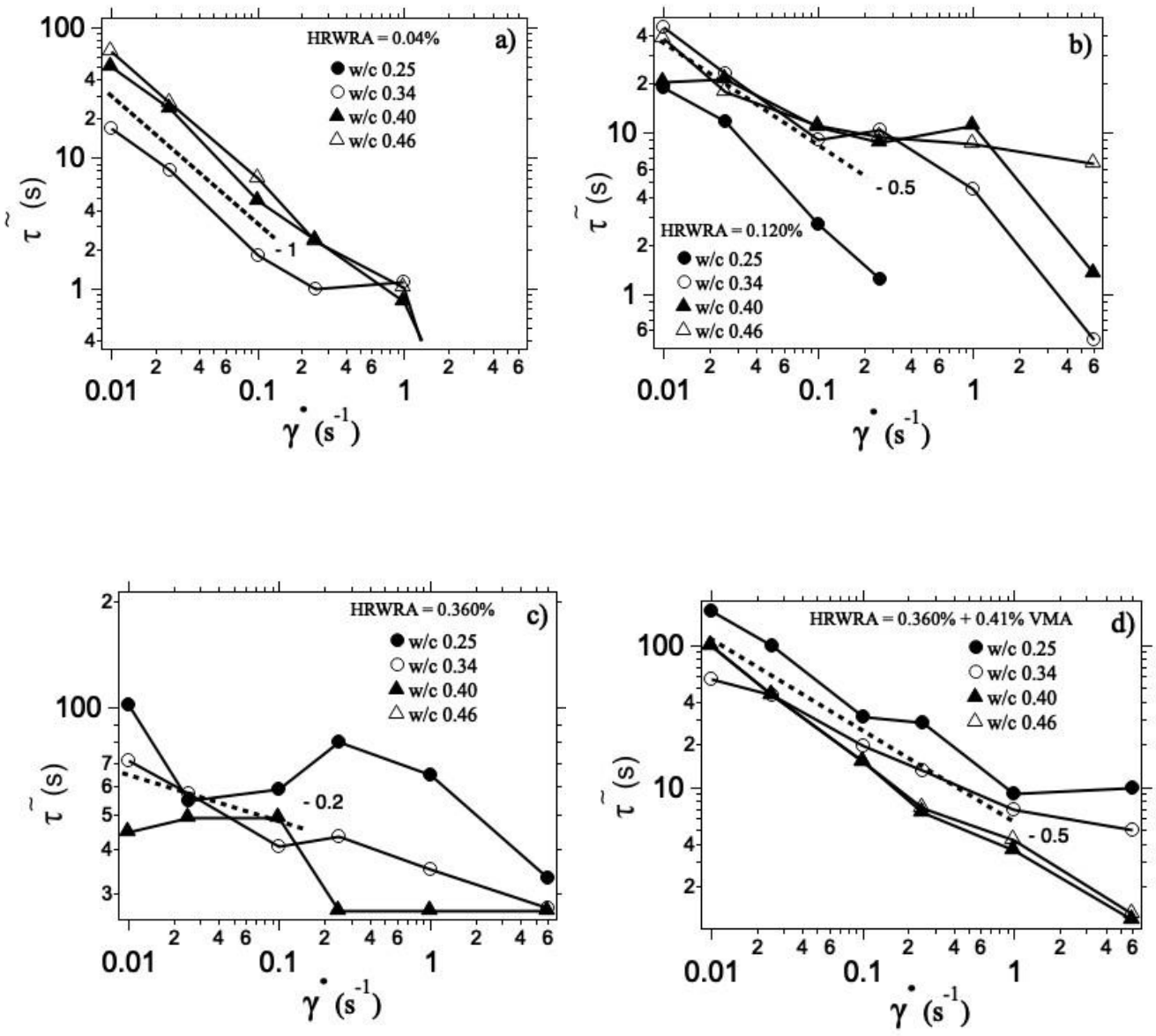

Figure 7.17 a) Value of the fit parameter τ~ as a function of the recovery shear-rate $\dot{\gamma}_r$ at a fixed concentration of polymer 0.04% for cement pastes with different w/c: 0.25 ●, 0.34 ○, 0.40 ▲ and 0.46 Δ. The dashed-line is a guide. b) HRWRA concentration 0.12%. c) HRWRA concentration of 0.36%. d) HRWRA concentration of 0.36% with 0.41% VMA added

7.2.3 Discussion

This set of experiments show the first kinetic is mainly controlled by the additives added in the cement paste. Superplasticizers are polymers adsorbing at the surface of the cement particles and therefore they changing the interactions between the cement particles.

Meanwhile, the viscosity modifying admixture used in this study possesses long chains which adsorb at the surface of different cement particles bridging them together. Thus, the first kinetics is controlled by the interaction between the cement particle and its origin is purely physical. A change in the interactions between the cement particles leads to a change in the first floculation kinetics. It can be explained by the fact that the lower is the interaction between the particles; the lower is the probability for two cement particles into contact to form a cluster because they can escape each other even at low-shear. This is observable in the experiment of Figure 7.17, where the higher is the shear-rate and the higher is the difference between the value of $\tilde{\tau}$ measured at different polymer concentrations.

In those build-up experiments, the increase of the cement viscosity over time has been observed as a consequence of both chemical and physical aging. By using a non-reactive thixotropic paste and by changing the physical interaction between the cement particles with the additives concentrations, the chemical and physical contributions to the thixotropic behavior can be uncoupled. Just after the end of the mixing, a rapid organization of the network occurs due to the particles mobility and clusters of particles are created because of their attractive interactions [127]. As a consequence, the average number of contacts between particles, initially very low after mixing, increases quickly leading to an exponential increase of the yield stress [128]. Once few contacts are connecting each particle, in a time scale which is about τ_1, the newly formed clusters are less mobile than single particles and the number of contacts and by consequence the yield stress is evolving slowly with time: a steady state is reached which corresponds to the viscosity plateau of the step (ii). From the moment at which the cement particles are mixed with water, dissolution of the cement and then precipitation of the hydrates at the surface of the particles occur. These phenomena are only due to the material chemistry and depend neither of the particle interactions nor of the presence of clusters, which explains why the time scale τ_2 is almost constant in all experiments. The precipitation of the hydrates leads to an increase of the total surface and therefore induced an increase of the number of contacts which leads to an increase of the yield stress. The viscosity evolution during precipitation phase is slower when compared to the physical aging, being linear with time as opposed to an exponential increase with time during the physical aging period. The time constant τ_2 value can be interpreted as the time needed to double the viscosity due to the precipitation of the hydrates on the particles surfaces. It is well known that a paste partially rigid due to the setting process is more thixotropic than a fresh one (like the one we used in those experiments): this can be explained by the fact that once re-mixed, the already existing layer of hydrates is destroyed and then precipitated much faster when the mixing stops which leads to a smaller value of τ_2 but also a couple contributions of chemical and physical aging.

7.2.4 Heat rate evolution of suspensions without admixtures

Figure 7.18 shows the evolution of the heat rate of suspensions without admixtures. At the beginning of hydration (pre-induction and induction periods), the curves show an apparently same development, the grains of cement are dissociated and the first hydration products (portlandite and CSH) are formed on its surface. During the acceleration period, it can be observed a decrease of the maximum hydration rate as well as a retard of cement hydration with the increase of water to cement ratio. This delay is associated with the low concentration of grains of cement and their large distance between them, delayed the growth of products at the surface of cement particles. A deacceleration period it can be observed the same development with a difference of heat rate. A clear effect of water to cement ratio on the hydration kinetics is observed in the result of calorimetry.

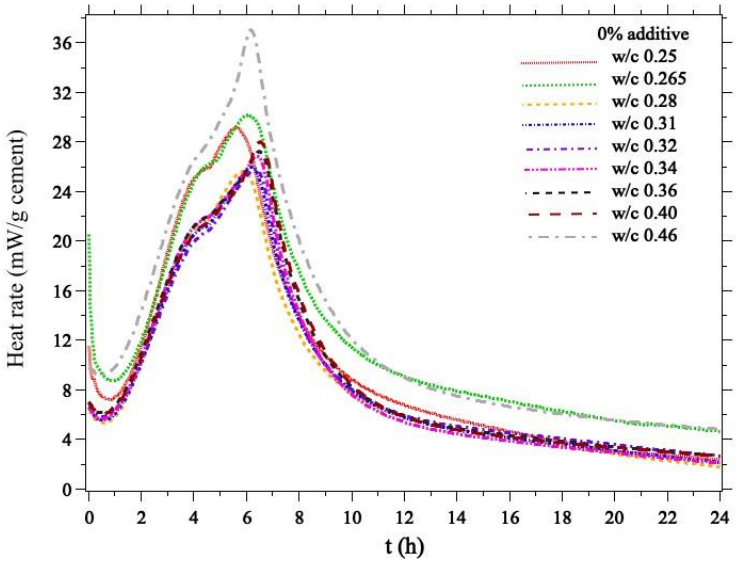

Figure 7.18 Evolution of heat rate as a function of time for pastes with water to cement ratios of 0.25, 0.265, 0.28, 0.31, 0.32, 0.34, 0.36, 0.40, and 0.46 without additives.

7.2.5 Heat rate evolution of suspensions and the influence of HRWRA and VMA

The influence of HRWRA concentration and its combination with a VMA was observed in heat rate evolution. Due to the hydration kinetics of cement pastes are directly linked to the mixing energy as was studied in [49] a mixing protocol has been established as is described in

section 6.4, in order to keep the same experimental conditions and reject the effect of mixer type on the hydration kinetics.

Table 7.3 shows the summary of the heat of hydration of cement suspensions, whereas the time evolution of heat rates is presented in Figure 7.19. In this plot, the concentration was fixed and the water to cement ratio was changing. As expected the higher is the water to cement ratio the higher is the hydration time as well. Both the dormant period and acceleration period are impacted, observing a lower heat flow rate at the end of the dormant period (second peak of the curve). It is known that at higher water to cement ratio, the particles of cement has a larger distance between them, leading to weaker network during the hydration process [90]. It can be observed that this behavior is kept for all concentrations analyzed. With the aim to compare the influence of HRWRA and VMA, the curves were also plotted at fixed water to cement ratio and changing the concentration of additives as is shown in Figure 7.20. It can also be observed that addition of HRWRA on the suspensions retard the cement hydration and decrease significantly the maximum hydration rate, especially in the suspensions with a high content of HRWRA and even with the content of VMA. HRWRA are polymers that act as dispersants, due to they are absorbed on the surface of the cement grains (alite and aluminate) and therefore changing the interactions inducing steric and electrostatic repulsion, especially at an early age, promoting a dismantling of the flocculated structure [129]. The higher is additive concentration the higher is the retarder of hydration reactions (lower yield stress), existing a linear relation between them [130].

Table 7.2 Heat evolution summary of the suspensions studied

	0.04% HRWRA		0.120% HRWRA		0.360% HRWRA		0.360% - 0.41% HRWR-VMA	
w/c	Max temp. (ºC)	Time (h)	Max temp. (ºC)	Time (h)	Max temp. (ºC)	Time (h)	Max temp. (ºC)	Time (h)
0.25	41.72	5.38	40.68	5.66	42.74	6.52	44.07	6.62
0.34	38.20	6.33	40.39	6.39	39.35	8.13	40.63	8.13
0.40	37.02	6.76	38.74	6.57	38.67	8.51	38.18	9.18
0.46	36.71	7.20	37.7	7.50	37.31	8.97	36.36	9.49

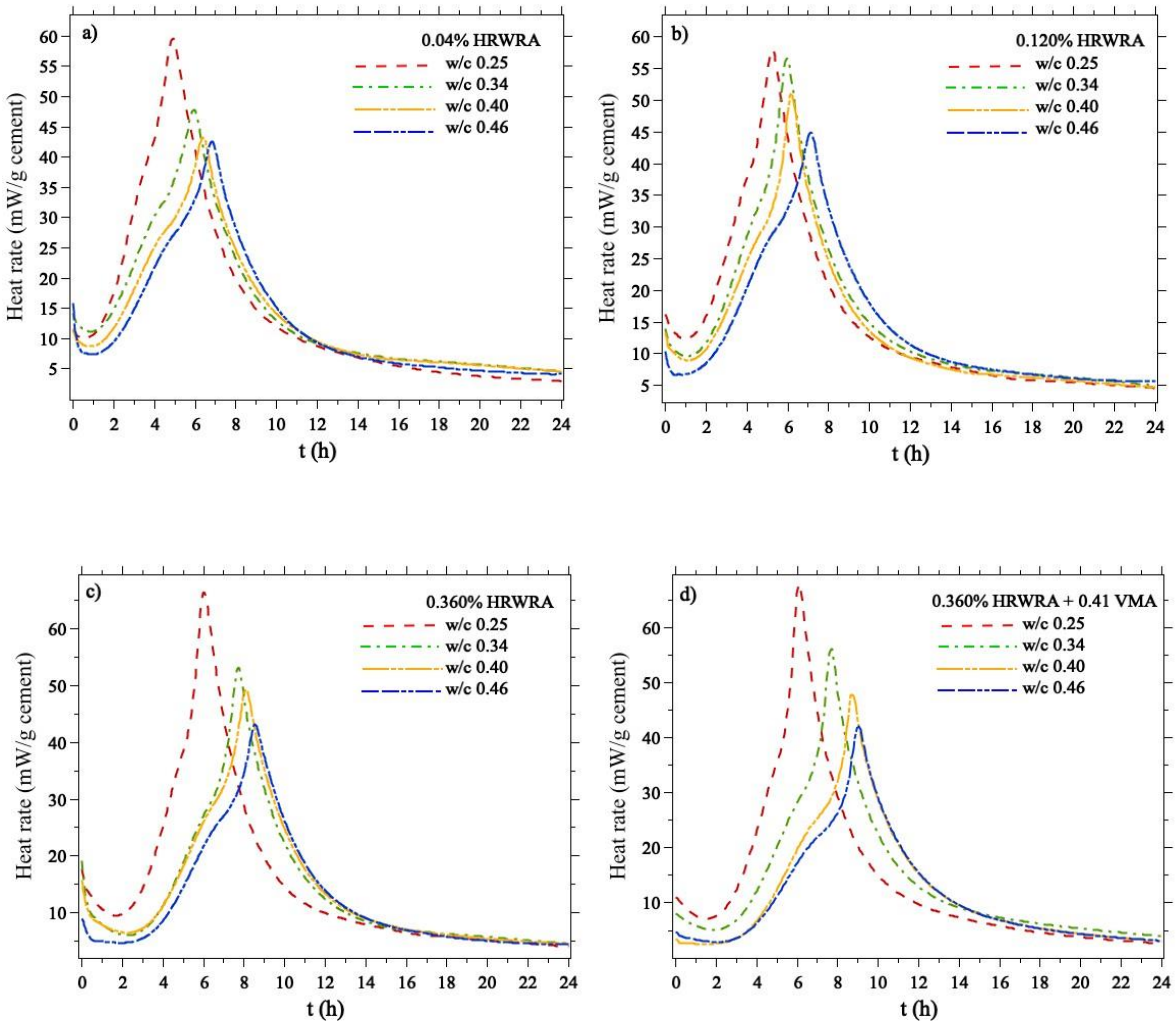

Figure 7.19 a) evolution of heat rate as a function of time for a fixed HRWRA concentration of 0.04% and changing water to cement ratio of 0.25 - - - - , 0.34 - · - · - · , 0.40 - ·· - ·· - ·· and 0.46 -- ·· -- ·· . b) 0.120% HRWRA . c) 0.360% HRWRA d) 0.360 HRWRA + 0.41% VMA

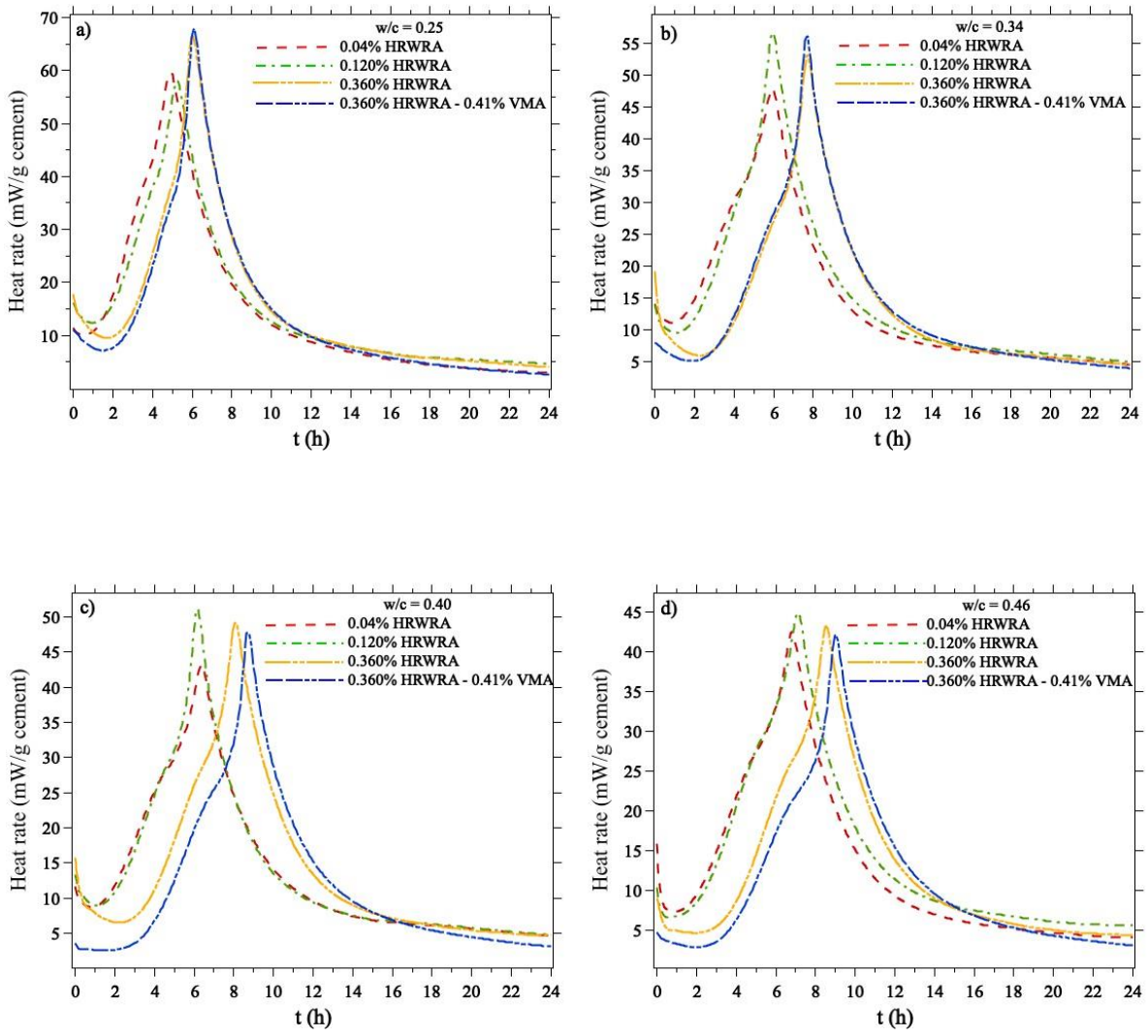

Figure 7.20 a) evolution of heat rate as a function of time for a fixed water to cement ratio of 0.25 and changing HRWRA concentration of 0.04% - - - - , 0.120% - · - · - · , 0.360% - ·· - ·· - and 0.360% HRWRA + 0.41 VMA -- ·· --. b) 0.34 . c) 0.40 d) 0.46.

7.2.6 Strength evolution of suspension without admixtures

The strength evolution of cement suspensions without additives is shown in Figure 7.21. As it can be observed, a high strength is related to less water to cement ratio. In fact, the setting time, rheological behavior and hydration kinetics change their behavior when water to cement ratio decrease [131]. The evolution of strength can also be associated with the evolution of heat rate over time, finding a good correlation between them [107]. For the plots of Figure 7.21, the shape of the strength curve can be divided into three zones. The first zone (around of

the first minutes) corresponds to the increase of viscosity due to the physical and chemical aging, which is a result of agglomeration of cement particles and the bridges formed by the connection of the first hydration products (portlandite, ettringite, and CSH). This period covers the pre-induction and dormant period where the ion dissolution is promoted until a barrier of products becomes the reaction slow. A second zone is characterized by the gain of strength and the setting is presented (around 2 and 10 hours). This zone corresponds to the acceleration period which is characterized by precipitation of hydration products. Finally, the diffusion mechanism decreases the kinetics, nevertheless, the growth of CSH continue due to the continuous hydration of alite and belite. The propose of this plot is to contrast the results of DWS with the development of kinetics of cement suspensions, identifying the zones discussed above into the autocorrelation function development results.

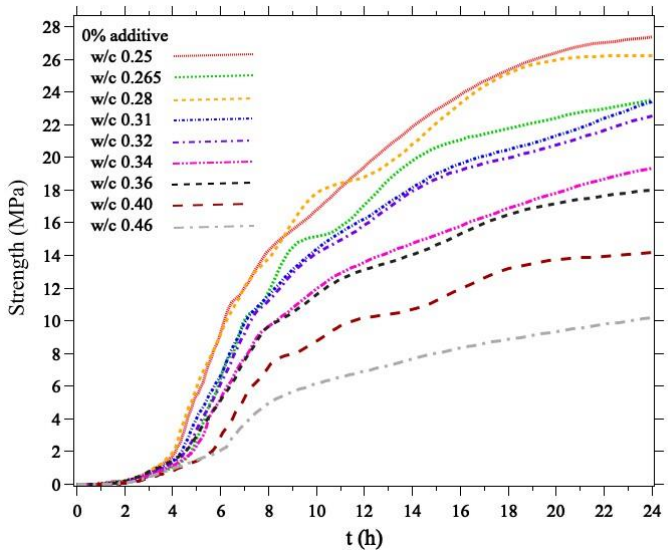

Figure 7.21 Strength evolution as a function of time for a cement suspensions prepared at a water to cement ratio 0.25, 0.265, 0.28, 0.31, 0.32, 0.34, 0.36, 0.40 and 0.46

7.2.7 Strength evolution of suspensions and the influence of HRWRA and VMA

The retardation of cement hydration reaction discussed above due to the addition of HRWRA is also perceived in the setting and hardening of the suspensions. Table 7.2 shows the result of strength evolution of suspensions when HRWRA is added at three concentrations, and when the higher concentration is combined with VMA. Figure 7.22 shows the result of strength evolution at a fixed concentration and changing the water to cement ratio. As it can be observed the higher is the water to cement ratio the lower is the final strength, observing also

an increase of initial and final setting times. It is known that the reduction of reactive powder of cement, decrease the evolution and gain of strength in cementitious materials. The large distance between particles due to the high content of water and the dispersive effect of the HRWRA decrease the kinetics of hydration. On the other hand, a high content of water dissolves quickly the phases of cement and then the gain of strength is limited.

Figure 7.23 shows the evolution of strength at fixed water to cement ratio and changing the HRWRA concentration. As it can be observed, the higher is the concentration of HRWRA the higher is the evolution of strength in all cases. This is not coherent with scientific and practical evidence, nevertheless, this result is due to the separation of phases (cement and water) as a consequence of high content of additive, therefore, the result of strength in these cases corresponds to sedimentation of paste and its direct contact with transductor of ultrasonic reflection equipment. As respect to low content (0.04%), medium content (0.120%) of HRWRA and the combination with VMA, a not significant variation of final strength is observed and this can be corroborated by the results of heat rate in the same suspensions.

Table 7.3 *Strength evolution summary of the suspensions studied*

w/c	0.04% HRWRA			0.120% HRWRA			0.360% HRWRA			0.360% HRWRA + 0.41 VMA		
	Inittial Setting Time (h)	Final Setting Time (h)	Strength 24 h (Mpa)	Inittial Setting Time (h)	Final Setting Time (h)	Strength 24 h (Mpa)	Inittial Setting Time (h)	Final Setting Time (h)	Strength 24 h (Mpa)	Inittial Setting Time (h)	Final Setting Time (h)	Strength 24 h (Mpa)
0.25	1.807	3.202	31.326	2.16	3.84	26.17	1.56	3.36	39.427	1.494	3.822	28.714
0.34	2.928	5.088	20.411	1.992	3.6	20.378	1.584	3.816	33.732	3.037	6.072	20.333
0.40	2.928	4.968	17.274	2.472	4.368	14.024	2.707	4.727	29.711	3.459	6.609	14.405
0.46	2.975	5.085	11.636	2.202	4.435	14.825	2.681	4.768	17.489	3.199	6.827	8.814

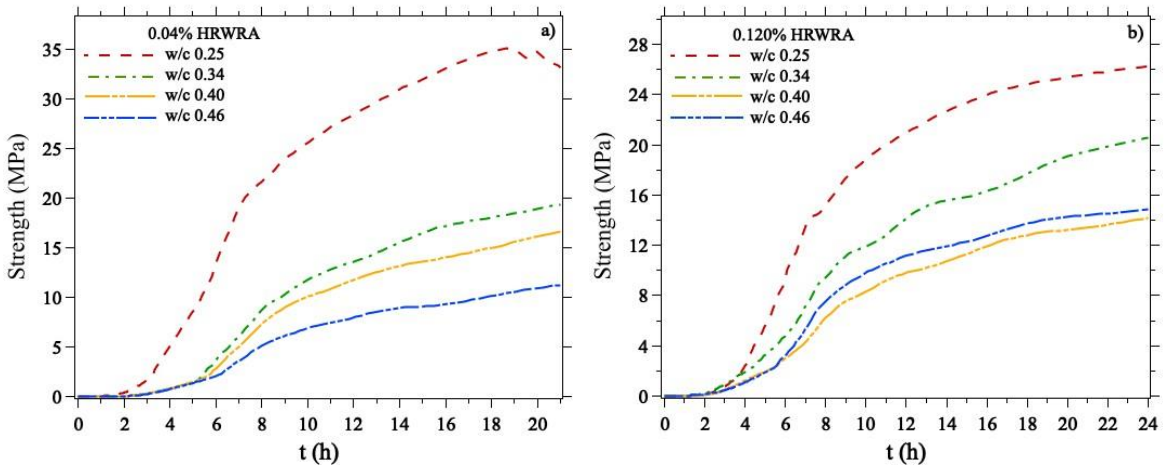

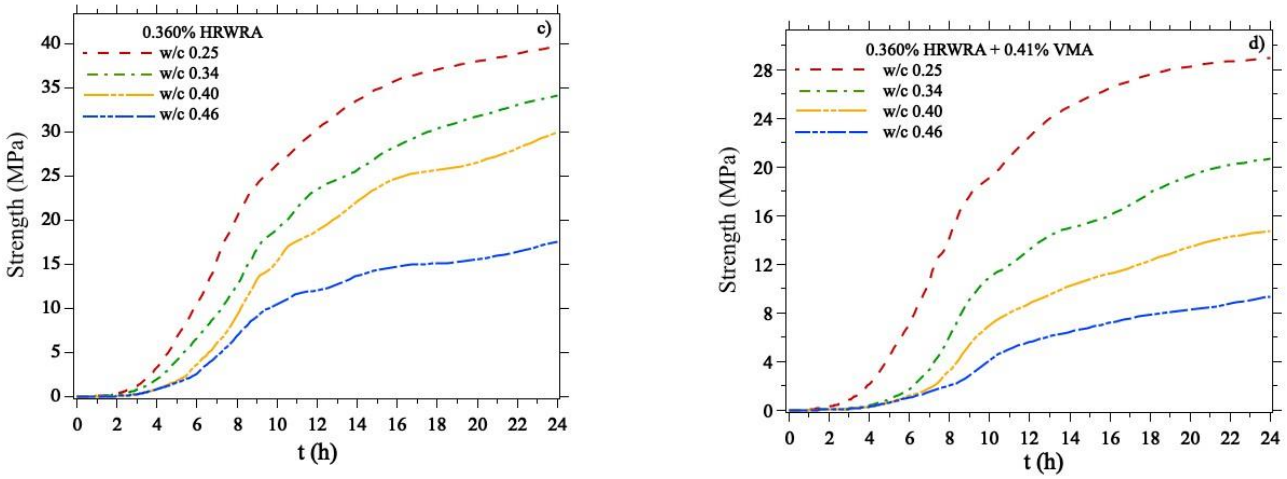

Figure 7.22 a) strength evolution as a function of time for a fixed HRWRA concentration of 0.04% and changing water to cement ratio of 0.25 - - - -, 0.34 - · - · -, 0.40 - ·· - ·· -. and 0.46 -- ·· -- ··. b) 0.120% HRWRA . c) 0.360% HRWRA d) 0.360 HRWRA + *0.41% VMA*

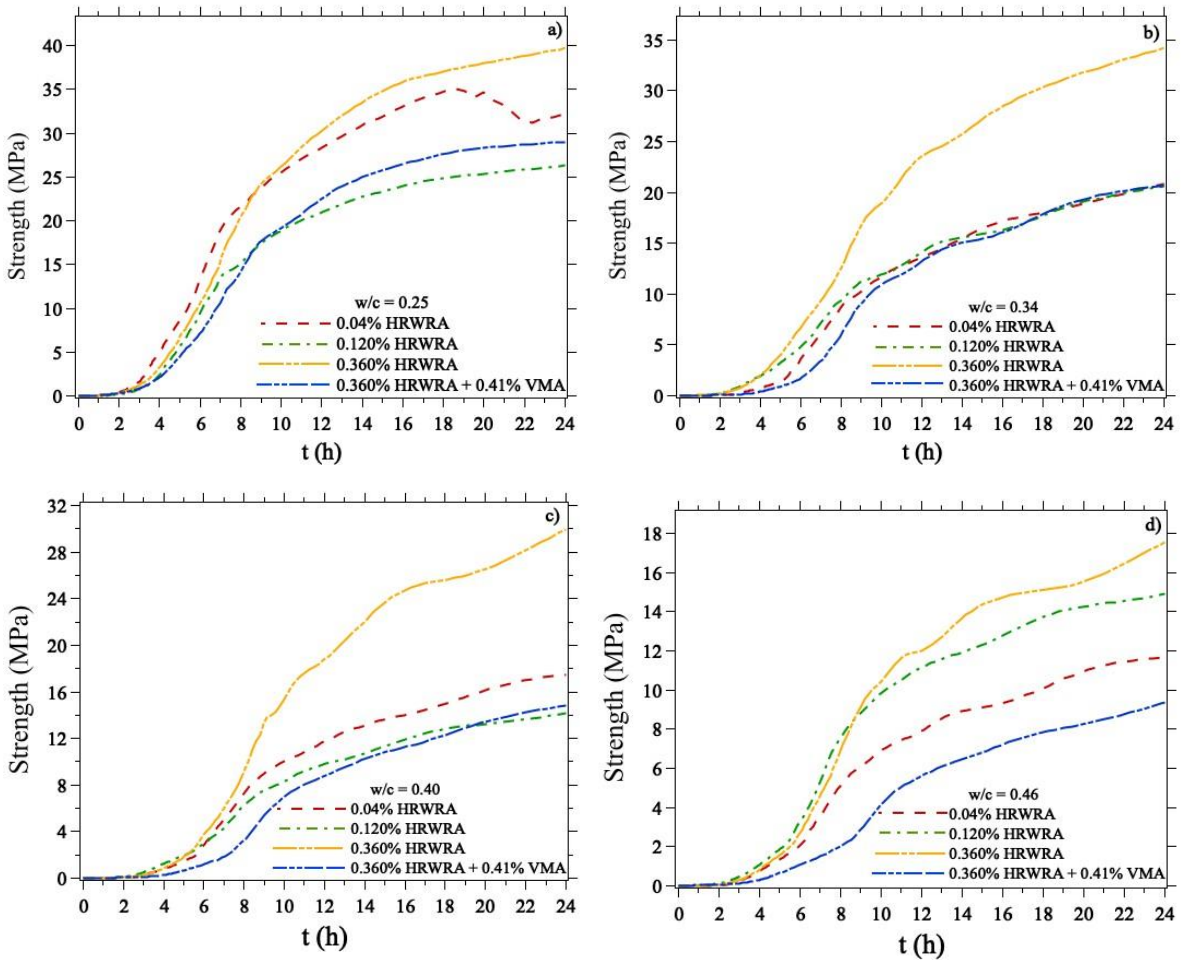

Figure 7.23 a) strength evolution as a function of time for a fixed water to cement ratio of 0.25 and changing HRWRA concentration of 0.04% - - - -, 0.120% - · - · -, 0.360% - ·· - ·· - and 0.360% HRWRA + 0.41 VMA -- ·· --. b) 0.34 c) 0.40 d) 0.46.

7.2.8 Discussion

Fresh properties of cementitious materials have been widely studied by viscosity, yield stress, and thixotropy, where the additives like HRWRA are the key in their behavior. The superplasticizer (HRWRA) delay the time of setting and therefore a long workability time is obtained. The experiments show that the hydration kinetics changes due to addition of HRWRA and VMA in the cement suspensions. Concentration of 0.04% and 0.120% that corresponds to low and optimal values show a steady state in both calorimetry and strength development, while higher addition of HRWRA show a significant modification of the kinetics retarding the formation of hydration products and delaying the aggregation process due to dispersive effect of the additives. Furthermore, phase separation can be observed at high content of HRWRA which is reduce by VMA addition due to the thickening effect on the suspensions. Our results complement the discussions about thixotropy development at 7.2.2, show that the effect of additives is present from the first minutes modifying the interaction and then aggregation of particles until the chemical reactions due to dispersive effect and by the optimal content of HRWRA and VMA the working time can be prolongated avoid phase separation.

7.2.9 Dynamics of cement suspension

Multiple light scattering experiments were used to study the dispersion particles of cement in water. By illumination with the laser, the backscattering light forms a speckled pattern which reveals the dynamics of internal structural changes of cement suspensions. The dynamics of cement suspensions is observed by determination of the intensity autocorrelation function of the set of images taken by diffusing wave spectroscopy technique. The experiments were carried out according to experimental design described in 6.2 and the results are presented and discussed below.

7.2.10 Intensity autocorrelation function of experiments

Just after the mixing of suspensions, the intensity autocorrelation function g_2 was determined at defined time intervals, therefore, the recovery of cement particles network or build-up condition was studied, finding that both suspensions with additives and without additives, the evolution of g_2 can be described by empirical equation 46.

$$g_2(t) = base + A\, e^{\left(-\left(\frac{t}{\tau}\right)^{\alpha}\right)} \qquad \text{Equation 46}$$

The time evolution of intensity autocorrelation function can be fitted with equation 46 with 4 fitting parameters as is showed in Figure 7.21, each one parameter controls the adjustment of

the curve. In the empirical model A is the value of intensity autocorrelation function at the plateau in the beginning regime of intensity, τ is the decay of the intensity which changes through the experiment, α is a power law-exponent of the relationship between intensity and time and base is a constant value very close to 1 that describes the long time asymptote of the correlated function. Figure 7.21 the intensity correlation function decay an experiment carried out on white portland cement suspension of water to cement ratio 0.34 without additive from a time 0 to one hour of the experiment are plotted. The higher is the time the higher is the value of decay time τ of intensity, keeping the value of α constant in the curves. The fit of the equation with experimental data is considered agreement.

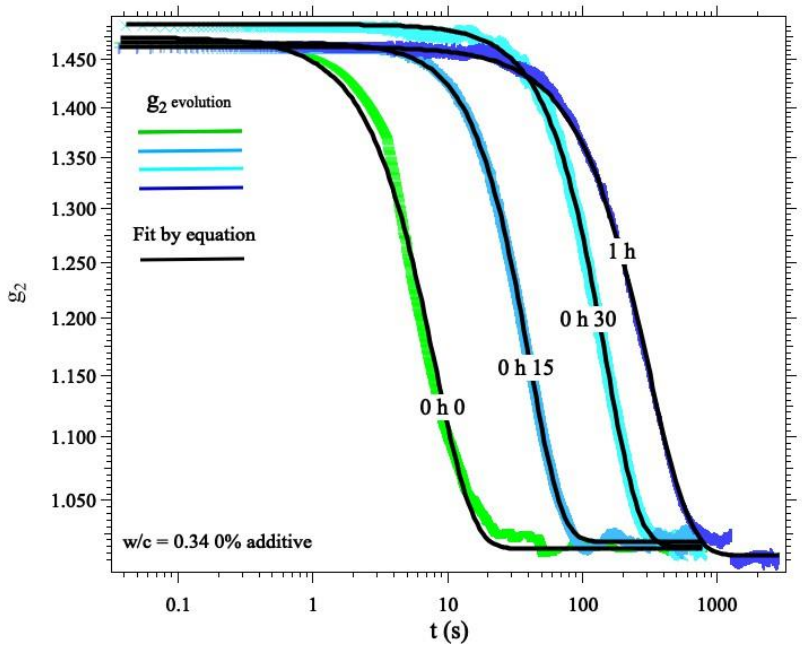

Figure 7.24 Time evolution of the intensity autocorrelation function g_2 of a cement paste at a w/c = 0.34 without additives at 0h0 ____ , 0h15 ___, 0h30 ___ and 1 h ___ of experiment and the fit following the equation 46 ____.

7.2.10.1 Intensity autocorrelation function on suspensions without additives

The autocorrelation functions determined by the analysis of a set of images taken on the suspension without additive are given from Figure 7.25 to Figure 7.33. The autocorrelation function was taken in a long lag time regime (3000 s). It can be observed that the behavior exhibit a two modes: A gradual evolution from a rapid decay at the first minutes ascribed to fast mobility of particles of cement until became it less relaxed as the setting time and

hardening is reached. These two modes can be observed in the plots of evolution of τ as a function of time, identifying two slopes over the time. As can be observed in the graphs of the evolution of the decay time τ as a function of time, the value of τ at the beginning of all experiments decreases as the water to cement ratio increases, this is due to the retard of hydration discussed above. A large distance between particles delay the agglomeration at in cement grains, therefore, its hydration kinetics as well as its strength development is delayed, as it was demonstrated in calorimetry and ultrasonic reflection results. The effect of flocculation of cement particles due to the attractive force present during the first contact between them can be observed in the increase of characteristic decay time of the light intensity autocorrelation function from the first minutes of study. In fact the first zone of strength evolution can be related with the first curves of intensity autocorrelation function (g_2) moment in which a fast mobility is observed, related with the pre-induction and the beginning of the dormant period of calorimetry test as well.

The experimental data obey the fit law proposal in all cases analyzed in this study, except for some curves that present a noise at a certain time, which will be discussed. Just after of mixing and once placed the suspension into the sampler, the experiment was carried out, finding a rapid decay time (less value of τ) which is less when water to cement ratio is higher. This is equivalent to say that the particles have fast mobility due to active Brownian motion [132], even though shows short duration, around some minutes. The mobility of particles decreases when the particles interacting forming clusters and when the ion dissolution occur, then first hydration products start to grow on the surface of cement, linked the particles by bridges of CSH. This behavior can be related with thixotropy development discussed in 3.2, where the increase of viscosity is a consequence of both chemical and physical aging, furthermore, this interval of time corresponds to pre-induction period and first zone of calorimetry and ultrasonic reflection tests.

As time goes by, the gradual evolution of decay time continues as the concentration of portlandite and CSH increase. In this moment induction period (called dormant period as well) is present, and the hydration becomes slow, as is showed in the heat flow of calorimetry curves. This decrease of reaction is due to metastable barrier discussed by several researchers mentioned in 2.1.4. A layer of CSH is formed impeding the migration of water, then this layer is broken due to osmotic pressure generating microcracks which can be detected by the noise of autocorrelation function particularly in experiments of w/c = 0.31, w/c = 0.32, w/c = 0.36. In order to prove this assumption, micrographics at time of noise have been taken with the aim to identify some products at the moment of the noise into the experiment. These micrographics can be observed in Figures 7. 28 and 7.29, where longer ettringite needles, portlandite, and gel CSH can be perceived which is an indication that the products have been formed on the surface of cement particles. The following curves of intensity autocorrelation functions become steady when the acceleration period starts, observing a constant strength evolution observing a second and third zone of strength development as it was discussed in

ultrasonic reflection results. This period is controlled by the growth of CSH and the nucleation of products, all calcium sulfate has been dissolved finalizing the set of suspensions and the gain of strength is gradual. In this period the evolution of decay time becomes large than at the beginning of the experiment, but continue to increase as the experiment is in progress. This fact can be related to the diffusion process, where the suspension continues to gain strength gradually.

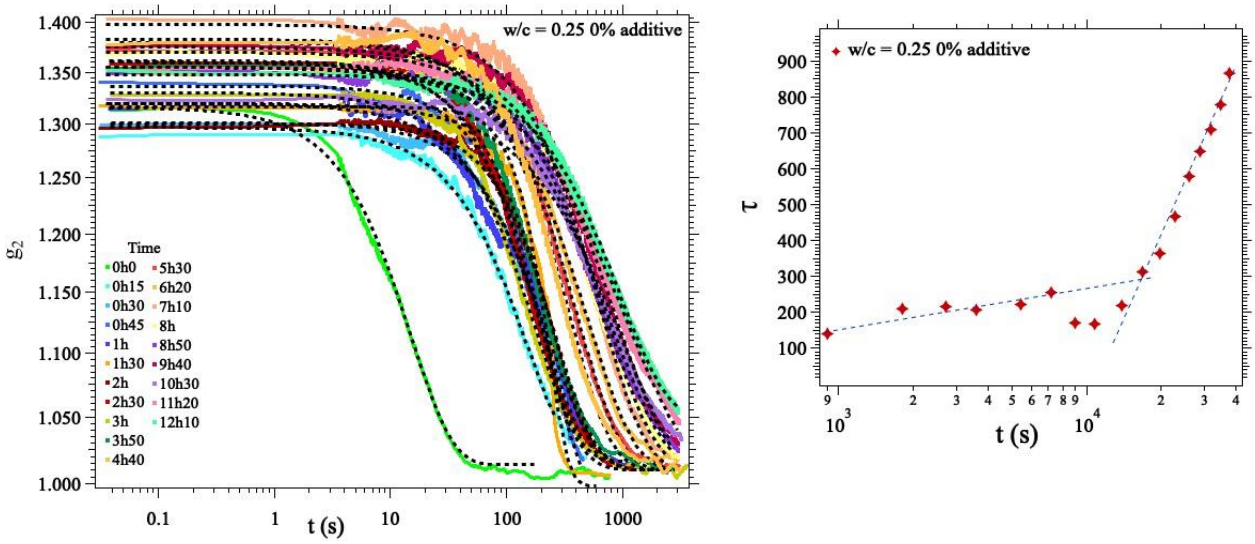

Figure 7.25 Left: Autocorrelation functions for suspension of w/c = 0.25. Discontinuous line corresponds to the fit law of equation 46. Right: Evolution of τ as a function of experimental time.

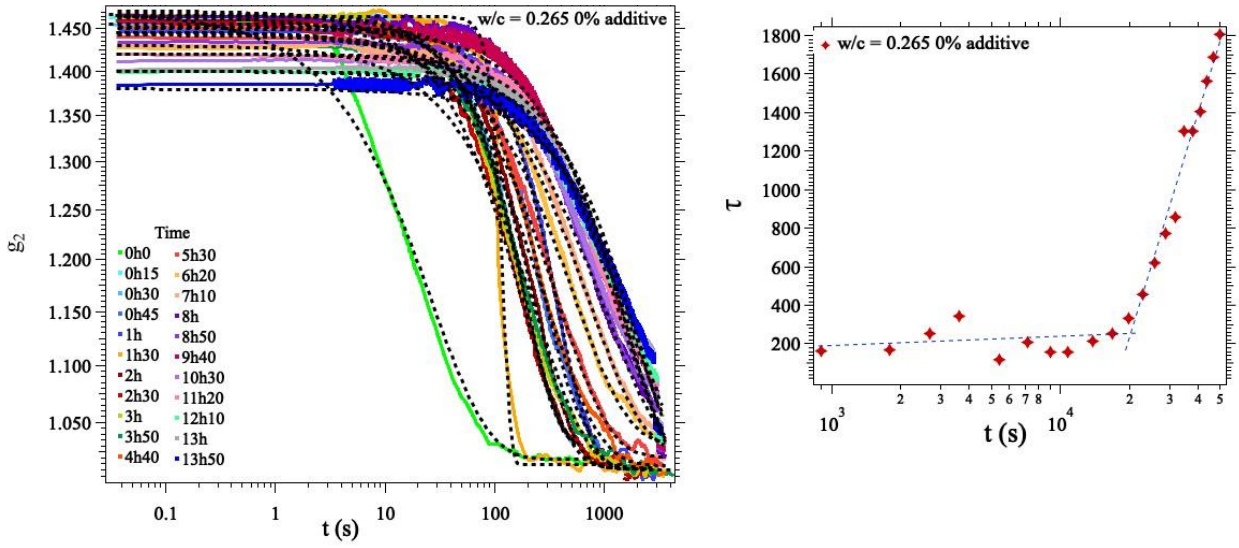

Figure 7.26 Left: Autocorrelation functions for suspension of w/c = 0.265. Discontinuous line corresponds to the fit law of equation 46. Right: Evolution of τ as a function of experimental time

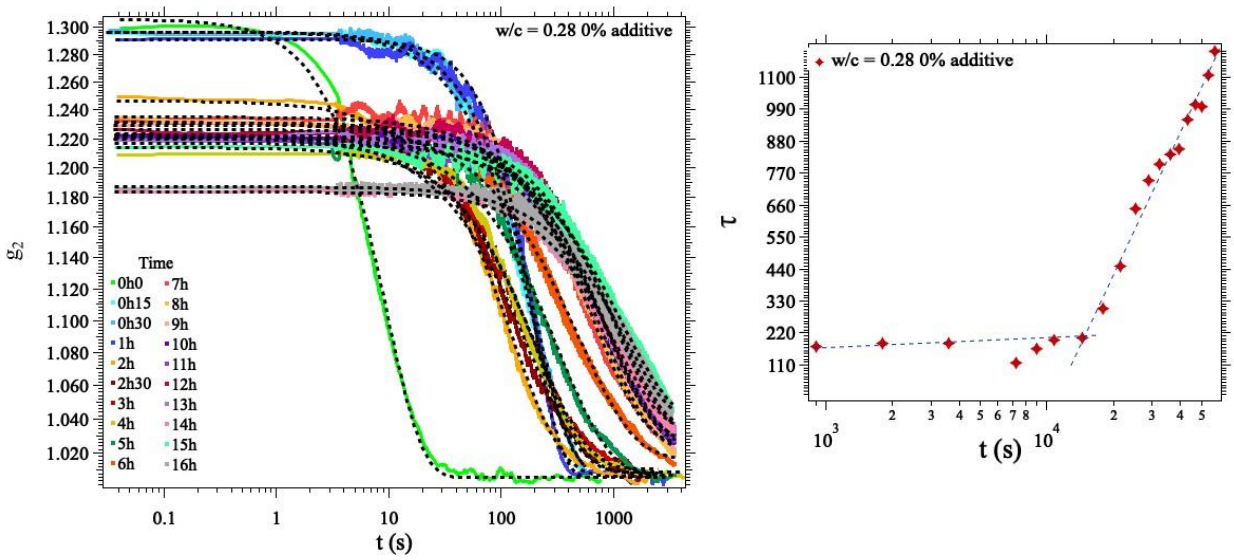

Figure 7.27 Left: Autocorrelation functions for suspension of w/c = 0.28. Discontinuous line corresponds to the fit law of equation 46. Right: Evolution of τ as a function of experimental time

An hypothesis for the mechanism responsible for the reactions of the dynamics of the paste at intermediate time and at intermediate concentration, in the fact that ettringite needles by growing put the network of already cohesive cement particles. At low concentration the network is loose, and the bridges generated by the ettringite needles does not induce rapid cracks of the structure; at high cement concentration, the aggregate paste is hard enough to maintain stress generated by the ettringite needles. Our results show that, at intermediate concentration, internal forces either resulting from the build-up of a consolidates network of cement particles, or due to growing ettringitte needles are strong enough to induce rapid rearrangements of the cement particles, that may result in microcracks as seen in the decorrelation function.

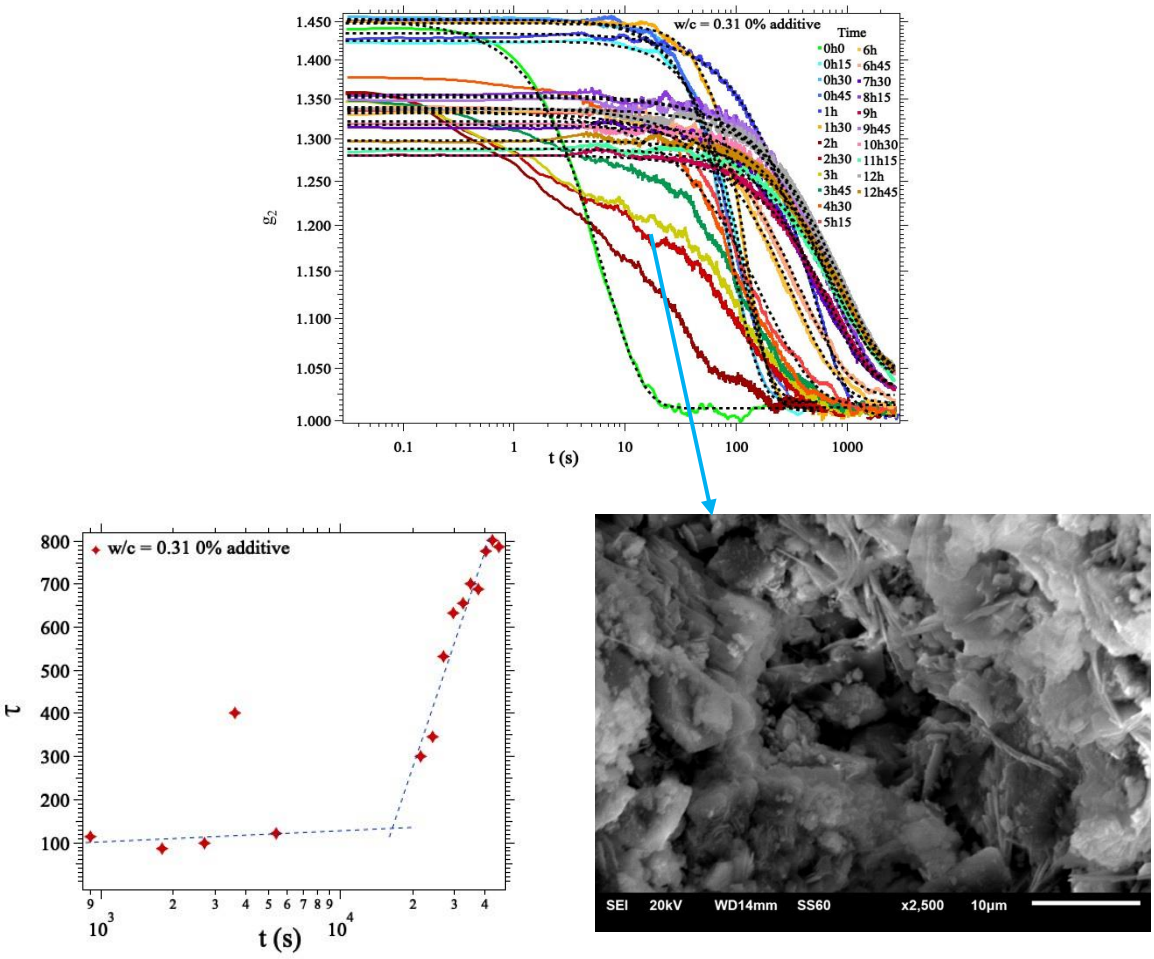

Figure 7.28 Top: Autocorrelation functions for suspension of w/c = 0.31. Discontinuous line corresponds to the fit law of equation 46. Bottom left: Evolution of τ as a function of experimental time. Bottom right: Micrographic at 3 h age

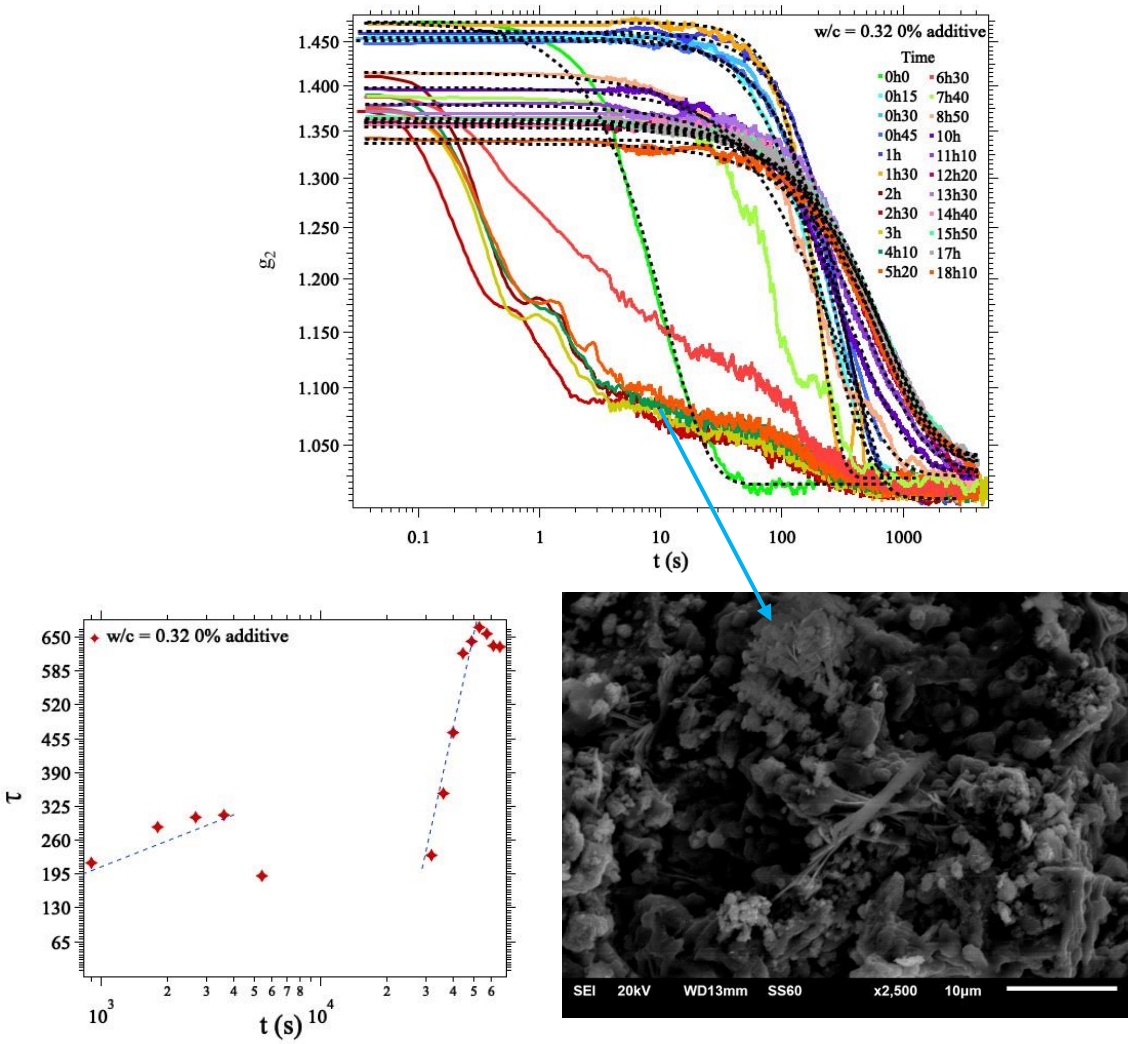

Figure 7.29 Top: Autocorrelation functions for suspension of w/c = 0.32. Discontinuous line corresponds to the fit law of equation 46. Bottom left: Evolution of τ as a function of experimental time Bottom right: Micrographic at 3 h age

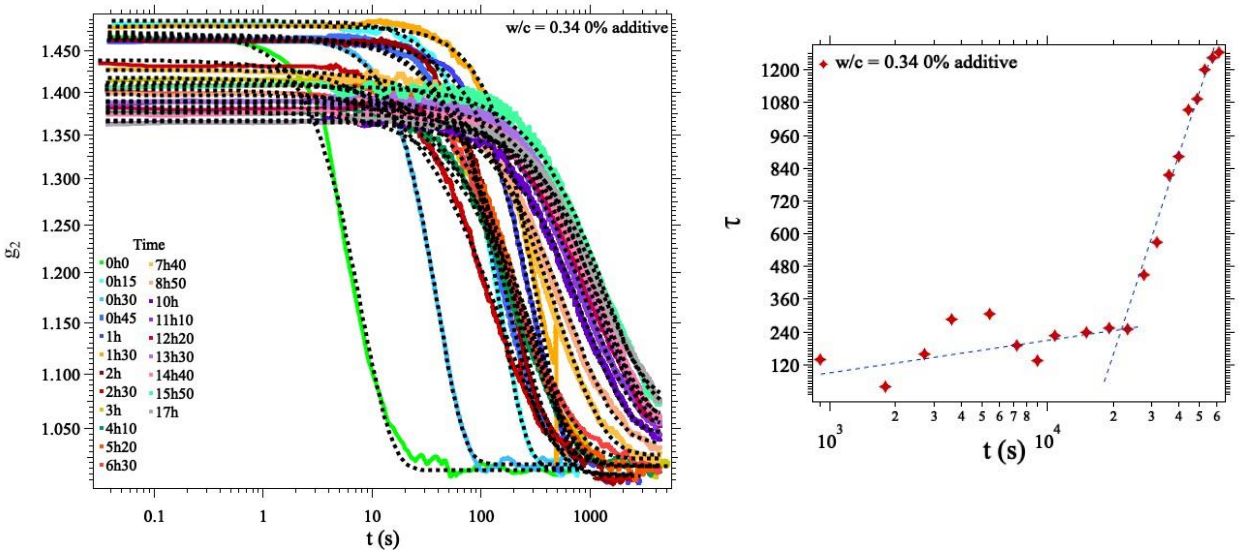

Figure 7.30 Left: Autocorrelation functions for suspension of w/c = 0.34. Discontinuous line corresponds to the fit law of equation 46. Right: Evolution of τ as a function of experimental time.

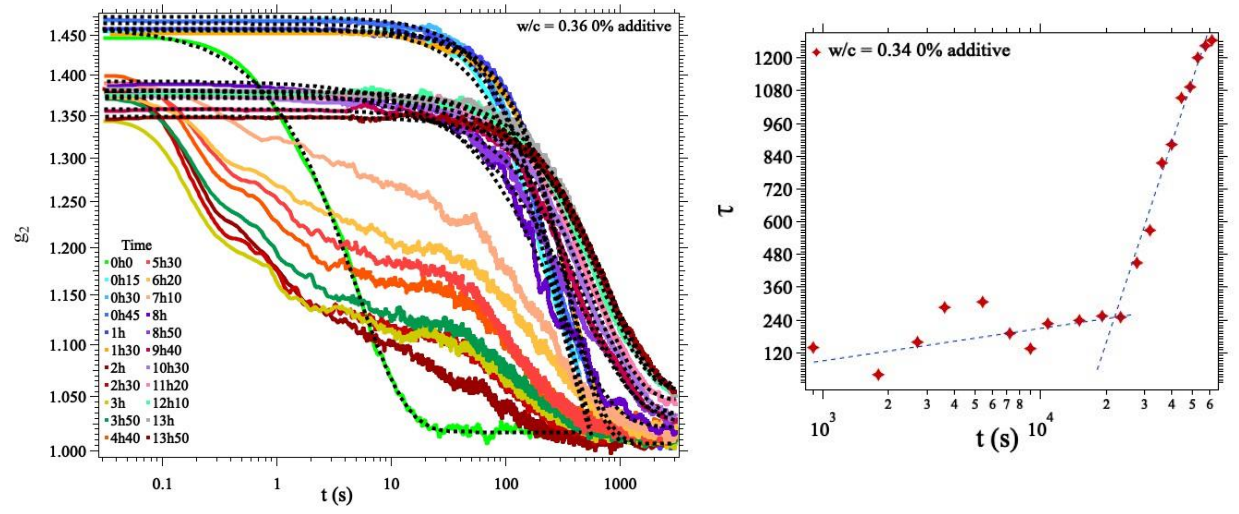

Figure 7.31 Left: Autocorrelation functions for suspension of w/c = 0.36 Discontinuous line corresponds to the fit law of equation 46. Right: Evolution of τ as a function of experimental time

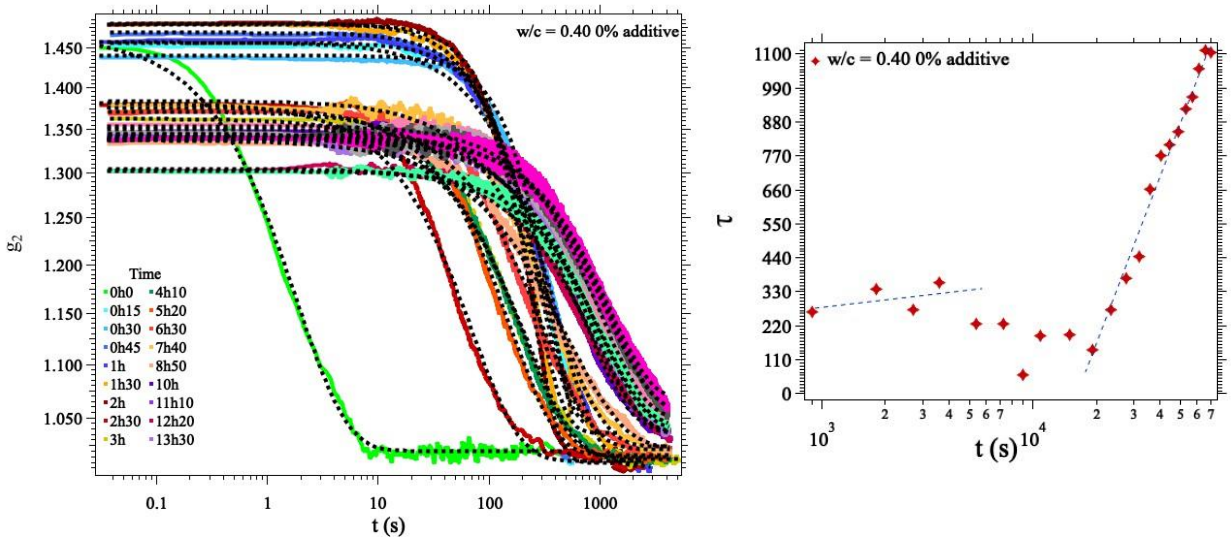

Figure 7.32 Left: Autocorrelation functions for suspension of w/c = 0.40. Discontinuous line corresponds to the fit law of equation 46. Right: Evolution of τ as a function of experimental time

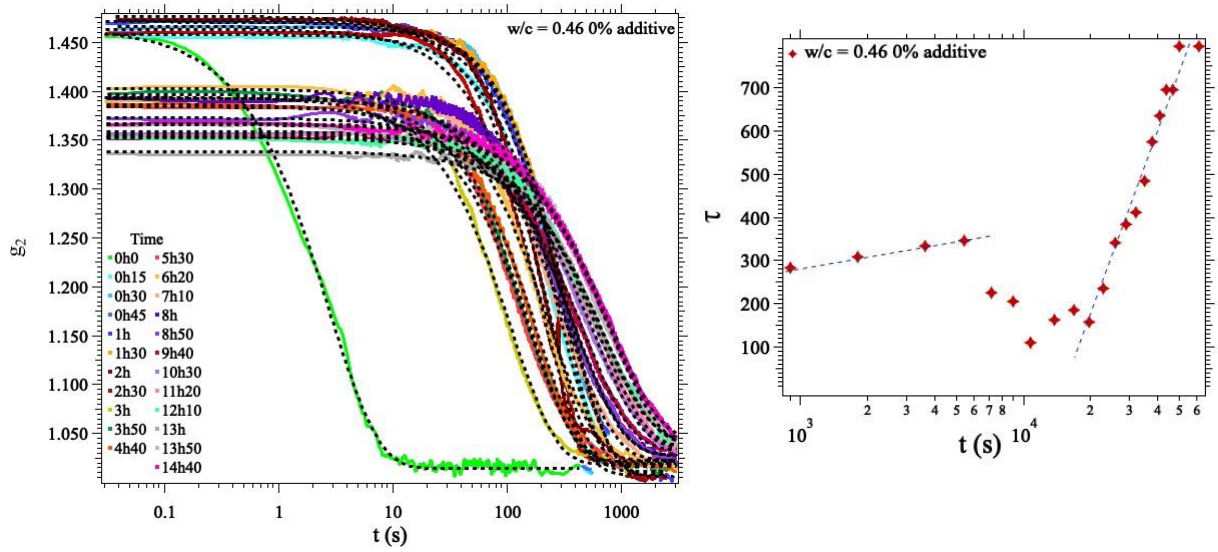

Figure 7.33 Left: Autocorrelation functions for suspension of w/c = 0.46 Discontinuous line corresponds to the fit law of equation 46. Right: Evolution of τ as a function of experimental time.

7.2.11 Intensity autocorrelation function of suspensions and the influence of HRWRA and VMA

The intensity autocorrelation functions and the influence of the concentration of HRWRA and VMA on their results is present in Figures 7.34 to 7.49. From analyze of plots can be observed that the higher is the HRWRA, especially in the 0.360% content, the evolution of decay time exhibit rapid decay time, in fact, the experiments of w/c = 0.34, 0.40 and 0.46 with 0.360% of HRWRA cannot be fitted with equation 46 due to the decay time is quickly reached and the shape of the curve differs from the equation. The high content of superplasticizers enhances the flowability but promoting phase separation. A high dispersant effect leads to non-homogeneously cement suspensions with no thixotropic effect. On the other hand, taken as reference the suspensions without additives, the addition of HRWRA in low and optimal content retards the agglomeration of cement particles. This is observed in the quick decay time in suspensions with HRWRA, interpreted as fast mobility of particles and slow relaxation of its mobility. This behavior is in agreement with results of the heat of hydration and evolution of strength where was observed a retard of kinetics due to the presence of polymers on the surface of cement particles.

Into all plots two modes can be identify that describe the decay time over experiment. The first mode corresponding around to first two hours of experimental has an evolution of decay time with a slope less prolongated than the second mode that has its beginning at the final of the first mode and its development is more intense, shows a higher slope until final of experiment. The first mode corresponds to pre-induction and dormant period of calorimetry curve and the first zone of the plots of strength evolution by ultrasonic reflection. The agglomeration of particles starts and the mobility is very fast and the formation of hydration products starts, observing that the higher is the water to cement ratio and HRWRA concentration the lower is the linear trend due to the delay in the kinetics of suspension. The second mode is ascribed to the acceleration period and the diffusion mechanism, the gain of strength and setting are observed due to the precipitation of hydration products. The diffusion mechanism decrease the kinetics but the growth of CSH, portlandite and ettringite continue. This is the reason why the slopes have a change aver the experimental time.

The addition of VMA on the high concentration of HRWRA does not modify significant the dynamics of cement suspensions, the thickening effect is not strong to change the dynamics of suspensions in study.

In these experiments the dynamics of the paste at intermediate time is presented in water to cement ratio of 0.34. The hypothesis discussed above can be explaining this mechanism.

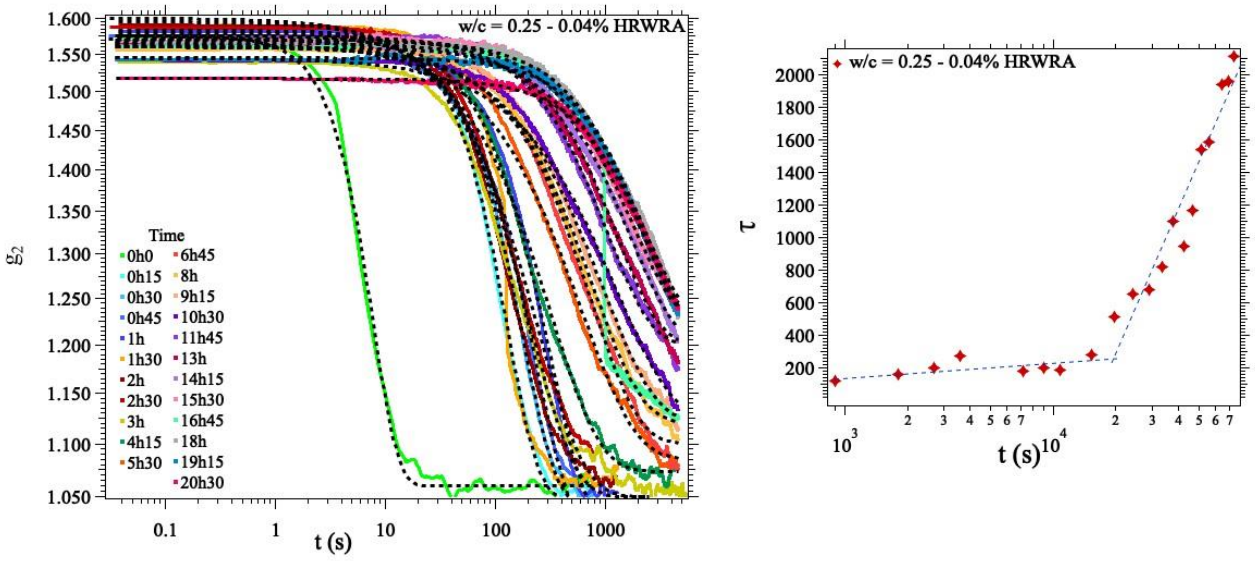

Figure 7.34 Left: Autocorrelation functions for suspension of w/c = 0.25 with 0.04% of HRWRA Discontinuous line corresponds to the fit law of equation 46. Right: Evolution of τ as a function of experimental time

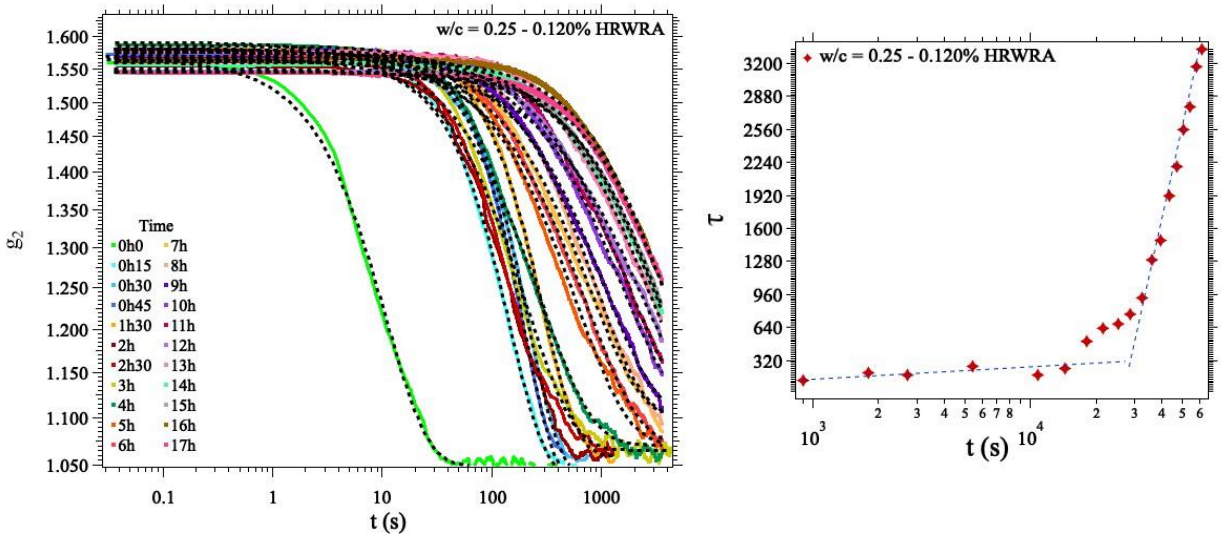

Figure 7.35 Left: Autocorrelation functions for suspension of w/c = 0.25 with 0.120% of HRWRA Discontinuous line corresponds to the fit law of equation 46. Right: Evolution of τ as a function of experimental time

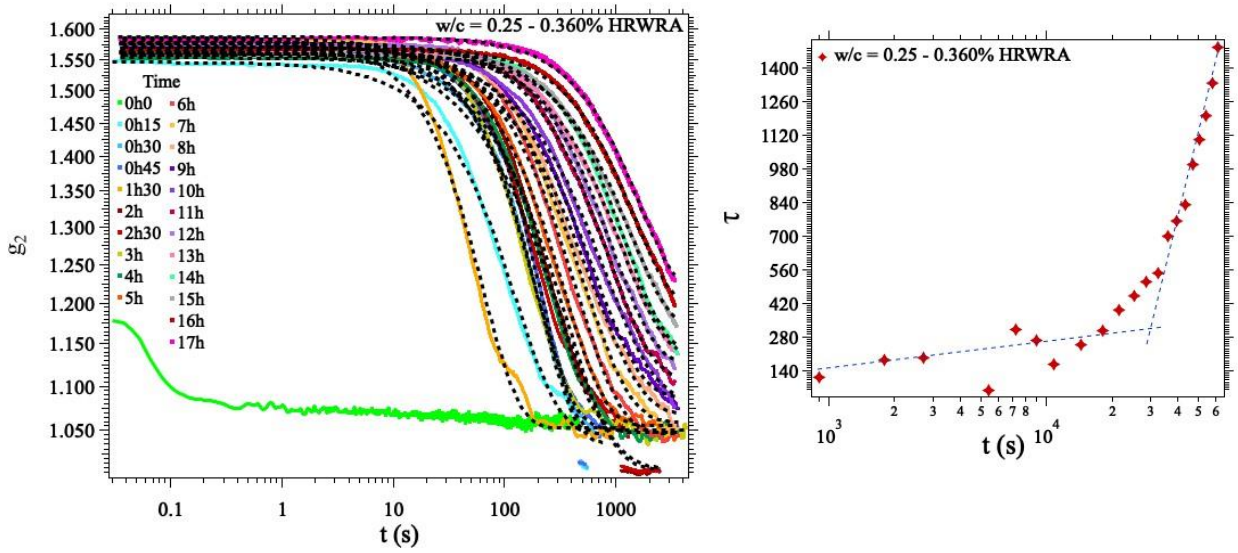

Figure 7.36 Left: Autocorrelation functions for suspension of w/c = 0.25 with 0.360% of HRWRA Discontinuous line corresponds to the fit law of equation 46. Right: Evolution of τ as a function of experimental time

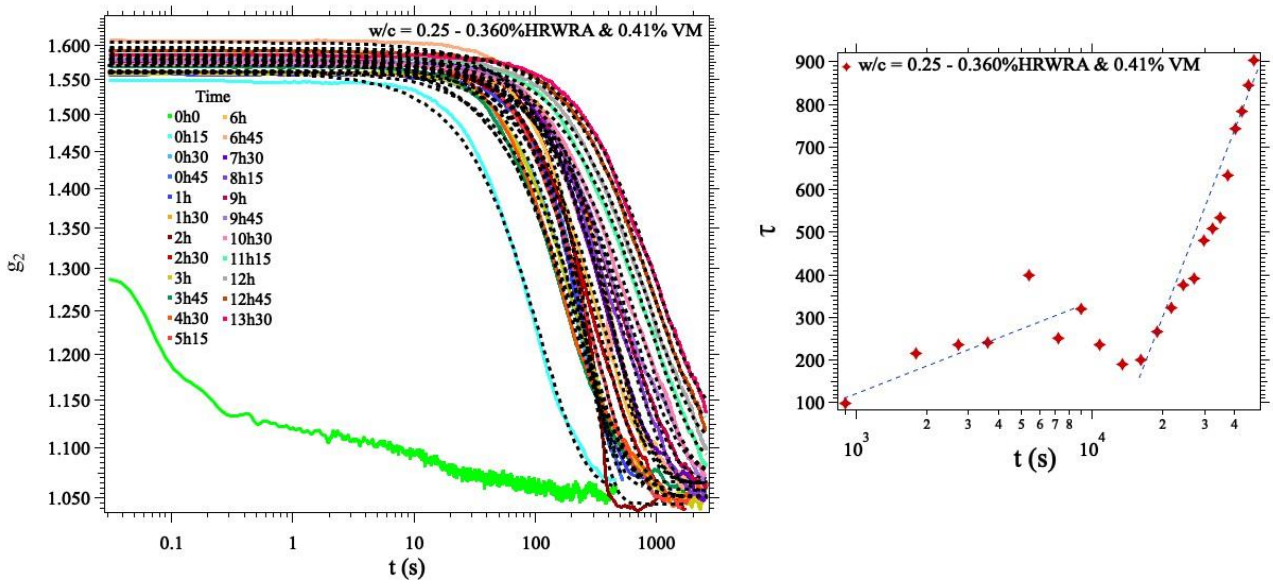

Figure 7.37 Left: Autocorrelation functions for suspension of w/c = 0.25 with 0.360% of HRWRA and 0.41% of VMA. Discontinuous line corresponds to the fit law of equation 46. Right: Evolution of τ as a function of experimental time

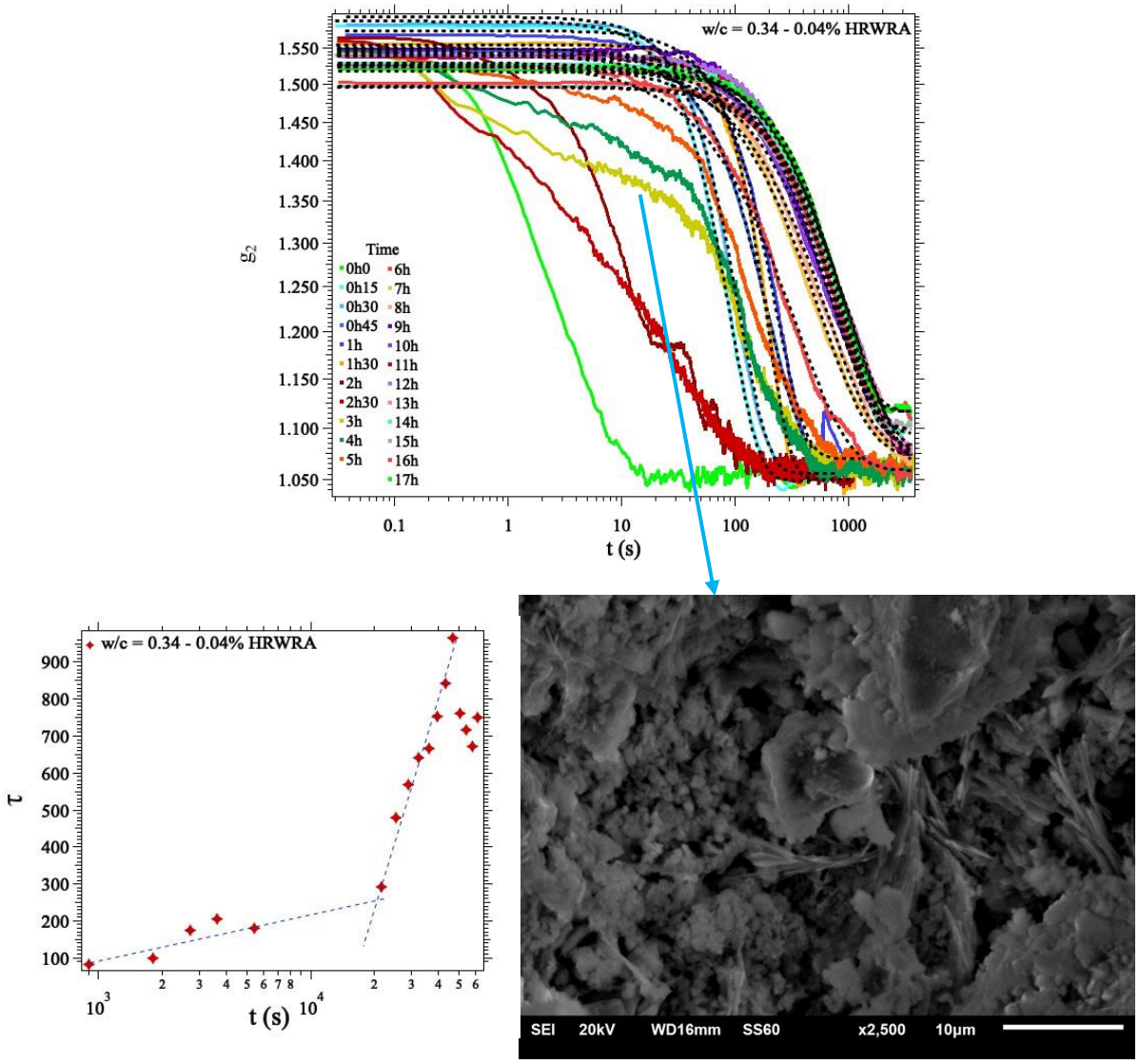

Figure 7.38 Top: Autocorrelation functions for suspension of w/c = 0.34 with 0.04% of HRWRA Discontinuous line corresponds to the fit law of equation 46. Bottom Left: Right: Evolution of τ as a function of experimental time. Bottom right: Micrographic at 3 h age.

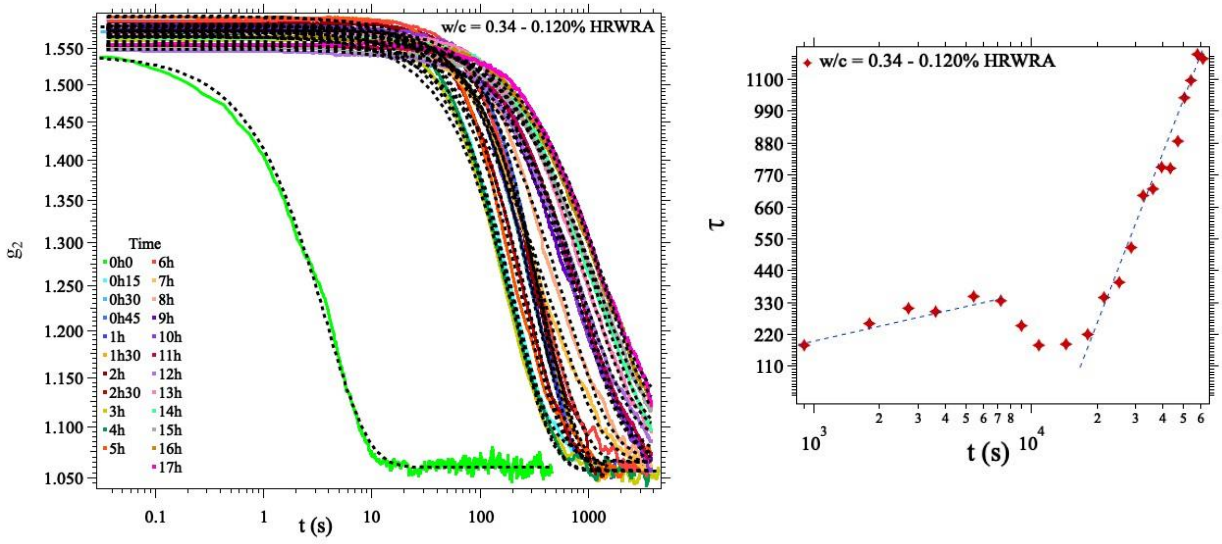

Figure 7.39 Left: Autocorrelation functions for suspension of w/c = 0.34 with 0.120% of HRWRA Discontinuous line corresponds to the fit law of equation 46. Right: Evolution of τ as a function of experimental time

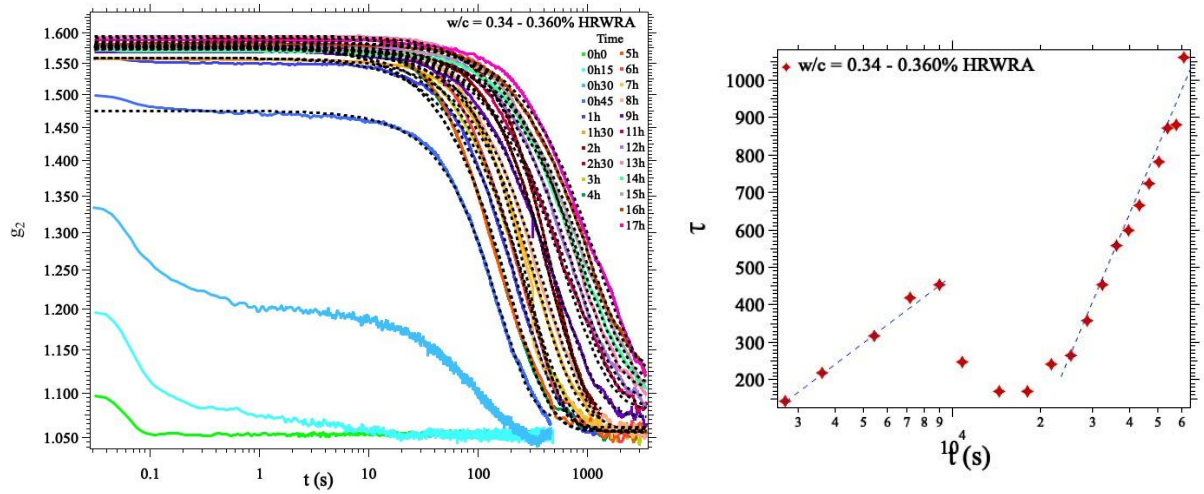

Figure 7.40 Left: Autocorrelation functions for suspension of w/c = 0.34 with 0.360% of HRWRA Discontinuous line corresponds to the fit law of equation 46. Right: Evolution of τ as a function of experimental time

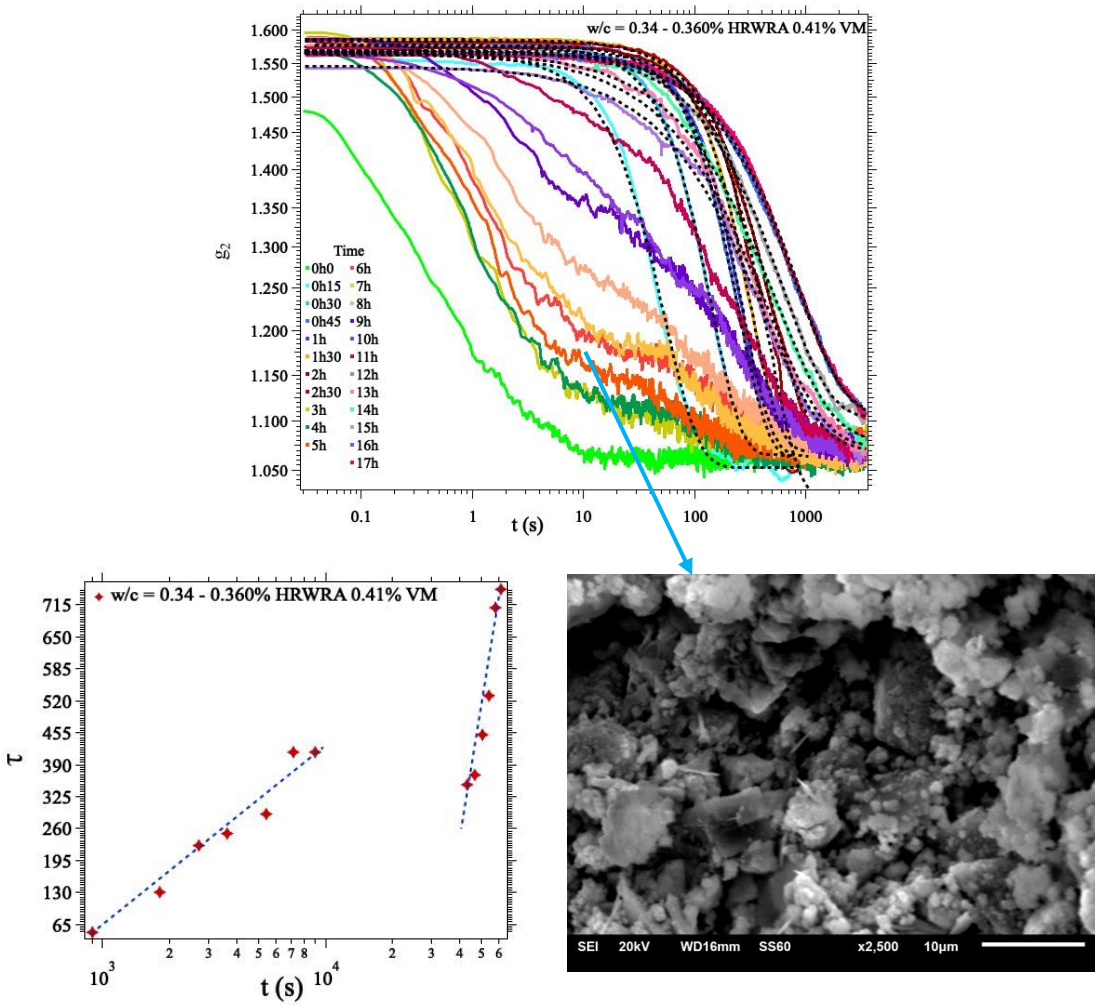

Figure 7.41 Top: Autocorrelation functions for suspension of w/c = 0.34 with 0.360% of HRWRA and 0.41% of VMA. Discontinuous line corresponds to the fit law of equation 46. Bottom Left: Evolution of τ as a function of experimental time. Bottom right: Micrographic at 3 h age.

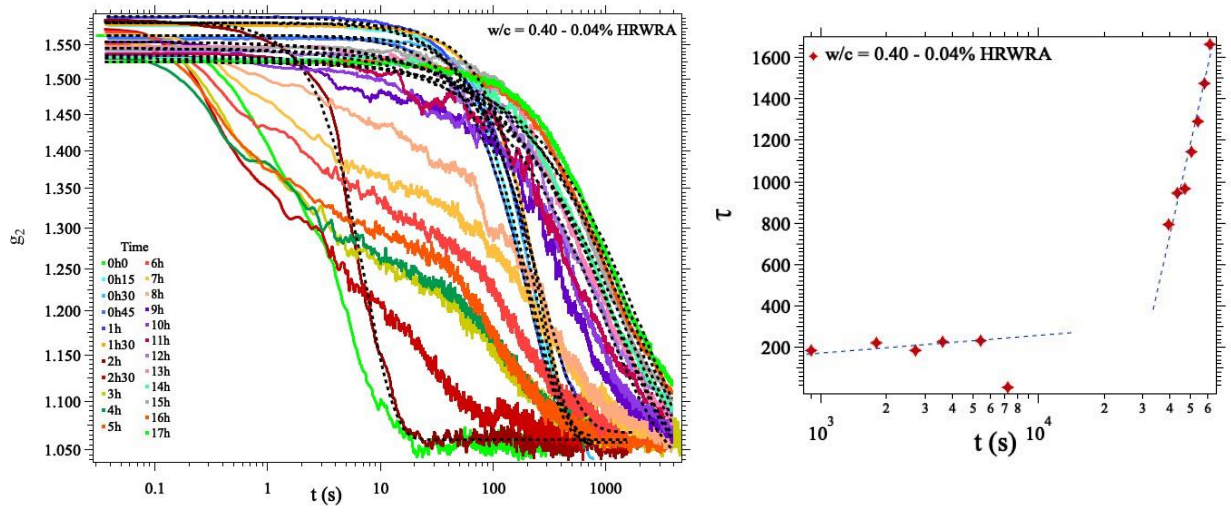

Figure 7.42 Left: Autocorrelation functions for suspension of w/c = 0.40 with 0.04% of HRWRA Discontinuous line corresponds to the fit law of equation 46. Right: Evolution of τ as a function of experimental time

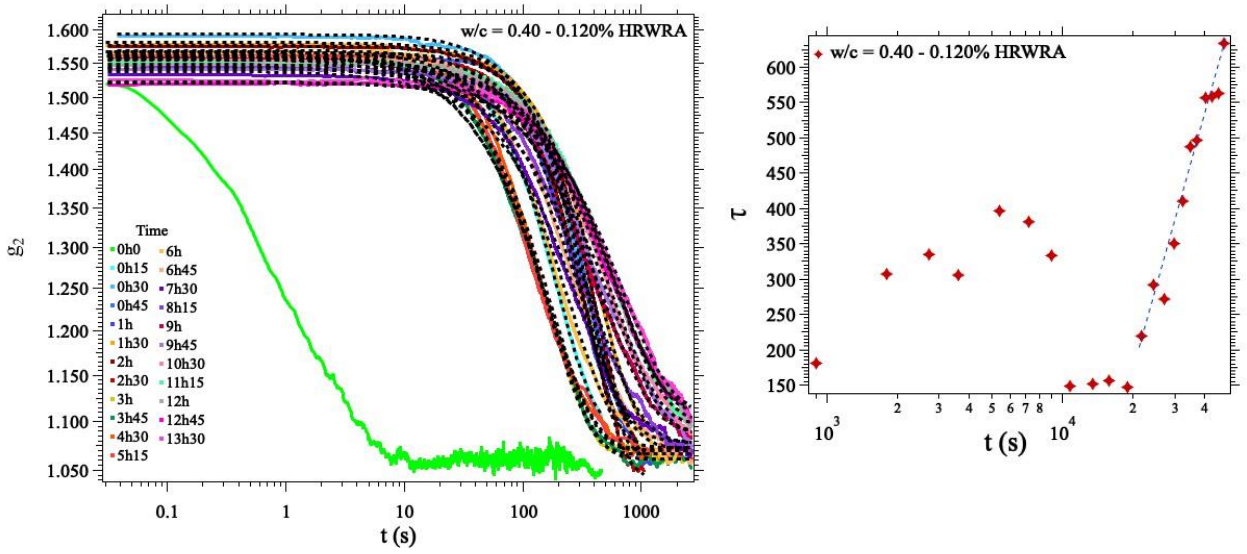

Figure 7.43 Left: Autocorrelation functions for suspension of w/c = 0.40 with 0.120% of HRWRA Discontinuous line corresponds to the fit law of equation 46. Right: Evolution of τ as a function of experimental time

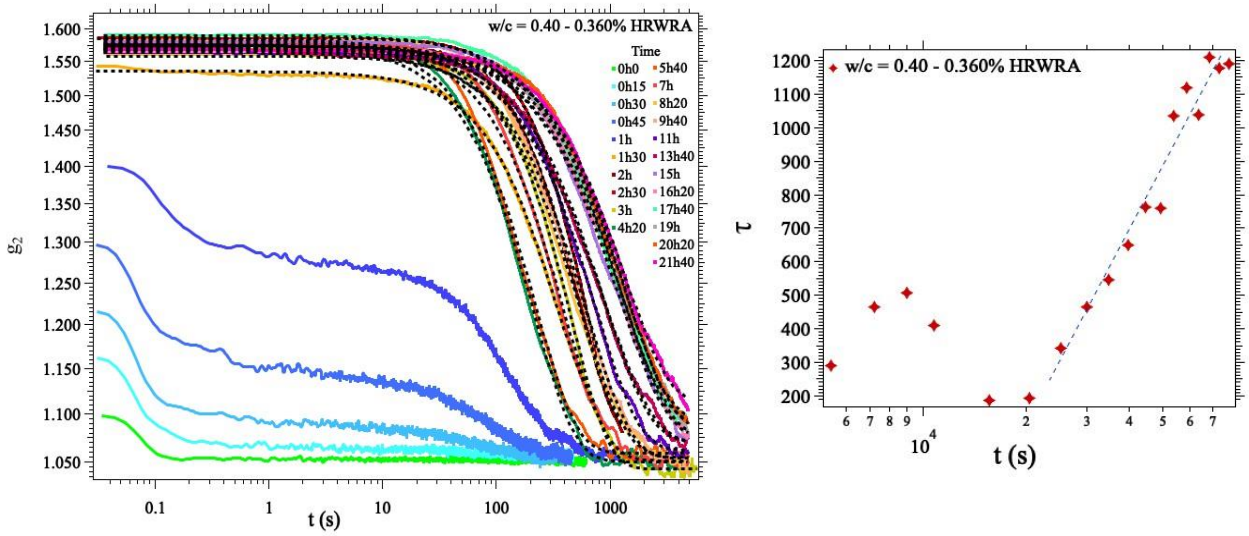

Figure 7.44 Left: Autocorrelation functions for suspension of w/c = 0.40 with 0.360% of HRWRA Discontinuous line corresponds to the fit law of equation 46. Right: Evolution of τ as a function of experimental time

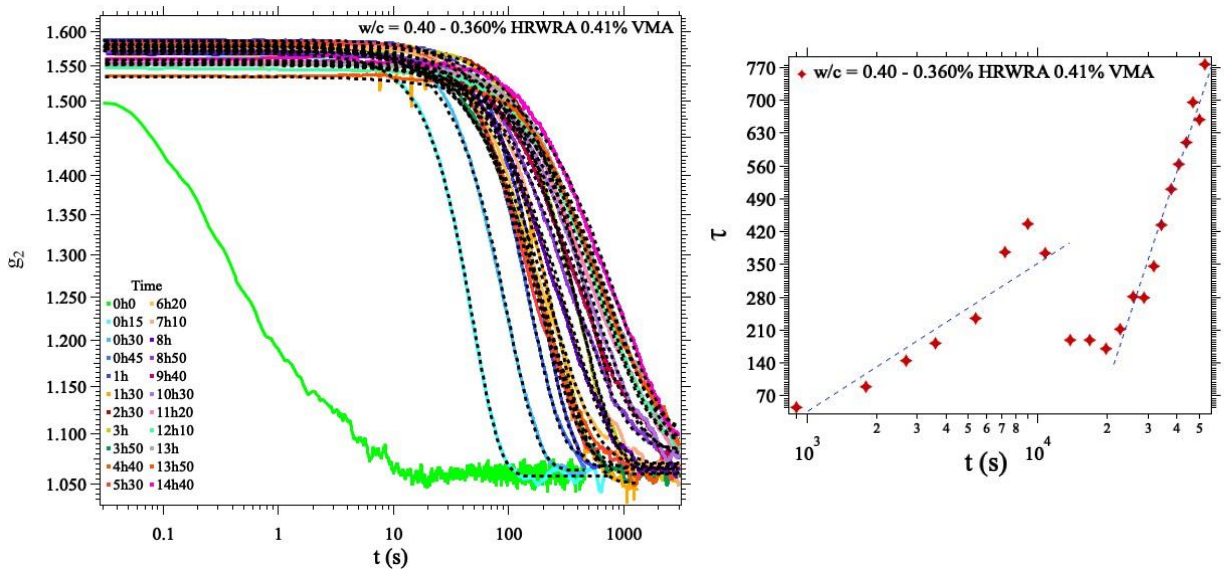

Figure 7.45 Left: Autocorrelation functions for suspension of w/c = 0.40 with 0.360% of HRWRA with 0.41 VMA. Discontinuous line corresponds to the fit law of equation 46. Right: Evolution of τ as a function of experimental time

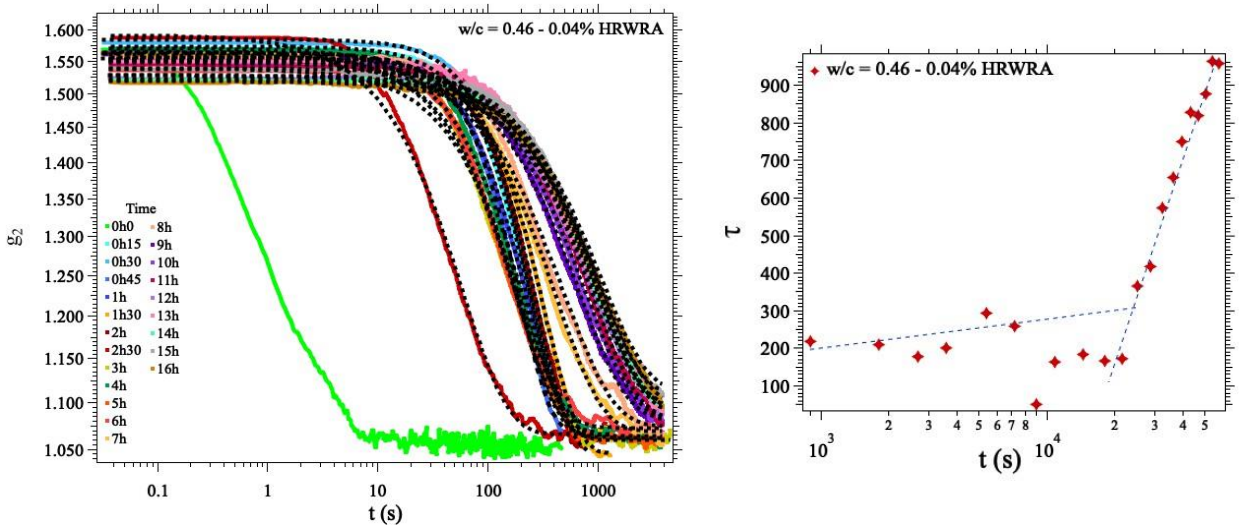

Figure 7.46 Left: Autocorrelation functions for suspension of w/c = 0.46 with 0.04% of HRWRA Discontinuous line corresponds to the fit law of equation 46. Right: Evolution of τ as a function of experimental time

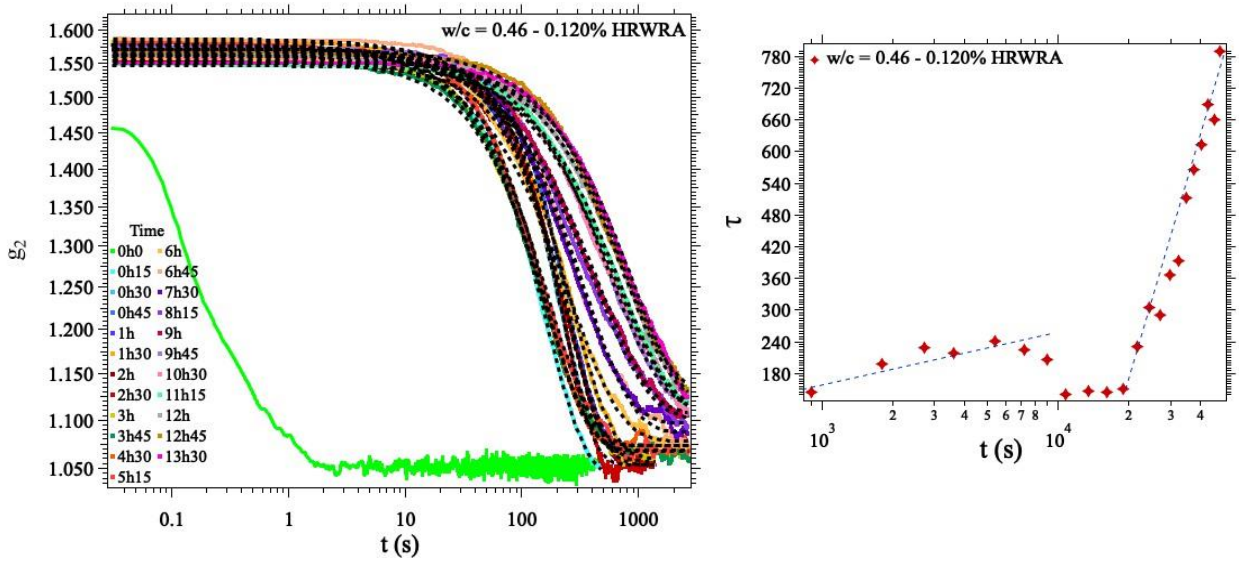

Figure 7.47 Left: Autocorrelation functions for suspension of w/c = 0.46 with 0.120% of HRWRA Discontinuous line corresponds to the fit law of equation 46. Right: Evolution of τ as a function of experimental time

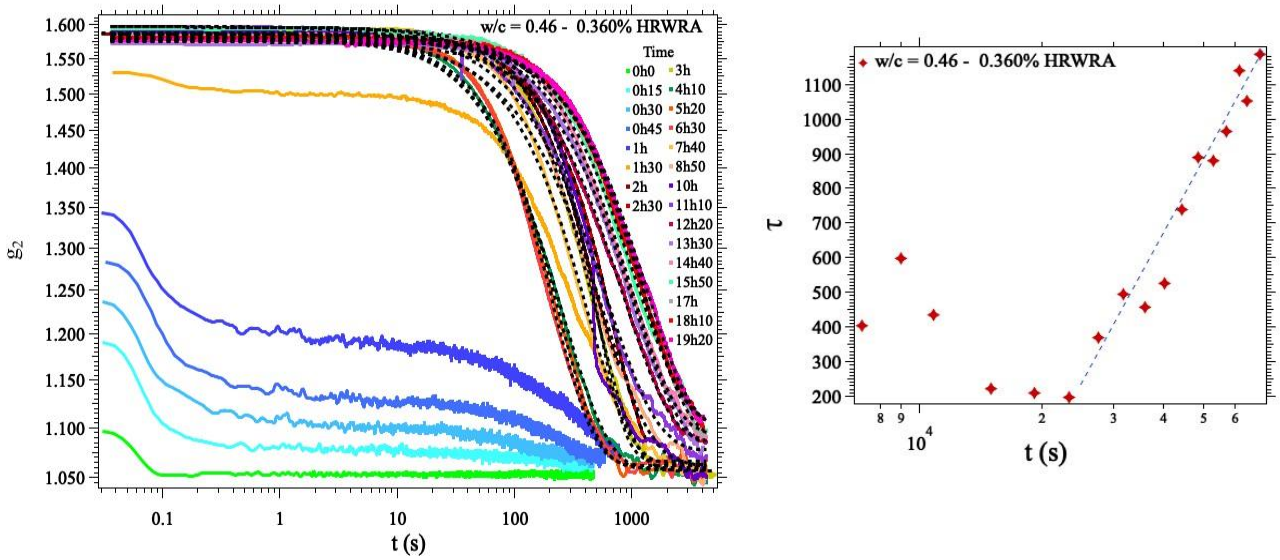

Figure 7.48 Left: Autocorrelation functions for suspension of w/c = 0.46 with 0.360% of HRWRA Discontinuous line corresponds to the fit law of equation 46. Right: Evolution of τ as a function of experimental time

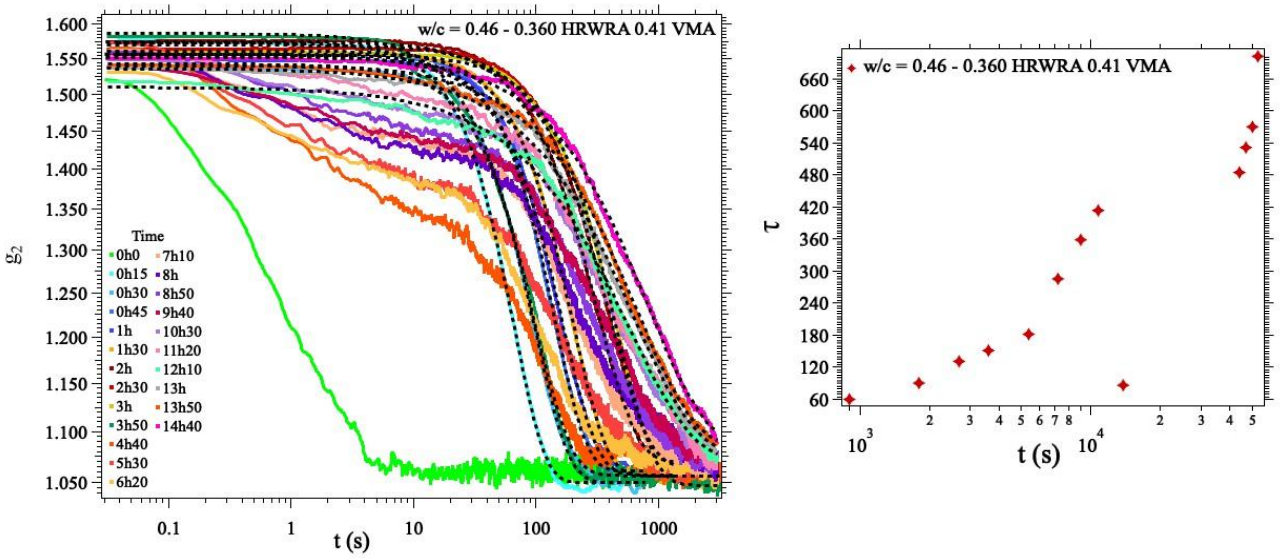

Figure 7.49 Left: Autocorrelation functions for suspension of w/c = 0.46 with 0.360% of HRWRA with 0.41% of VMA. Discontinuous line corresponds to the fit law of equation 46. Right: Evolution of τ as a function of experimental time

7.2.12 Discussion

The dynamics of cement suspensions are strongly related with rheological behavior and development of setting and hardening. In fact, the thixotropy of cement suspensions depends of the microstructural changes during the build-up of the network by the physical and chemical process. Our experimental results of MSDWS show that the dynamics of several cement suspensions during the build-up process can be represent by two evolution modes obtained from the evolution of decay time τ of the set of intensity autocorrelation function curves. The first evolution shows fast mobility and low stiffness, so the values of τ has a rapid decay, keeping this behavior around the pre-induction and dormant periods located in calorimetry curves. This dynamics is associated to the dissolution of ions and the formation of the first products where the strength is low enough to permit a manipulation of cement suspensions, in other words, the workability time is present. The second evolution is characterized by the increase of stiffness, therefore the mobility decrease and the decay time becomes slow increasing faster than the first evolution. At this moment the acceleration period is occur, the hydration of alite and belite is the most stronger and the gain of strength fast forward. Products like CSH, portlandite and ettringite precipitate on the surface of cement grains forming a layer that covering the cement grains. In fact, this layer is broken due to internal forces as have been reported by several researches. Our results shows hypothetically that mechanism, due to the dynamics of the suspensions at intermediate time and at intermediated concentrations is modified, ascribed it to the microcracks propagation which can be seem in the decorrelation function.

The influence of HRWRA and VMA can be observed in the dynamics of the suspensions, especially in the second evolution of the decay time. The higher is the HRWRA the lower is the decay time, this is due to the addition of superplasticizer retards the kinetics of the suspensions as was observed in the calorimetry and ultrasonic reflections tests. In the first evolution the addition of HRWRA and VMA caused variability in the values of decay time, this is ascribing to the high dispersion and mobility of particles of cement.

7.2.13 Flexural Strength

Figure 7.50 shows the results of flexural strength at the water to cement ratios 0.25, 0.30, 0.32, 0.34, 0.36, 0.38, 0.40 and 0.46 without additives, studied by diffusing wave spectroscopy as well. As expected, flexural strength decreases with the increase of water to cement ratio down to 56.4%. The mechanism through which, the flexural strength decrease is due to the emergence of cracks propagation during the hydration time. The crack propagation can be observed in the experiments of MS DWS. From the Figure 7.50, it can be distinguished two behaviors. At the water to cement ratios > 0.35, the flexural strength begins to decrease more rapidly. If may be ascribed to the rapid rearrangement observed at 0.36 and 0.40 by MSDWS.

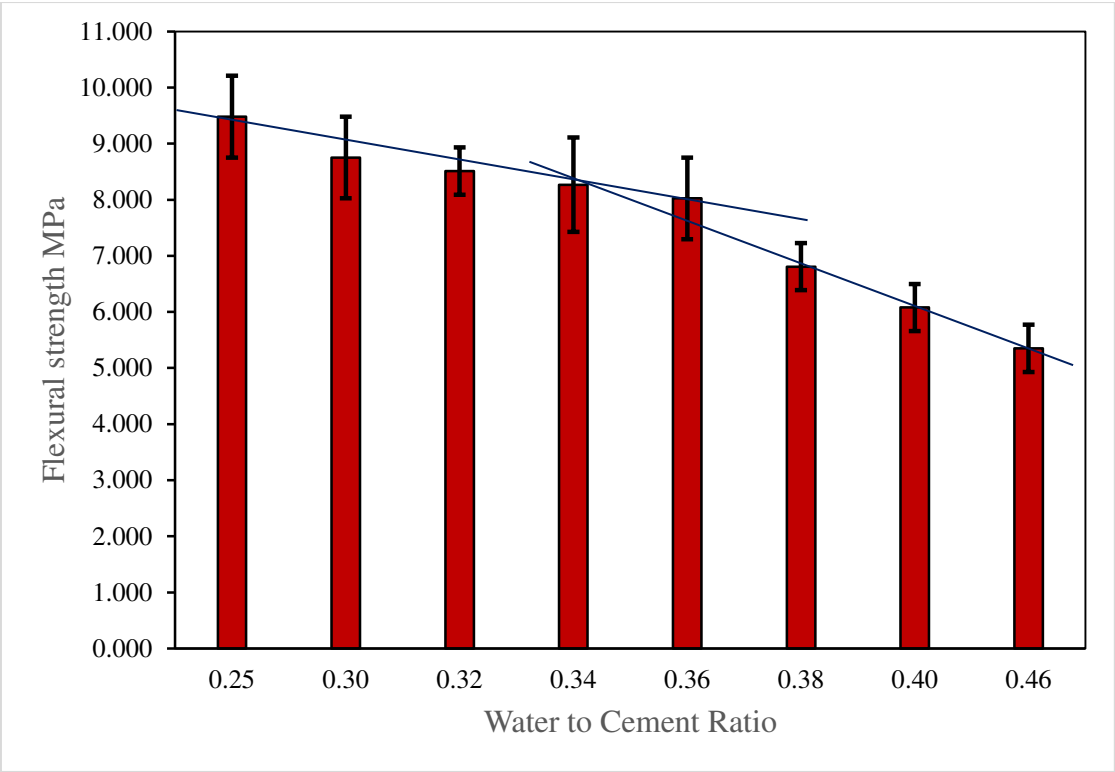

Figure 7.50 Evolution of flexural strength as a function of water to cement ratio at 30 h of age

8 CONCLUSIONS

Based on the experiments carried out to study the thixotropic behaviour of white portland cement suspensions, the following conclusions can be made:

By measuring the viscosity over time on a fresh paste it is possible to uncouple the contribution of the chemical and physical thixotropies. The physical thixotropy is due to the reconstruction of the contact network due to the attractive interaction between particles inducing a structuration of their network and the chemical thixotropy is due to the precipitation of the hydrates on the surface of particles which increases the total available surfaces of the particles.

The two contributions lead to an increase of the amount of contacts between the particles and therefore to an increase of the viscosity over-time. The physical aging appears on shorter time scale than the chemical one. The attractive nature of the particles induces a rapid restructuration of their network leading to an exponential increase of the suspension viscosity. The continuous precipitation of the hydrates on the surfaces of the particles is not changing the network organization but rather increasing its global surface and as a consequence increases the contact strength between the particles. This surface increases lead to a macroscopic linear increase of the suspension viscosity.

An empirical model is proposed here to study the thixotropy of a cement paste. The model can be understood as a combination of physical behavior, which is caused by the attractive nature of cement particles and of chemical behavior due to the reactivity of the cement in water. Two different time constants τ_1 and τ_2 have been proposed and tested successfully in the experiments. The model is described by equation 43 but can be simplified in most cases by assuming $\alpha = \beta = 1$ to equation 43 $\eta(t) = \eta_0 \left(1 - e^{\frac{-t}{\tau_1}}\right)\left(1 + \frac{t}{\tau_2}\right)$ reducing the fitting parameter drastically. A key result of our study lies in the observation that physical aging is exponential in time whereas the chemical aging is linear with time.

The addition of additives only affects the physical aging but does not interfere with the chemical thixotropy. The investigation of the admixtures effect on the thixotropy could be used to formulate cement paste with fast or slow thixotropy depending of the application.

An empirical model is proposed to study the intensity autocorrelation function. The key of the model is the identification of the decay time τ over the several correlated functions, which describes the dynamics of the suspensions at build-up over experimental time.

The dynamics of cement suspensions behaves into two behavior modes dictated by evolution of the decay time τ. The first mode is associated to the fast mobility and a slow rearrangement of cement particles a physical aging is observed. The second mode is ascribed to the gain of

strength due to the precipitation of hydration products; the increase of stiffness is purely chemistry.

A reaction of dynamics of the suspensions at intermediate time and concentration of cement has been identified. The mechanism of reaction is ascribing to the internal forces that leads to microcracks propagation which were observed in the decorrelation function. The microcracks affect the microstructure evolution then the flexural strength is affected.

9 WORKS CITED

[1] S. H. Kosmatka, B. Kerkhoff y W. C. Panarese, Desing and Control of Concrete Mixtures, 14th edition ed., Skokie, Illinois: Portland Cement Association, 2002, p. 358 pages.

[2] W. Kurdowski, Cement and Concrete Chemistry, Kraków: Springer, 2014.

[3] V. S. Ramachandran y J. J. Beaudoin, Handbook of Analytical Techniques in Concrete Science and Technology, Ottawa: Noyes Publications, 2001.

[4] N. Spiratos, M. Page, N. P. Mailvaganam, V. M. Malhotra y C. Jolicoeur, Superplasticizers for concrete, Ottawa: supplementary Cementing Materials for Sustainable Development, 2003.

[5] H. M. Ludwig y W. Zhang, «Research review of cement clinker chemistry,» *Cement and Concrete Researh,* vol. 78, nº Part A, pp. 24-37, 2015.

[6] ASTM C150/C150M-18, «Standard Specification for Portland Cement,» *ASTM International,* pp. 1-9, 2018.

[7] ASTM C595/C595 M-18, Standard Specification for Blended Hydraulic Cements, West Conshohocken: ASTM International, 2018.

[8] NMX-414-ONNCCE-2017, «Industria de la Construcción - Cementantes Hidráulicos - Especificaciones y Métodos de Ensayo,» *Organismo Nacional de Normalización y Certificación de la Construcción y Edificación, S.C.,* pp. 1-17, 2017.

[9] M. A. Sanjuan y C. Argiz, «The new european standard on common cements specifications EN 197-1:2011,» *Materiales de Construcción,* vol. 62, nº 307, pp. 425-430, 2012.

[10] B. S. Hamad, «Investigations of chemical and physical properties of white cement concrete,» *Advance cement based materials,* vol. 2, nº 4, pp. 161-167, 1995.

[11] K. K. Veiga y A. L. Gastaldini, «Sulfate attack on a white Portland cement with activated slag,» *Construction and building materials,* vol. 34, pp. 494-503, 2012.

[12] A. Lübeck, A. L. Gastaldini, D. S. Barin y H. C. Siqueira, «Compressive strength and electrical properties of concrete with white Portland cement and blast-furnace slag,»

Cement and Concrete Composites, vol. 34, nº 3, pp. 392-399, 2012.

[13] A. Subaşi y M. Emiroğlu, «Effect of metakaolin substitution on physical, mechanical and hydration process of white Portland cement,» *Construction and Building Materials,* vol. 95, pp. 257-268, 2015.

[14] A. P. Kirchheim, V. Rheinheimer, D. C. C. y D. Molin, «Comparative study of white and ordinary concretes with respect of carbonation and water absorption,» *Construction and building materials,* vol. 85, pp. 320-330, 2015.

[15] V. S. Ramachandran, R. M. Paroli, J. J. Beaudoin y A. H. Delgado, Handbook of thermal analysis of construction materials, Ottawa: Noyes Publications, 2002.

[16] I. G. Richardson, A. V. Girão, R. Taylor y S. Jia, «Hydration of water and alkali-activated white Portland cement pastes and blends with low-calcium pulverized fuel ash,» *Cement and Concrete Research,* vol. 83, pp. 1-18, 2016.

[17] D. P. Bentz, «Cementitious Materials: Hydration Chemistry and Characterization,» http://doi.org/10.13140/rg.2.1.1734.2163, 2015.

[18] H. F. W. Taylor, Cement Chemistry, 2nd Edition ed., vol. I, London: Thomas Telford, 1997.

[19] M. H. Noël, H. Van Damme y P. Hébraud, «Building of a thermoresponsive cement,» *Cement and Concrete Research,* vol. 41, nº 9, pp. 975-980, 2011.

[20] A. C. Muller, K. L. Scrivener, J. Skibsted, A. M. Gajewicz y P. J. McDonald, «Influece of silica fume on the microstructure of cement pastes: New insights from H NMR relaxometry,» *Cement and Concrete Reseacrh,* vol. 74, pp. 116-125, 2015.

[21] J. W. Bullard, H. M. Jennings, R. A. Livingston, A. Nonat, G. W. Scherer, J. S. Schweitzer, K. L. Scrivener y J. J. Thomas, «Mechanisms of cement hydration,» *Cement and Concrete Research,* vol. 41, nº 12, pp. 1208-1223, 2011.

[22] P. C. Hewlett, Lea's Chemistry of Cement and Concrete, Oxford: Elsevier, 2006.

[23] S. Rahimi-Aghdam, Z. P. Bazant y M. A. Qomi, «Cement hydration from hours to centuries controlled by diffusion through barrier shells of C-S-H,» *Journal of the Mechanics and Physics of Solids,* vol. 99, pp. 211-224, 2017.

[24] K. L. Scrivener, P. Juilland y P. J. Monteiro, «Advances in understanding hydration of Portland cement,» *Cement and Concrete Research,* vol. 78, nº Part A, pp. 38-56, 2015.

[25] B. Lothenbach y A. Nonat, «Calcium silicate hydrates: Solid and liquid phase composition,» *Cement and Concrete Research,* vol. 78, nº Part A, pp. 57-70, 2015.

[26] F. Irgens, Rheology and Nen-Newtonian Fluids, Trondheim: Springer, 2014.

[27] D. R. Dinger, Rheology for Ceramists, D. C. C. Service, Ed., Clemson, 2002.

[28] R. Moreno-Botella, Reología de Suspensiones cerámicas, Madrid: CSIC, 2005.

[29] A. P. Deshpande, J. M. Krishnan y P. B. Sunil-Kumar, Rheology of Complex Fluids, Madras: Springer, 2010.

[30] F. Irgens, Rheology and Non-Newtonian Fluids, Trondheim: Springer, 2013.

[31] T. G. Mezger, The Rheology Handbook, Hanover: Vincentz, 2014.

[32] J. Mewis y N. J. Wagner, «Thixotropy,» *Advances in Colloidal and Interface Science,* Vols. %1 de %2147 - 148, pp. 214- 227, 2009.

[33] M. Bellour, M. Skouri, J. P. Munch y P. Hébraud, «Brownian motion of particles embedded in a solution of giant micelles,» *The European Physical Journal E,* vol. 8, nº 4, pp. 431-436, 2002.

[34] F. Puertas, H. Santos, M. Palacios y S. Martinez-Ramirez, «Polycarboxylate superplasticiser admixtures: effect on hydration, microstructure and rheological behaviour in cement pastes,» *Advances in Cement Research,* vol. 17, nº 2, pp. 77-89, 2005.

[35] C. Tropea, A. L. Yarin y J. F. Foss, Springer Handbook of Experimental Fluid Mechanics, Berlin, 2007.

[36] V. A. Rinaldi y J. J. Clariá Jr, «Time dependent stress-strain behavior of bentonite slurries; effect of thixotropy,» *Powder Technology,* vol. 291, pp. 311-321, 2016.

[37] D. Lowke, «Thixotropy of SCC - A model describing the effect of particle packing and superplasticizer adsorption on thixotropic structural build-up of the mortar phase based on interparticle interactions,» *Cement and Concrete Research,* vol. 104, pp. 94-104, 2018.

[38] Z. Quanji, G. R. Lomboy y K. Wang, «Influence of nano-sized highly purified magnesium alumino silicate clay on thixotropic behavior of fresh cement pastes,» *Construction and Building Materials,* vol. 69, pp. 295-300, 2014.

[39] P. Coussot, Rheophysics. Matter in all its states, Paris-Est: Springer, 2014.

[40] F. Babick, Suspensions of Colloidal Particles and Aggregates, Dresden: Springer, 2016.

[41] D. Lootens, P. Hébraud, E. Lécolier y V. Damme, «Gelation, shear-thining and shear-thickening in cement slurries,» *Oil and Gas Science and Technology,* vol. 59, nº 1, pp. 31-40, 2004.

[42] M. Finessi, I. Szilagyi y P. Maroni, «Dendrimer induced interaction forces between colloidal particles revealed by direct force and aggregation measurements,» *Journal of Colloidal and Interface Science,* vol. 417, pp. 346-355, 2014.

[43] A. Regalado Mendez y O. A. Noriega Ramos, «Comportamiento reológico de un fluido,» *Ciencia y Mar,* vol. XII, nº 36, pp. 35-42, 2008.

[44] S. Farrokhpay, «The importance of rheology in mineral flotation: A review,» *Minerals Engineering,* Vols. %1 de %236-38, pp. 272-278, 2012.

[45] J. Mewis y N. Wagner, «Suspension Rheology,» University of Delaware and K. U. Leuven, Belgium - USA, 2012.

[46] G. Sant, C. F. Ferrairis y J. Weiss, «Rheological properties of cement pastes: A discussion of structure formation and mechanical property development,» *Cement and Concrete Research,* vol. 38, nº 11, pp. 1286-1296, 2008.

[47] N. Roussel, A. Lemaître, R. J. Flatt y P. Coussot, «Steady state flow of cement suspensions: A micromechanical state of the art,» *Cement and Concrete Research,* vol. 40, nº 1, pp. 77-84, 2010.

[48] L. Ferrara, M. Cremonesi, N. Tregger, A. Frangi y S. P. Shah, «On the identification of rheological properties of cement suspensions: Rheometry, Computational Fluid Dynamics modeling and field test measurements,» *Cement and Concrete Research,* vol. 42, nº 8, pp. 1134-1146, 2012.

[49] M. Liard, L. Oblak, M. Hachim, M. Vachon y D. Lootens, «Impact of Viscosity on Hydration Kinetics and Setting Properties of Cementitious Materials,» *Advances in Civil Engineering Materials,* vol. 3, nº 2, pp. 117-126, 2014.

[50] D. Jiao, C. Shi y Q. Yuan, «Influences of shear-mixing rate and fly ash on rheological behavior of cement pastes under continuous mixing,» *Construction and Building Materials,* vol. 188, pp. 170-177, 2018.

[51] D. Lootens, Ciments et suspensions concentrées modèles. Écoulement, encombrement et floculation, Paris VI: Université Pierre et Marie Curie, 2004.

[52] H. Jae Yim y J. Hong kim, «Physical Characterization of Cementitious Materials on Casting and Placing Process,» *Materials,* vol. 7, nº 4, pp. 3049-3064, 2014.

[53] H. A. Barnes, «Thixotropy a review,» *Journal of Non-Newtonian Fluid Mechanics,* vol. 70, nº 1-2, pp. 1-33, 1997.

[54] J. Miranda, V. Flores-Ales y J. Barrios, «Aportaciones al estudio reológico de pastas y morteros de cemento portland,» *Materiales de Construcción,* vol. 50, nº 257, pp. 47-56, 2000.

[55] K. Vance, G. Sant y N. Neithalath, «The rheology of cementitious suspensions: A closer look at experimental parameters and property determination using common rheological models,» *Cement and Concrete Composites,* vol. 59, pp. 38-48, 2015.

[56] J. E. Wallevik, «Thixotropy behavior of cement pastes,» *Annual Transactions of the Nordic Rheology Society,* vol. 12, pp. 21-28, 2004.

[57] J. E. Wallevik, «Thixotropy investigation on cement paste: Experimental and numerical approach,» *Journal of Non-Newtonian Fluid Mechanics,* vol. 132, nº 1-3, pp. 86-99, 2005.

[58] S. Jarny, N. Roussel, S. Rodts, F. Bertrand, R. Roy Le y P. Coussot, «Rheological behavior of cement pastes from MRI velocimetry,» *Cement and Concrete Research,* vol. 35, nº 10, pp. 1873-1881, 2005.

[59] N. Roussel, «A thixotropy model for fresh fluid concretes: Theory, validation and applications,» *Cement and Concrete Research,* vol. 36, nº 10, pp. 1797-1806, 2006.

[60] N. Roussel, G. Ovarlez, S. Garrault y C. Brumaud, «The origins of thixotropy of fresh cement pastes,» *Cement and Concrete Research,* vol. 42, nº 1, pp. 148-157, 2012.

[61] S. Kawashima, M. Chaouche, D. J. Corr y S. P. Shah, «Rate of thixotropy rebuilding of cement pastes modified with highly purified attapulgite clays,» *Cement and Concrete Research,* vol. 53, pp. 112-118, 2013.

[62] L. Reiter, T. Wangler, N. Roussel y R. J. Flatt, «The role of early age structural build-up in digital fabrication with concrete,» *Cement and Concrete Research,* vol. 112, 2018.

[63] C. Pedrajas, V. Rahhal y R. Talero, «Determination of characteristic rheological

parameters in Portland cement pastes,» *Construction and Building Materials,* vol. 51, pp. 484-491, 2014.

[64] A. M. Mostafa y A. Yahia, «New approach to assess build-up of cement-based suspensions,» *Cement and Concrete Research,* vol. 85, pp. 174-182, 2016.

[65] A. M. Mostafa y A. Yahia, «Physico-chemical kinetics of structural build-up of neat cement-based suspensions,» *Cement and Concrete Research,* vol. 97, pp. 11-27, 2017.

[66] Q. Yuan, D. Zhou, K. H. Khayat, D. Feys y C. Shi, «On the measurement of evolution of structural build-up of cement paste with time by static yield stress test vs. small amplitude oscillatory shear test,» *Cement and Concrete Research,* vol. 99, pp. 183-189, 2017.

[67] Y. Qian y S. Kawashima, «Distinguishing dynamic and static yield stress of fresh cement mortars through thixotropy,» *Cement and Concrete Research,* vol. 86, pp. 288-296, 2018.

[68] D. Galvez-Moreno, Robustez de un concreto autocompactable producido con materiales disponibles en la región de Monterrey, Nuevo León, Monterrey: Universidad Autónoma de Nuevo León, 2015.

[69] K. D. Kabagire, A. Yahia y M. Chekired, «Toward the prediction of rheological properties of self-consolidating concrete as diphasic material,» *Construction and Building Materials,* vol. 195, pp. 600-612, 2019.

[70] M. M. Alonso, O. Burgos-Montes, C. Varga, F. Puertas y M. Palacios, «Influencia de aditivos PCE en el comportamiento reologico, mecanico y durable de morteros de CAC,» de *3º Congreso Iberoamericano sobre hormigon autocompactante. Avances y oportunidades*, Madrid, 2012.

[71] R. S. Ahari, T. K. Erdem y K. Ramyar, «Time-dependet rheological characteristics of self-consolidating concrete containing various mineral admixtures,» *Construction and Building Materials,* vol. 88, pp. 134-142, 2015.

[72] S. Ng y H. Justnes, «Influence of plasticizers on the rheology and early heat of hydration of blended cements with high content of fly ash,» *Cement and Concrete Composites,* vol. 65, pp. 41-54, 2016.

[73] J. Liu, K. Wang, Q. Zhang, F. Han, J. Sha y J. Liu, «Influence of Superplasticizer dosage on the viscosity of cement paste with low water-binder ratio,» *Construction and*

Bulding Materials, vol. 149, pp. 359-366, 2017.

[74] H. Y. Ghorab, I. M. Kenawi y Z. G. Abdel-All, «Interaction between cements with different composition and superplasticizers,» *Materiales de Construccion,* vol. 62, nº 307, pp. 359-380, 2012.

[75] E. Janowska-Renkas, «The influence of the chemical structure of polycarboxylic superplasticizers on their effectiveness in cement pastes,» de *7th Scientific-Technical Conference Material Problems in Civil Engineering*, 2015.

[76] J. Hot, H. Bessaies-Bey, C. Brumaud, M. Duc, C. Castella y N. Roussel, «Adsorbing polymers and viscosity of cement pastes,» *Cement and Concrete Research,* vol. 63, pp. 12-19, 2014.

[77] H. Bessaies-Bey, R. Baumann, M. Schmitz, M. Radler y N. Roussel, «Organic admixtures and cement particles: Competitive adsorption and its macroscopic rheological consequences,» *Cement and Concrete Research,* vol. 80, pp. 1-9, 2016.

[78] D. N. Pinder, A. J. Swanson, P. Hebraud y Y. Hemar, «Micro-rheological investigation of dextran solutions using diffusing wave spectroscopy,» *Food hydrocolloids,* vol. 20, nº 2-3, pp. 240-244, 2006.

[79] J. Galvan-Miyoshi, J. Delgado y R. Castillo, «Diffusing wave spectroscopy in Maxwellian fluids,» *The European Physical Journal E,* vol. 26, pp. 369-377, 2008.

[80] T. A. Waigh, «Advances in the microrheology of complex fluids,» *Reports on Progress in Physics,* vol. 79, nº 7, pp. 1-62, 2016.

[81] H. Yang, W. Kang, H. Wu, Z. Li, Y. Yu, Y. Lu, L. Zhang, M. Wang y Y. He, «Passive microrheology for measurement of gelation behavior of a kind of polymer gel P(AM-AA-AMPS),» *Journal of Applied Polymer Science,* vol. 133, nº 17, 2016.

[82] C. Tisserand, M. Fleury, L. Brunel, P. Bru y G. Meunier, «Passive Microrheology for measurement of the concentrated dispersions stability,» *Progr Colloid Polym Sci,* vol. 139, pp. 101-105, 2012.

[83] J. L. Harden y V. Viasnoff, «Recent advances in DWS-based micro-rheology,» *Current Opinion in Colloid & Interface Science,* vol. 6, nº 5-6, pp. 438-445, 2001.

[84] R. Sarcia y P. Hébraud, «Crackling of a coagulating suspension,» *Physical Review E 72,* vol. 72, pp. 11402-1 - 11402-5, 2005.

[85] M. Reufer, A. H. E. Machado, A. Niederquell, K. Bohnenblust, B. Müller, A. C. Völker y M. Kuentz, «Introducing Diffusing Wave Spectroscopy as a Process Analytical Tool for Pharmaceutical Emulsion Manufacturing,» *Journal of Pharmaceutical Sciences,* vol. 103, nº 12, pp. 3902-3913, 2014.

[86] H. M. Wyss, S. Romer, F. Scheffold, P. Schurtenberger y L. J. Gauckler, «Diffusing-Wave Spectroscopy of Concentrated Alumina Suspensions during Gelation,» *Journal of Colloid and Interface Science,* vol. 241, nº 1, pp. 89-97, 2001.

[87] N. Isert, G. Maret y C. M. Aegerter, «Studying foam dynamics in levitated, dry and wet foams using diffusing wave spectroscopy,» *Colloids and Surface A: Physicochemical and Engineering Aspects,* vol. 413, pp. 40-45, 2015.

[88] R. Höhler, S. Cohen-Addad y D. J. Durian, «Multiple light scattering as a probe of foams and emulsions,» *Current Opinion in Colloid and Interface Science,* vol. 19, nº 3, pp. 242-252, 2014.

[89] G. J. Oh, J. W. Hwang, K. W. Bong y H. W. Jung, «Particle Dynamics and Relaxation in Bimodal Suspensions During Drying Using Multispeckle Diffusing Wave Spectroscopy,» *American Institute of Chemical Engineers Journal,* vol. 63, nº 3, pp. 1114-1121, 2016.

[90] Y. Zhang, X. Kong, L. Gao, Z. Lu, S. Zhou, B. Dong y F. Xing, «In-situ measurement of viscoelastic properties of fresh cement paste by a microrheology analyzer,» *Cement and Concrete Research,* vol. 79, pp. 291-300, 2016.

[91] Z. Lu, X. Kong, C. Zhang, F. Xing y Y. Zhang, «Effect of colloidal polymers with different surface properties on the rheological property of fresh cement pastes,» *Colloids and Surface A: Physicochemical and Engineering Aspects,* vol. 520, pp. 154-165, 2017.

[92] ASTM C494 / C494M-17, «Standard Specification for Chemical Admixtures for Concrete,» *ASTM International,* pp. 1-10, 2017.

[93] S. Brunauer, P. H. Emmett y E. Teller, «Adsorption of gases in multimolecular layers,» *Journal of the American Chemical Society,* vol. 60, nº 2, pp. 309-319, 1938.

[94] Z. Stojanovic y S. Markovic, «Determination of particle size distribution by laser diffraction,» *Technics - New Materials,* vol. 21, pp. 11-20, 2012.

[95] ASTM C188-17, «Standard Test Method for Density of Hydraulic Cement,» *ASTM*

International, p. 3, 2017.

[96] ASTM C187 - 16, «Standard test method for amount of water required for normal consistency of hydraulic cement paste,» *ASTM International,* pp. 1-3, 2016.

[97] Y. L. Yaphary, Z. Yu, R. H. Lam y D. Lau, «Effect of triethanolamine on cement hydration toward inittial setting time,» *Construction and Building Materials,* vol. 141, pp. 94-103, 2017.

[98] ASTM C191-18, «Standard Test Methods for Time of Setting of Hydraulic Cement by Vicat Needle,» *ASTM International,* p. 8, 2018.

[99] K. Wien, D. Wissmann, M. Kölling y H. D. Schulz, «Fast application of X-ray fluorescence spectroscopy aboard ship: how good is the new portable Spectro Xepos analyser?,» *Geo-Mar Lett,* vol. 25, nº 4, pp. 248-264, 2005.

[100] R. Salamo Clapera, «Energy Dispersive X-Ray Fluorescence: Measuring Elements in Soild and Liquid Matrices,» KdG & EPS, Girona, 2006.

[101] S. A. Speakman, Basics of X-Ray Powder Diffraction, Massachusetts: MIT, 2018.

[102] H. F. W. Taylor, La quimica de los cementos, vol. II, Londres: Ediciones Urmo, 1964.

[103] M. Sardela, Practical Materials Characterization, Illinois: Springer, 2014.

[104] D. Han y R. D. Ferron, «Effect of mixing method on microstructure and rheology of cement paste,» *Construction and Building Materials,* vol. 93, pp. 278-288, 2015.

[105] D. Han y R. D. Ferron, «Influence o high mixing intensity on rheology, hydration, and microstructure of fresh cement paste,» *Cement and Concrete Research,* vol. 84, pp. 95-106, 2016.

[106] A. Olivas, C. F. Ferraris, N. Martys, W. George, E. Garboczi y B. Toman, «Certification of SRM 2493: Standard Reference Mortar of Rheological Measurements,» *NIST special Publication,* pp. 187-260, 2017.

[107] D. Lootens y D. P. Bentz, «On the relation of setting and early-age strength development to porosity and hydration in cement-based materials,» *Cement and Concrete Composites,* vol. 68, pp. 9-14, 2016.

[108] D. P. Bentz, A. Ardani, T. Barrett, S. Z. Jones, D. Lootens, M. A. Peltz, T. Sato, P. E. Stutzman, J. Tanesi y W. J. Weiss, «Multi-scale Investigation of the Performance of

Limestone in Concrete,» *Construction and Building Materials,* vol. 75, pp. 1-10, 2015.

[109] V. Meacci, S. Ricci, A. Bruehwiler y D. Lootens, «Non Destructive Ultrasound Equipment to Evaluate the Concrete Compressive Strength,» de *Applications in Electronics Pervading Industry, Enviromental and Society, Lecture Notes in electrical Engineering*, vol. 429, Cham, Springer, 2016.

[110] A. Z. M. Badruddoza, S. V. MacWillians, D. A. Sebben, M. Krasowska, D. Beattie, D. J. Durian y J. K. Ferri, «Diffusing wave spectroscopy (DWS) methods applied to double emulsions,» *Colloid and Interface Science,* vol. 37, pp. 74-87, 2018.

[111] Z. Fahimi, F. J. Aangenendt, P. Voudouris, J. Mattsson y H. M. Wyss, «Diffussing-wave spectroscopy in a standard dynamic light scattering setup,» *Physical Review E,* vol. 96, nº 6, pp. 62611-1 - 62611-13, 2017.

[112] R. Tacail, «Mesures de diffusion multiple de la luminière sur des échantillons de pâtes cimentaires prises,» IUT Louis Pasteur Institut universitaire de technologie - Université de Strasbourg, Strasbourg, 2018.

[113] D. A. Weitz y D. J. Pine, «Diffusing-wave spectroscopy,» de *Dynamic Light Scattering: The methods and Some Applications* , Oxford, Oxford Science Publications, 1993, pp. 652-720.

[114] A. Eloy, Z. Yao, R. Bachelard, W. Guerin, M. Fouche y R. Kaiser, «Diffusing-wave spectroscopy of cold atoms in ballistic motion,» *Physical Review A,* vol. 97, pp. 13810-1 - 13810-7, 2018.

[115] Y. Hemar, D. N. Pinder, R. J. Hunter, H. Sing, P. Hebraud y D. S. Horne, «Monitoring of flocculation and creaming of sodium-caseinate-stabilized emulsions using diffusing-wave spectroscopy,» *Journal of colloid and Interface Science,* vol. 264, nº 2, pp. 502-508, 2003.

[116] V. Viasnoff, F. Lequeux y D. J. Pine, «Multispeckle diffusing-wave spectroscopy: A tool to study slow relaxation and time-dependent dynamics,» *Review of Scientific Instruments,* vol. 73, nº 6, pp. 2336-2344, 2002.

[117] T. Narita, C. Beauvais, P. Hebraud y F. Lequeux, «Dynamics of concentrated colloidal suspensions during drying-aging, rejuvenation and overaging,» *The European Physical Journal E,* vol. 14, nº 3, pp. 287-292, 2004.

[118] ASTM D790-17, «Standard Test Method for Flexural Properties of Unreinforced and

Reinforced Plastics and Electrical Insulating Materials,» pp. 1-12, 2017.

[119] I. F. Sáez del Bosque, S. Martínez-Ramírez y M. T. Blanco-Varela, «Combined effect of amorphous nanosilica and temperature on white portland cement hydration,» *Industrial and Engineering Chemistry Research,* vol. 52, pp. 11866-11874, 2013.

[120] W. Kunther, Z. Dai y J. Skibsted, «Thermodynamic modeling of hydrated white Portland cement-metakaolin-limestone blends utilizing hydration kinetics from Si MAS NMR spectroscopy,» *Cement and Concrete Research,* vol. 86, pp. 29-41, 2016.

[121] D. P. Bentz, «Cementitious Materials: Hydration Chemistry and Characterization,» National Institute of Standards and Technology, 2015.

[122] J. Peng, D. Deng, H. Huang, Q. Yuan y j. Peng, «Influence of superplasticizer on the rheology of frsh cement asphalt paste,» *Case Studies in Construction Materials,* vol. 3, pp. 9-18, 2015.

[123] M. Liard, Suspensions Concentrées: Systems non Newtoniens et thixotropie sous écoulement, Strasbourg: Université de Strasbourg - IPCMS, 2015.

[124] G. Ovarlez y X. Chateau, «Influence of shear stress applied during flow stoppage and rest period on the mechanical properties of thixotropy suspensions,» *Physical Review E: Statical, Non-linear, and Soft Matter Physics, American Physical Society,* vol. 77, nº 6, pp. 1-35, 2008.

[125] L. Nachbaur, J. C. Mutin, A. Nonat y L. Choplin, «Dynamic mode rheology of cement and tricalcium silicate pastes from mixing to setting,» *Cement and Concrete Research,* vol. 31, nº 2, pp. 183 - 192, 2001.

[126] F. Ianni, D. Lasne, R. Sarcia y P. Hébraud, «Relaxation of jammed colloidal suspensions after shear cessation,» *Physical Review E,* vol. 74, nº 1, pp. 11401-1 - 11401-6, 2006.

[127] N. S. Martys, D. Lootens, W. George y P. Hébraud, «Contact and stress anisotropies in start-up flow of colloidal suspensions,» *Phys. Rev. E,* vol. 80, nº 3, pp. 31401 - 31407, 2009.

[128] D. Lootens, P. Jousset, L. Martinie, N. Roussel y R. J. Flatt, «Yield stress during setting of cement pastes from penetration test,» *Cement and Concrete Research,* vol. 39, nº 5, pp. 401 - 408, 2009.

[129] R. J. Flatt, «Dispersion forces in cement suspensions,» *Cement and Concrete Research,*

vol. 34, pp. 399-408, 2004.

[130] F. Puertas y T. Vazquez, «Early hydration cement. Effect of admixtures superplasticizers,» *Materiales de Construcción,* vol. 51, nº 262, 2001.

[131] R. C. De oliveira-Romano, M. Hark-Maciel, R. Giuliano-Pileggi y M. Alba-Cincotto, «Monitoring of hardening of portland cement suspensions by vicat test, oscillatory rheometry, and isothermal calorimetry,» *Applied Rheology,* vol. 27, nº 3, 2017.

[132] M. Khan y T. G. Mason, «Local collective motion analysis for multi-probe dynamic imaging and microrheology,» *Journal of Physics: Condensed Matter: An Institute of Physics Journal,* Vols. %1 de %228-30, 2016.